Max-Planck-Institut für Meteorologie
Max Planck Institute for Meteorology

The influence of aerosols on North Atlantic cyclones

Dorothea F. Banse

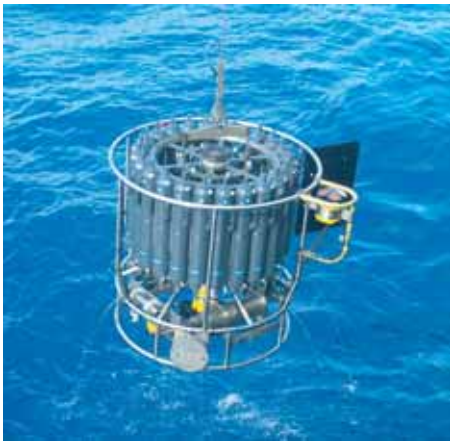

Berichte zur Erdsystemforschung 53/2008

Reports on Earth System Science

Hinweis

Die Berichte zur Erdsystemforschung werden vom Max-Planck-Institut für Meteorologie in Hamburg in unregelmäßiger Abfolge herausgegeben.

Sie enthalten wissenschaftliche und technische Beiträge, inklusive Dissertationen.

Die Beiträge geben nicht notwendigerweise die Auffassung des Instituts wieder.

Die "Berichte zur Erdsystemforschung" führen die vorherigen Reihen "Reports" und "Examensarbeiten" weiter.

Notice

The Reports on Earth System Science are published by the Max Planck Institute for Meteorology in Hamburg. They appear in irregular intervals.

They contain scientific and technical contributions, including Ph. D. theses.

The Reports do not necessarily reflect the opinion of the Institute.

The "Reports on Earth System Science" continue the former "Reports" and "Examensarbeiten" of the Max Planck Institute.

Anschrift / Address

Max-Planck-Institut für Meteorologie
Bundesstrasse 53
20146 Hamburg
Deutschland

Tel.: +49-(0)40-4 11 73-0
Fax: +49-(0)40-4 11 73-298
Web: www.mpimet.mpg.de

Layout:

Bettina Diallo, PR & Grafik

Titelfotos:
vorne:
Christian Klepp - Jochem Marotzke - Christian Klepp
hinten:
Clotilde Dubois - Christian Klepp - Katsumasa Tanaka

Berichte zur Erdsystemforschung 53/2008

The influence of aerosols on North Atlantic cyclones

Dissertation zur Erlangung des Doktorgrades der Naturwissenschaften
im Departement Geowissenschaften der Universität Hamburg
vorgelegt von

Dorothea F. Banse
aus Erfurt

Hamburg 2008

Reports on Earth System Science 53/2008

ISSN 1614-1199

Dorothea F. Banse
Max-Planck-Institut für Meteorologie
Bundesstrasse 53
20146 Hamburg
Germany

Als Dissertation angenommen
vom Departement Geowissenschaften der Universität Hamburg

auf Grund der Gutachten von
Prof. Dr. Hartmut Graßl
und
Dr. Johann Feichter

Hamburg, den 7. April 2008
Prof. Dr. Kay-Christian Emeis
Leiter des Departements für Geowissenschaften

ISSN 1614-1199

The influence of aerosols on North Atlantic cyclones

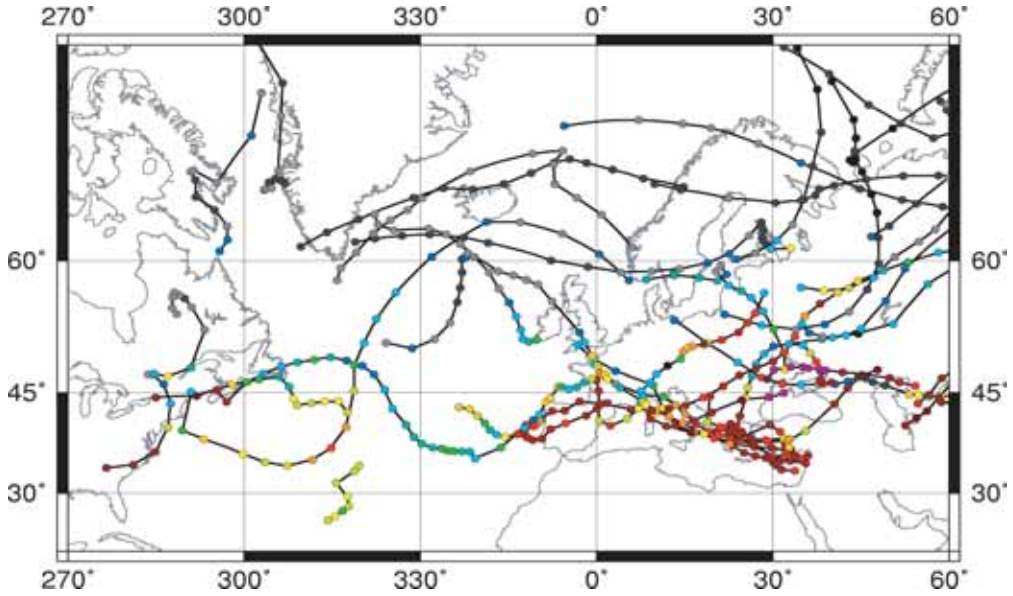

Dorothea F. Banse

Hamburg 2008

The rights to the quotation of Antoine de Saint-Exupéry are as follows:

The figure on the previous page shows selected cyclone tracks of March 2000 identified in a nudged run performed with ECHAM5/HAM (courtesy of Philip Stier, archived as experiment E220). The filled circles indicate the sulphate burden in mg(S)/m^2 along the track according to the following scale:

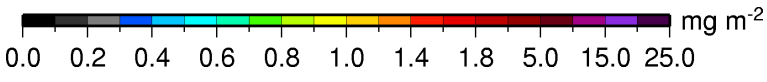

UNSER WERDEN IST NOCH NICHT VOLLENDET, SOLANGE WIR HUNGER SPÜREN. . . .
DARUM MÜSSEN WIR UNS UNSERER SELBST UND DER WELT BEWUSST WERDEN.

CE QUE NOUS SENTONS QUAND NOUS AVONS FAIM . . . C'EST QUE LA GENÈSE N'EST POINT ACHEVÉE ET QU'IL NOUS FAUT PRENDRE CONSCIENCE DE NOUS-MÊMES ET DE L'UNIVERS.

WHAT WE FEEL WHEN WE ARE HUNGRY . . . IS THAT THE BIRTH OF MAN IS NOT YET ACCOMPLISHED, THAT WE MUST TAKE STOCK OF OURSELVES AND OUR UNIVERSE.

Antoine de Saint-Exupéry

Abstract

Extratropical low-pressure systems or cyclones, which mainly originate over the North Atlantic, characterise the everyday weather in Europe. Severe cyclones can cause large amounts of damage due to high wind speeds and heavy precipitation. The question arises if and how cyclones will change due to future anthropogenic impacts. Previous studies of the response of cyclonic activity to global climate change have primarily focussed on the effect caused by increasing greenhouse gas concentrations and the associated global warming. It is uncertain, though, how this warming will influence the number, intensity and locations of cyclones in the North Atlantic/European region. This uncertainty is caused by two competing energetic effects that occur simultaneously: the meridional temperature gradient decreases because of the differential warming of polar and tropical regions and the latent heat content of the atmosphere increases. In addition to the anthropogenic greenhouse forcing, radiatively active aerosol particles modify the earth's energy budget. Therefore, they should also be taken into account when studying cyclonic activity.

In this study, the influence of the direct sulphate aerosol effect on North Atlantic cyclones is investigated in simulations of the ECHAM4/OPYC3 coupled climate model with respect to temperature, baroclinicity and cyclone tracks. The simulations include a control experiment (CTL) and two transient experiments from 1860 to 2050, one with increasing concentrations of greenhouse gases (GHG) and the other additionally allowing for the direct radiative effect of anthropogenic sulphate aerosol (GSD). Different cyclone characteristics in CTL agree well with those in the ECMWF Re-Analysis ERA40 which gives confidence in the performance of the climate model and in its use to address the uncertainty mentioned above.

The comparison of a present to a future simulation period leads to the following results: The greenhouse gas effect causes a warming in both winter and summer whereas the aerosol effect causes a cooling, but of smaller magnitude. Considering the effects together, the sulphate aerosol present in GSD attenuates the warming projected in the GHG simulation. Regarding the atmospheric baroclinicity, greenhouse gases tend to increase it while the sulphate aerosol effect tends to decrease it. The cyclone track density shifts northward in both winter and summer in GHG. In GSD, this shift is distinctly dampened and almost negligible. The number of all cyclones detected in the North Atlantic/European region does not change significantly in either experiment. Deep cyclones with core pressures below 970 hPa occur more often in the future in GHG, but not in GSD. The direct radiative effect of sulphate aerosol thus strongly

moderates the response of the climate system to the increase in greenhouse gas concentrations, but does not reverse it.

In another part of this study, the influence of aerosols on the cyclone *Grace*, which developed over the North Atlantic in March 2000, is investigated in a case study setup with respect to the change in certain meteorological parameters along the cyclone track. For this case study, which covers a 10-day period, two ensembles of 13 simulations each are produced. For one ensemble, ECHAM5-HAM is used considering the full AeroCom emission inventory. For the other, the anthropogenic contributions to the emissions are neglected. The two ensembles exhibit differences in the sulphate burden along the track. However, these differences have no impact on the track of *Grace* itself or on the along-track aerosol optical depth, net surface solar radiation and precipitation. While the current setup proves to be an inappropriate tool for the case study analysis, the simulations do reveal an interesting phenomenon south of the actual region of interest in this study: they indicate long-distance transport of sulphur dioxide and sulphate from Europe towards northern Africa where both species accumulate due to inefficient sink processes. The prevailing winds during the case study period suggest that the accumulated sulphur species are transported across the Sahara towards the North Atlantic where they are partly transported toward the north again. This possible transport mechanism has not yet been validated, though, since the observational data are not sufficient.

Zusammenfassung

Die Abfolge von außertropischen Tiefdruckgebieten oder Zyklonen, die hauptächlich über dem Nordatlantik entstehen, charakterisiert das Wetter in Europa. Besonders stark ausgeprägte Tiefs können aufgrund der hohen Windgeschwindigkeiten und Starkniederschläge, die sie mit sich bringen, große Schäden verursachen. Es stellt sich die Frage, ob und wie sich die Tiefs durch zukünftige anthropogene Einflüße ändern werden. Frühere Studien zur Reaktion der Zyklonenaktivität auf den globalen Klimawandel konzentrierten sich vor allem auf den Effekt, der durch ansteigende Treibhausgaskonzentrationen und die damit verbundene globale Erwärmung verursacht wird. Es besteht jedoch Unsicherheit darüber, wie diese Erwärmung sich auf Anzahl, Intensität und geographisches Vorkommen der Zyklonen auswirken wird. Diese Unsicherheit kommt durch zwei energetische Effekte, die gleichzeitig auftreten und miteinander konkurrieren, zustande: Zum einen nimmt der meridionale Temperaturgradient aufgrund der unterschiedlich starken Erwärmung in den tropischen und den Polargebieten ab, zum anderen kann eine wärmere Atmosphäre mehr latente Wärme speichern. Zusätzlich zum anthropogenen Treibhausgasantrieb beeinflussen auch strahlungsaktive Aerosolpartikel den Energiehaushalt der Erde. Deshalb sollten diese bei Untersuchungen zur Zyklonenaktivität auch berücksichtigt werden.

In dieser Arbeit wird der direkte Sulfataerosoleffekt auf nordatlantische Zyklonen bezüglich Temperatur, Baroklinität und Zyklonenzugbahnen in Simulationen des gekoppelten Klimamodells ECHAM4/OPYC3 untersucht. Die Simulationen umfassen ein Kontrollexperiment (CTL) und zwei transiente Experimente von 1860 bis 2050, von denen eins (GHG) steigende Treibhausgaskonzentrationen als externen Antrieb beinhaltet, während das andere (GSD) auch den direkten Strahlungseffekt des anthropogenen Sulfats berücksichtigt. Verschiedene Zykloneneigenschaften der CTL-Simulation stimmen gut mit denen der EZMW Reanalyse ERA40 überein, was Vertrauen in die Leistung des Klimamodells und seiner Anwendbarkeit, die oben erwähnte Unsicherheit anzugehen, erweckt.

Der Vergleich einer gegenwärtigen mit einer zukünftigen Modellperiode führt zu folgenden Ergebnissen: Der Treibhausgaseffekt verursacht eine Erwärmung sowohl im Winter als auch im Sommer, während der Aerosoleffekt eine Abkühlung, wenn auch geringeren Ausmaßes, bewirkt. Betrachtet man beide Effekte zusammen, offenbart sich, dass das Sulfat in GSD die in GHG projizierte Erwärmung schwächt. Bezüglich der atmosphärischen Baroklinität lässt sich feststellen, dass Treibhausgase diese eher verstärken, das Sulfat sie jedoch eher schwächt. Die Zugbahndichte erfährt im Winter und im Sommer eine Nordwärtsverschiebung in GHG. In GSD ist diese Verschiebung deutlich geringer und fast vernachläs-

sigbar. Die Gesamtanzahl der im nordatlantisch-europäischen Raum detektierten Zyklonen weist weder in GHG noch in GSD eine signifikante Änderung auf. Intensive Tiefdruckgebiete, deren Kerndrücke unter 970 hPa fallen, treten in GHG in der zukünftigen Periode verstärkt auf, aber nicht in GSD. Der direkte Strahlungseffekt von Sulfataerosol verursacht folglich eine starke Abmilderung der Reaktion des Klimasystems auf steigende Treibhausgaskonzentrationen, aber kann diese nicht rückgängig machen.

Ein weiterer Teil dieser Arbeit beschäftigt sich mit dem Einfluss von Aerosolen auf bestimmte meteorologische Größen entlang der Zugbahn des Tiefs *Grace*, das sich im März 2000 über dem Nordatlantik bildete. Für dieses Fallbeispiel wurden zwei Ensembles mit jeweils 13 Simulationen gerechnet. Für ein Ensemble greift ECHAM5-HAM auf den vollständigen AeroCom-Emissionsdatensatz zurück. Für das andere Ensemble werden die anthropogenen Emissionen vernachlässigt. Beide Ensemble zeigen Unterschiede in der Sulfatbelastung entlang der Zugbahn. Diese Unterschiede haben jedoch keinerlei Einfluss auf die Zugbahn von *Grace* selbst oder auf die aerosoloptische Dicke, die solare Nettostrahlung am Boden oder den Niederschlag entlang der Zugbahn. Es zeigt sich also, dass der gewählte Untersuchungsmethode nicht für die Fallbeispielanalyse geeignet ist. Die Simulationen offenbaren jedoch ein interessantes Phänomen südlich des eigentlichen Untersuchungsgebietes: Anscheinend werden Schwefeldioxid und Sulfat von Europa nach Nordafrika transportiert, wo sie aufgrund ineffizienter Senkenprozesse akkumulieren. Die vorherschenden Winde deuten einen westwärtsgerichteten Transport der Schwefeloxide über die Sahara an. Über dem Nordatlantik werden Teile dieser Schwefeloxide scheinbar wieder nach Norden transportiert. Dieser mögliche Transportmechanismus konnte jedoch noch nicht bewertet werden, da nicht ausreichend Beobachtungsdaten vorhanden sind.

Table of Contents

List of Tables

List of Figures

Chapter 1

Introduction

1.1 Motivation

Extratropical cyclones of the North Atlantic constitute a major component of the weather in Europe. Together with high pressure systems, they are responsible for the incessant alteration from sunny and calm to rainy and windy conditions. Severe cyclones are accompanied by heavy precipitation and strong winds which may cause large damage. An important role of the cyclones is the redistribution of temperature, momentum and moisture between polar and tropical regions. The two main factors influencing the life cycle of a cyclone are the meridional temperature gradient between the Equator and the Poles and the latent heat content of the atmosphere. Both of these are expected to change with the enhanced greenhouse effect caused by anthropogenic emissions of carbon dioxide and other radiatively active gases. Modelling studies show that the enhanced greenhouse effect will result in a general cooling of the stratosphere and a warming of the mid-troposphere (IPCC, 2007). The largest tropospheric warming is expected in the high latitudes of the Northern Hemisphere. Therefore, the meridional temperature gradient between the North Pole and the Equator is expected to decrease in the lower troposphere. In turn, the baroclinicity, which is a measure of the baroclinic instability of the atmosphere, is expected to decrease so that the number of extratropical cyclones may decrease as well. On the other hand, a warmer atmosphere has a higher latent heat content so that cyclones have a larger energy reservoir to draw from during their developmental stages. It is still uncertain how these two competing effects will influence the development of cyclonic activity in the future. Furthermore, aerosols are known to have a significant influence on the climate system (IPCC, 2007). They can exert a notable radiative forcing and hence also influence both the meridional temperature gradient and the latent heat content of the atmosphere. The motivation for this study was therefore to investigate if and to what extent aerosols affect cyclone occurrence and characteristics in the North Atlantic/European region.

Section 1.2 describes the role of aerosols in the climate system due to their radiative impacts . Section 1.3 summarises the current knowledge on cyclonic behaviour in the North Atlantic/European region.

Section 1.4 discusses methods for detecting and tracking cyclones and Section 1.5 provides an overview of climate change and its impact on cyclonic activity as presented in the literature. The introductory chapter concludes with the objectives and outline of this thesis (Section 1.6).

1.2 The role of aerosols in the global climate system

1.2.1 Sources of atmospheric aerosols

An aerosol is, by definition, the suspension of liquid and/or solid particles in air. Atmospheric aerosol particles originate from a variety of natural and anthropogenic sources. They are either emitted in particulate form, then referred to as primary aerosol, or nucleated in the atmosphere from gaseous precursors, then referred to as secondary aerosol. The sizes of atmospheric aerosol particles cover a range that spans several orders of magnitude. Newly-nucleated Aitken particles with diameters of a few nanometers represent the lower end of the size distribution. Primary particles may reach a diameter of several tens of micrometers. The upper end of the size distribution is considered to be about 100 μm since particles of that size and larger can generally not be considered as suspended in the air anymore.

The main contributors to the atmospheric aerosol load are dust from mineral soil, sea salt, carbonaceous aerosol particles, sulphates, ammonium and nitrates. Their principal sources are wind-driven emissions of particles and droplets from land and water surfaces, combustion processes and the emission of gaseous aerosol precursors.

The source regions of dust, which is emitted by wind-driven mobilisation of erodible soil dust particles, are deserts, dry lakes and river beds as well as arid zones with anthropogenically disturbed vegetation.

Sea salt is predominantly natural in origin and is formed from partly-evaporating sea spray droplets.

Carbonaceous aerosols are generally grouped into organic, referred to as particulate organic matter (POM), and elemental, referred to as black carbon (BC). Combustion processes represent the largest source of carbonaceous aerosols are combustion processes, i.e. vegetation fires and the burning of fossil fuels, biofuels and agricultural waste. Other sources of primary organic aerosols are plants (pollen and plant debris) and bacteria. POM also originates from volatile organic compounds which either condensate on pre-existing aerosol particles or nucleate new particles.

Atmospheric sulphate, SO_4^{2-}, originates from chemical reactions of gaseous sulphur dioxide, SO_2, and dimethylsulphide, DMS. The main anthropogenic sources of SO_2 are fossil fuels, industry and biofuels. The main natural sources are volcanoes for SO_2 and the marine biosphere for DMS.

1.2.2 Radiative effects of aerosols

Aerosols play an important role in the climate system. They interact with both solar (shortwave) and thermal-infrared (longwave) radiation in a variety of ways. Fig. 1.1 shows the various radiative mechanisms associated with aerosols. By scattering and absorbing radiation aerosol particles directly alter the earth's radiation budget (Ångström, 1962; McCormic & Ludwig, 1967). This mechanism is known as the direct aerosol effect. Aerosol particles that predominantly scatter solar radiation cause a net cooling of the earth's surface. Sulphates and sea salt belong to this group of aerosol particles. On the other hand, strongly absorbing aerosol, e.g. black carbon in the form of soot, warms the atmosphere (e.g. Haywood & Shine, 1995).

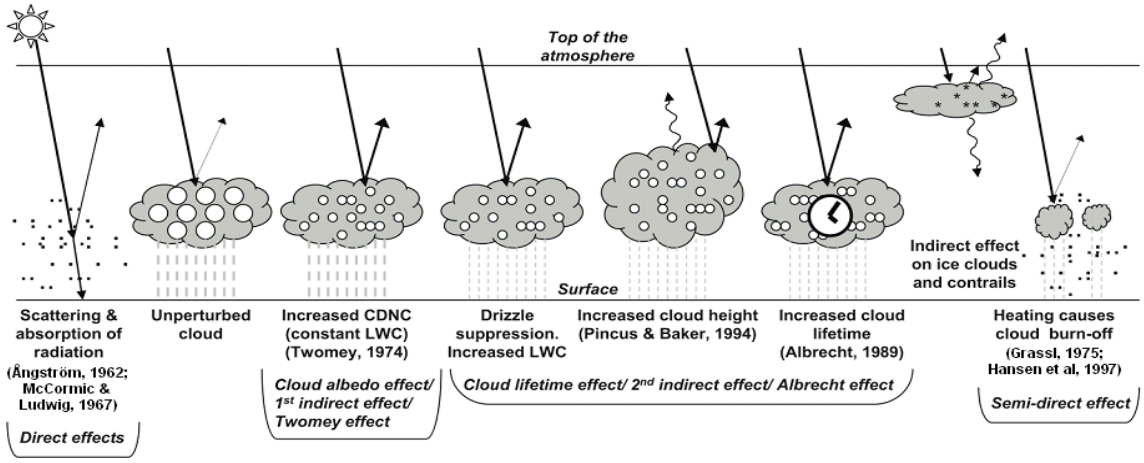

Figure 1.1: Schematic diagram of radiative aerosol effects (modified from IPCC (2007)). Small black dots: aerosol particles; larger open circles: cloud droplets; straight lines: incident and reflected solar radiation; wavy lines: terrestrial radiation; vertical grey dashes: rainfall; LWC: liquid water content.

In addition to the direct effects, aerosols alter the radiation budget indirectly by modifying cloud properties. The major indirect effects are: the cloud effect, the cloud lifetime effect, the semi-direct effect and the glaciation indirect effect. These effects will be briefly described below. Lohmann & Feichter (2005) provide a comprehensive review on indirect aerosol effects.

Cloud albedo effect. This is also known as the first indirect or the Twomey effect. Since aerosols act as cloud condensation nuclei (CCN), increasing numbers of aerosol particles lead to higher cloud droplet number concentrations (CDNC) with smaller droplet radii. In turn, the cloud albedo increases (Twomey, 1974).

Cloud lifetime effect. This is also known as the second indirect or the Albrecht effect. It refers to the increasing cloud lifetime and enhanced cloud thickness caused by higher CDNC (Albrecht, 1989; Pincus & Baker, 1994).

Semi-direct effect. Absorbing aerosols heat the atmosphere and reduce low cloud cover by reducing relative humidity (Graßl, 1975; Hansen et al., 1997; Ackerman et al., 2000). The reduction in cloud cover is a combination of inhibiting the formation of new droplets and the evaporation of existing droplets.

Glaciation indirect effect. Certain aerosol particles act as ice nuclei. Therefore, they potentially enhance the precipitation formation in mixed-phase clouds decreasing the cloud lifetime and hence the global albedo (Lohmann, 2002).

Another effect of aerosol scattering and absorption is the dampening of the hydrological cycle (Liepert et al., 2004; Feichter et al., 2004). The reduction of incoming shortwave radiation at the surface is only partly offset by increases in the downwelling longwave radiation. To reach equilibrium, the system responds partly by reductions in the out-going longwave radiation and partly by reductions in the fluxes of sensible and latent heat, i.e. reductions in evapotranspiration.

In-situ and remote observations prove the existence of radiative aerosol effects. For example, the direct aerosol effect can be estimated from satellite retrievals relying on instruments such as MODIS (Moderate Resolution Imaging Spectrometer) and CERES (Clouds and the Earth's Radiant Energy System; see Yu et al., 2006, for a review). *Ship tracks*—distinctive bright streaks observed in satellite images of marine stratocumulus clouds associated with plumes of ship exhaust (e.g., Ferek et al., 1998; Feingold et al., 2003)—are observational evidence for the cloud albedo effect. Smaller droplet sizes in polluted compared to clean clouds were also observed (e.g., Brenguier et al., 2000). Krüger & Graßl (2002, 2004) demonstrated the semi-direct aerosol effect by analysing long-term satellite observations of cloud reflectance. They found a considerable decrease of the planetary albedo over Europe and China from the late 1980s to the late 1990s.

1.3 Cyclones in the North Atlantic and Europe

In the following, *cyclone* or *feature* refers to a single extratropical low pressure centre identified at a specific location at a specific time. A *cyclone track* is the trajectory of one specific cyclone during its lifetime. *Storm tracks*, finally, represent regions of enhanced eddy variance/covariance statistics (Blackmon, 1976).

1.3.1 The analysis region

The region chosen for this study of North Atlantic cyclones extends from 20°N to 80°N and from 90°W to 60°E (Fig. 1.2) A number of geographical locations relevant within the context of cyclone research are indicated on the map for better identification.

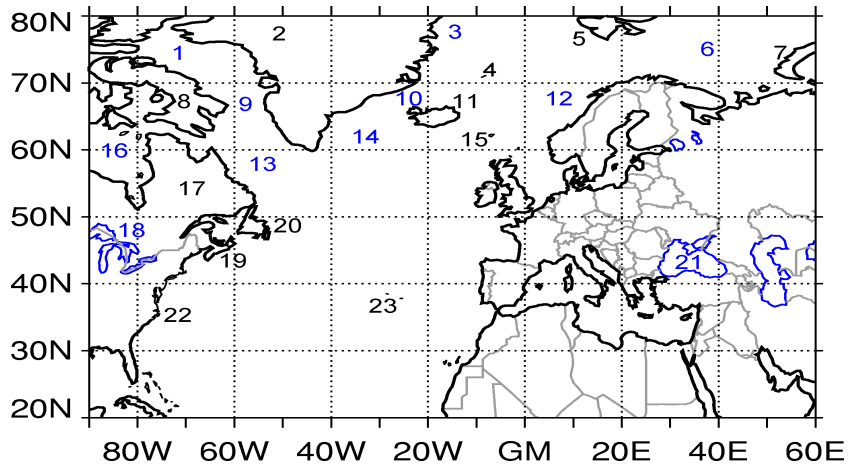

Figure 1.2: Map of the region analysed within the framework of this thesis. Numbers reference the following: 1—Baffin Bay, 2—Greenland, 3—Greenland Sea, 4—Jan Mayen, 5—Svalbard, 6—Barents Sea, 7—Novaya Zemlya, 8—Baffin Island, 9—Davis Strait, 10—Denmark Strait, 11—Iceland, 12—Norwegian Sea, 13—Labrador Sea, 14—Irminger Sea, 15—Faroe Islands, 16—Hudson Bay, 17—Labrador, 18—Great Lakes, 19—Nova Scotia, 20—Newfoundland, 21—Black Sea, 22—Cape Hatteras, 23—Azores.

1.3.2 Measuring cyclonic activity

The two approaches to describe cyclonic activity are of an Eulerian and a Lagrangian nature. Blackmon (1976) introduced an Eulerian diagnostic derived from a gridded data set of 500 hPa geopotential height as a general measure of the variability in tropospheric eddy activity over a frequency band of 2 to 6 days, which he considered to be the synoptic time scale. Regions of strongest eddy activity are referred to as storm tracks. Synoptic activity is particularly intense in the North Atlantic storm track extending from the US east coast towards Iceland and Europe and in the Mediterranean storm track extending from the Gulf of Genoa towards southern Italy.

Since both cyclonic and anticyclonic eddies contribute to the bandpass filtered variance, it is not possible to differentiate between cyclonic or anticyclonic activity in the storm track. Therefore, a different approach, the Lagrangian approach, is needed. It considers individual weather systems and goes back to Köppen (1881) and van Bebber (1891) who recognised the key role played by cyclones in synoptic-scale variability.

1.3.3 Overview of cyclone climatologies

1.3.3.1 Manual analyses

The first long-term cyclone climatologies, i.e. statistical descriptions of cyclonic activity, were only published more than half a century after the endeavours of Köppen and van Bebber: Pettersen (1956) and Klein (1957) provided frequency maps of cyclone centres and cyclone days, respectively, which they derived from synoptic charts of the Northern Hemisphere for the period 1899 to 1939. Subsequently

published climatologies were often regional in scope, focussing for instance on North America (e.g., Reitan, 1974), the North Atlantic (e.g., Reitan, 1979), the Mediterranean (e.g., Radinovic, 1987) or the Arctic (e.g., Overland & Pease, 1982). Hemisphere-wide climatologies were compiled again after 1980 (e.g., Whittaker & Horn, 1984).

Due to the data scarcity in the Southern Hemisphere, the first cyclone climatologies there were of a regional nature (e.g., Karelsky, 1961). From the additional data gathered during the International Geophysical Year (IGY, 1957–1958), Taljaard (1967) compiled the first definite synoptic climatology for the entire Southern Hemisphere. Contrary to northern hemispheric climatologies, though, southern hemispheric climatologies (e.g., Streten & Troup, 1973; Le Marshall & Kelly, 1981) were rarely based on periods longer than 10 years and partly relied on the analysis of cloud imagery instead of mean sea level pressure (MSLP) data.

Manual tracking requires time and effort which often limits the geographical region explored and the number of phenomena that can be followed. It was the principal tool in studying cyclonic activity until the Eulerian approach gained momentum due to its ease of application to the gridded analyses provided by numerical weather prediction (NWP) and climate model data. With the increase in computer power, though, automated Lagrangian procedures to compile cyclone climatologies have been more and more extensively used since the late 1980s.

1.3.3.2 Automated analyses

Similarly to the manual analyses, cyclone climatologies derived from the automated analysis of meteorological data are available on a variety of spatial and temporal scales. The majority of the climatologies were derived from reanalysis data sets, others from operational NWP analyses or gridded observational data. Table A.1 provides an overview of cyclone climatologies based on observational and reanalysis data sets.

Within the context of this thesis, which focusses on the North Atlantic/European region, only selected climatologies covering this region of interest are discussed below.

Global-scale studies. The term *global* here refers to climatologies that consider the extratropical regions of both hemispheres. Comprehensive climatologies, i.e. ones providing a broad picture of cyclonic activity and not only considering one specific aspect of it, have only been published for about five years. To the knowledge of the author, the first of these comprehensive climatologies was compiled by Hodges et al. (2003) who compared data from four reanalysis projects: ERA15 (Gibson et al., 1997) of the European Centre for Medium-Range Weather Forecasts (ECMWF), the reanalysis of the National Centers for Environmental Prediction and Atmospheric Research, henceforth referred to as NCEP/NCAR reanalysis (Kistler et al., 2001), the reanalysis of NCEP and the Department of Energy (NCEP/DOE; Kanamitsu

et al., 2000) and the reanalysis of the first version of the Goddard Earth Observing System assimilation system of the National Aeronautics and Space Administration (NASA-GEOS1; Schubert et al., 1993). They found that the tracking statistics correspond very well for all re-analyses in the Northern Hemisphere. However, the cyclone mean intensities of the ECMWF reanalysis were systematically stronger in the main storm track regions, but weaker around major orographic features. A direct comparison of the identified tracks revealed differences between the re-analyses for small-scale weak systems, in particular in secondary development regions. Hodges et al. (2003) restricted their analysis to the satellite era, i.e. after 1979, to exclude the data inhomogeneity caused by the introduction of satellite data into the NCEP/NCAR reanalysis and to obtain similar study periods for all re-analyses.

Wang et al. (2006) compared the climatology and changes of extratropical cyclone activity of ERA40, the 45-year reanalysis project of ECMWF, and NCEP/NCAR for 1958–2001. They introduced a cyclone activity index, defined as the product of the number of cyclones per season per year and the mean intensities of these cyclones in terms of the local Laplacian of pressure. Similarly to Hodges et al. (2003), the re-analyses are in reasonably good agreement in the Northern Hemisphere with ERA40 showing systematically stronger cyclone activity over the oceans. This overestimation in ERA40 compared to NCEP/NCAR is attributed to the higher model resolution, updated assimilation system and improved observational data used for ERA40.

Northern Hemisphere. The majority of climatologies for the Northern Hemisphere are based on the NCEP/NCAR reanalysis. Furthermore, many studies only look at the winter season, although the length of these winter seasons often differs between the studies.

Lambert (1996) presented a climatology of intense cyclone events, defined as MSLP minima with a core pressure below 970 hPa, for the period 1899–1991. In particular, he investigated the trend in the number of intense cyclones. Before about 1970, the trend is negligible, but afterwards it is positive for both the Pacific and the Atlantic. In the Pacific, the number of intense events and the sea surface temperature (SST) were temporally correlated indicating a relationship between SST gradients averaged between the Equator and the midlatitudes and cyclone behaviour. In the Atlantic, there was no evidence for such a relationship.

Sickmöller et al. (2000) investigated cyclone behaviour in the North Atlantic and the North Pacific in an extended ERA15 data set from 1980 to 1997. They related cyclonic activity to the dominant teleconnection patterns, i.e. the NAO and the Southern Oscillation (El Niño Southern Oscillation, ENSO), and found evidence for an interaction between the storm tracks in the two ocean basins.

Hoskins & Hodges (2002) tracked extrema in a variety of meteorological fields (MSLP, geopotential height $z_{850\,\mathrm{hPa}}$ and $z_{250\,\mathrm{hPa}}$, meridional wind $V_{850\,\mathrm{hPa}}$ and $V_{250\,\mathrm{hPa}}$, temperature $T_{850\,\mathrm{hPa}}$ and $T_{250\,\mathrm{hPa}}$, vertical velocity $\omega_{500\,\mathrm{hPa}}$, relative vorticity $\xi_{850\,\mathrm{hPa}}$ and $\xi_{250\,\mathrm{hPa}}$, potential temperature $\theta_{PV=2}$, potential

vorticity $PV_{\theta=330\mathrm{K}}$) to explore the nature and comparative magnitudes of northern hemispheric storm tracks in winter. The data cover the period 1979–2000 and are from ERA15 extended by operational ECMWF analyses. They showed that the oceanic storm track regions are conspicuous in the tracking statistics of all the fields. The magnitude of the storm track does depend on the field, though, i.e. for some fields the Atlantic storm track is stronger, for others the Pacific storm track.

Paciorek et al. (2002) interpreted the winter cyclone activity of the NCEP/NCAR reanalysis in 1949–1999 with the help of a variety of indices. They found a moderately strong correlation between baroclinicity, temperature variance and extreme wind with the counts of cyclones and intense cyclones, here defined as cyclones with a core pressure below 980 hPa, over much of the storm tracks when the counts are offset 7.5° to the north. Furthermore, an increase in intense cyclones over the Atlantic, the Pacific, and Eurasia occurred while the total number of cyclones remained either stable or decreased, depending on the region.

Rudeva & Gulev (2007) studied cyclone size characteristics and changes during the cyclone life cycle in the NCEP/NCAR reanalysis for 1948–2004. Their results indicated that cyclones are significantly larger over the oceans (mean effective radii >900 km) than over the continents (mean effective radii 300–400 km). The cyclone effective radius is proportional to cyclone lifetime and intensity with the longest lived and most intense cyclones having the largest radii.

North Atlantic and Europe. Contrary to northern hemispheric cyclone climatologies, the majority of cyclone climatologies in the North Atlantic/European region are derived from reanalysis and operational NWP products of the ECMWF. The focus on the winter season remains the same, though.

Haak & Ulbrich (1996) identified cyclone positions in initialised analyses of the ECMWF for 1980–1993. A comparison of automatically and manually determined positions of cyclone centres with core pressures below 950 hPa revealed a median difference in distance between corresponding cyclone centres of 100 km. Furthermore, the cyclone core pressures were about 4.5 hPa higher in the numerical analysis.

Blender et al. (1997) performed a cluster analysis for cyclones identified and tracked in 5 years of ECMWF analyses (1990–1994). They used 3 clusters differentiating between stationary, north-eastward and zonally moving cyclones. The clusters are characterised by different geographical positions, life-cycles and mean-square displacements of their respective members.

Hanson et al. (2004) and Trigo (2006) compared the cyclone climatologies derived from the ECMWF and the NCEP/NCAR re-analyses for 1979–2001 and 1958–2000, respectively. The two studies agreed that the spatial distribution of the cyclones is similar in both reanalysis data sets and that the number of detected cyclones is higher in ERA40 than in the NCEP/NCAR data. Regarding the time series of cyclone frequency, though, Hanson et al. (2004) found only weak correlations between the re-analyses. They concluded that analysing the ECMWF data set leads to a more comprehensive climatology of North

Atlantic cyclones at all scales.

Benestad & Chen (2006) provided another comparison of two data sets: the ERA40 reanalysis and the gridded ds195.5 MSLP data set from the National Meteorological Center (NMC; now NCEP). Their investigation showed that the results of the cyclone identification routine depend more on the choice of the data set than on the parameters of the identification method such as the spatial resolution of the interpolation.

The studies summarised above and listed in Table A.1 often highlight specific characteristics of cyclone behaviour. Taken together, they provide a comprehensive picture of cyclonic activity, particularly in recent decades, helping to better understand cyclonic activity and its causes on global and regional scales. They also represent different methods of the automatic identification and tracking of cyclones. Such automatic methods have proven to be an indispensable tool to analyse long-time data series and will be discussed below.

1.4 Cyclone identification and tracking methods

Automatic cyclone identification and tracking algorithms were initially used as forecast validation tools (Williamson, 1981; Akyildiz, 1985; Reed et al., 1986). Their application to global climate data began towards the end of the 1980s. Since then, many studies on the subject have been published (Table 1.1).

Table 1.1: Overview of cyclone identification and tracking schemes.

Author(s)	Studies based on the same or a slightly adapted version of the algorithm referenced in the left column
Alpert et al. (1990a)	Alpert et al. (1990b); Picornell et al. (2001); Campins et al. (2006)
Ayrault & Joly (2000a)	Baehr et al. (1999); Ayrault & Joly (2000b)
Bardin & Polonsky (2005)	
Bartholy et al. (2006)	
Beersma et al. (1997)	
Bell & Bosart (1989)	Key & Chan (1999); Smith et al. (2002)
Benestad & Chen (2006)	
Blender et al. (1997)	Schubert et al. (1998); Trigo et al. (1999); Sickmöller et al. (2000); Merkel & Latif (2002); Trigo et al. (2002); Hanson et al. (2004); Raible & Blender (2004); Luksch et al. (2005); Trigo (2006); Gaffney et al. (2007); Raible et al. (2007b); Raible (2007); Raible et al. (2007a); Schneidereit et al. (2007), diploma theses Affeld (1996); Schubert (1996); Wilshusen (1996); Schneidereit (2007), PhD theses Gaffney (2004)
Cao & Zhang (2004)	
Chandler & Jonas (1999)	Bauer & Del Genio (2006)
Chang & Song (2006)	
Dean (1993)	Lefevre & Nielsen-Gammon (1995); Dean & Bosart (1996)
Favre & Gershunov (2006)	
Fyfe (2003)	
Geng & Sugi (2001)	Geng & Sugi (2003)
Graham & Diaz (2001)	
Grigoriev et al. (2000)	Gulev et al. (2001); Zolina & Gulev (2001); Gulev et al. (2002); Ruprecht et al. (2002); Zolina & Gulev (2002, 2003); Sepp et al. (2005); Jung et al. (2006); Löptien et al. (2007); Rudeva & Gulev (2007), diploma thesis Ubl (2001)
Haak & Ulbrich (1996)	Knippertz et al. (2000)

Table 1.1: Continued from previous page.

Reference	Related studies
Hodges (1994)	Hodges (1995, 1996); Hodges & Thorncroft (1997); Hodges (1998, 1999a,b); Thorncroft & Hodges (2001); Hoskins & Hodges (2002); Hodges et al. (2003); Anderson et al. (2003); Bengtsson et al. (2004a,b); Martin et al. (2004); Stratton (2004); Bengtsson et al. (2005); Hoskins & Hodges (2005); Sorteberg et al. (2005); Bengtsson et al. (2006a,b); Byrkjedal et al. (2006); Gray & Dacre (2006); Greeves et al. (2006); Mailier et al. (2006); Ringer et al. (2006); Bengtsson et al. (2007a,b); Bromwich et al. (2007); Froude et al. (2007a,b); Hopsch et al. (2007); McDonald (2007), MSc thesis dos Santos Mesquita (2006), PhD theses Anderson (2000); Dacre (2004); Froude (2005); Song (2007)
König et al. (1993)	Carnell et al. (1996); Carnell & Senior (1998); Lozano et al. (2004); Gaffney et al. (2007)
Lambert (1988)	Lambert (1995); Lambert et al. (2002); Lambert (2004); Lambert & Fyfe (2006)
Le Treut & Kalnay (1990)	
Lionello et al. (2002)	
Löptien & Ruprecht (2005)	
Maheras et al. (2001)	
Murray & Simmonds (1991a)	Godfred-Spenning & Simmonds (1996); Jones & Simmonds (1993); Jones et al. (1994); Keable et al. (2002); Leckebusch & Ulbrich (2004); Leckebusch et al. (2006); Lim & Simmonds (2006, 2007); Murphy et al. (2002); Murray & Simmonds (1991b); Pezza & Ambrizzi (2003, 2005); Pinto et al. (2005, 2006, 2007); Raible et al. (2007a); Simmonds & Wu (1993); Simmonds & Law (1995); Simmonds & Murray (1999); Simmonds & Keay (2000b,a); Walland & Simmonds (1997); Condron et al. (2006); Wassermann et al. (2006); White & Simmonds (2006), PhD theses Pinto (2002); Lim (2005), diploma thesis Zacharias (2006), with slightly adapted detection, but same tracking: Sinclair (1994, 1995, 1997); Sinclair et al. (1997); Sinclair & Watterson (1999)
Muskulus & Jacob (2005)	
Nieto et al. (2005)	Porcù et al. (2007)
Serreze et al. (1993) (only detection), Serreze (1995) (also tracking)	Eichler & Higgins (2006); McCabe et al. (2001); Serreze et al. (1997); Wang et al. (2004, 2006); Zhang et al. (2004)
Spanos et al. (2003)	
Terry & Atlas (1996)	Leonard et al. (1999)
Ueno (1991a)	Ueno (1991b, 1993)
Wang & Rogers (2001)	
Wernli & Schwierz (2006)	Raible et al. (2007a)
Wile (2006)	
Zhang & Wang (1997)	Paciorek et al. (2002); Watterson (2006)
Zhu et al. (2007)	

The automated algorithms emulate the manual analysis and partly eliminate its subjective component. They allow comparisons of cyclone statistics obtained from different data sets, especially model-generated data, with the advantage of being independent of the analysist and of being repeatable. Similarly to the manual analyses, there are basically two steps in the Lagrangian procedures: (1) the identification of features, i.e., minima or maxima, in specific meteorological fields, and (2) the tracking of these features in time. A third step, which involves filtering the tracks according to certain requirements regarding cyclone lifetime and minimum distance travelled, may be included. During all of these steps, suitable parameters have to be chosen. These parameters are not always determined purely on a physical basis which makes direct comparisons of the schemes difficult. While the choice of parameters does introduce an arbitrary element to the analysis, the automation ensures that all cases that occured are subject to the same analysis criteria which is not the case for manual analyses.

Several authors (Lambert, 1988, 1995; Haak & Ulbrich, 1996; Lambert, 1996; Beersma et al., 1997; Zhang & Wang, 1997; Knippertz et al., 2000; Maheras et al., 2001; Lambert et al., 2002; Paciorek et al., 2002; Smith et al., 2002; Fyfe, 2003; Lambert, 2004; Bardin & Polonsky, 2005; Benestad & Chen, 2006;

Chang & Song, 2006; Keller et al., 2006; Lambert & Fyfe, 2006) applied only the first step to determine climatologies of cyclone centre density. While easily applicable to gridded data sets, this non-tracking technique does not provide information about the life cycle of the cyclones. For this purpose, cyclones are tracked in time, which constitutes the second step in the Lagrangian procedures, to study additional cyclone characteristics, such as genesis and lysis densities, deepening rates and lifetime. The most widely used tracking algorithms are Murray & Simmonds (1991a), König et al. (1993), Hodges (1994), Serreze (1995), Blender et al. (1997) and Grigoriev et al. (2000).

1.4.1 The choice of a suitable meteorological parameter

A large number of cyclone identification and tracking algorithms are applied to the fields of MSLP or geopotential height at the 1000 hPa level ($z_{1000\,\mathrm{hPa}}$, e.g., Benestad & Chen, 2006; Blender et al., 1997; Bauer & Del Genio, 2006; Carnell et al., 1996; Favre & Gershunov, 2006; Gulev et al., 2001; König et al., 1993; Lambert, 1996; Muskulus & Jacob, 2005; Serreze, 1995; Wernli & Schwierz, 2006; Zolina & Gulev, 2003). While this guarantees consistency with the manual cyclone analyses, there are also drawbacks. First, MSLP is strongly influenced by the large-scale background, i.e. the central pressure of a cyclone changes with the regional (latitudinal) climate mean pressure (Hoskins & Hodges, 2002). Second, strong background flows, for instance during an enhancement of the subtropical jets, can mask weak, fast moving synoptic features until significant development has occurred. Hence, MSLP-based tracking algorithms are biased toward well-developed and relatively slow-moving systems and underestimate cyclone duration and extent (Sinclair, 1994, 1997; Gulev et al., 2001). MSLP-based tracking also overlooks open-wave systems, which can overrun stationary lows or pass through the strong background pressure gradients associated with enhanced westerly winds. Such open-wave systems are often associated with comma cloud structures and strong precipitation bands (Sinclair, 1997). Furthermore, the extrapolation of pressure data to mean sea-level can introduce bias over high terrain. MSLP may be sensitive to how this extrapolation is performed and to the representation of the orography in the model. The same considerations apply to tracking features in the $z_{1000\,\mathrm{hPa}}$ field.

Tracking based on some kind of curvature measure offers an alternative. Murray & Simmonds (1991a) opted for the Laplacian of MSLP, $\nabla^2 MSLP$, which is related to cyclonic geostrophic vorticity by $\xi_g \approx \frac{1}{\rho f}\nabla^2 p$, where ρ is air density and f the Coriolis parameter. Sinclair (1994) tracked minima of geostrophic relative vorticity computed from $z_{1000\,\mathrm{hPa}}$. Ayrault & Joly (2000a) and Hodges (1996) applied their tracking algorithms to the 850 hPa relative vorticity, $\xi_{850\,\mathrm{hPa}}$. Vorticity is less influenced by the background flow and allows an earlier identification of the features. However, vorticity fields can be very noisy in high-resolution data and smaller-scale structures such as frontal systems may be resolved. Therefore, smoothing or a reduction in resolution is necessary for feature tracking. When considering the 1000 hPa level, the sensitivity of the field to its extrapolation to this level needs to be taken into account

as well.

When comparing trajectories of $\xi_{850\,\mathrm{hPa}}$ maxima and MSLP minima in the Northern Hemisphere, a spatial shift of about 100 km can be observed between the two trajectories (Mailier et al., 2006). This is caused by the interaction of zonal geostrophic wind and cyclonic geostrophic vorticity: Sinclair (1994) illustrated that adding a zonal geostrophic wind component to a stationary circular region of cyclonic geostrophic vorticity leads to a poleward shift of the corresponding pressure minimum.

In the literature, contradictory statements regarding the appropriateness of pressure, geopotential height or vorticity as the basic variable for tracking can be found: on the one hand, Murray & Simmonds (1991a) stated that the existence of a midlatitude depression is better represented by a pronounced cyclonic vorticity maximum than by a pressure minimum for synoptic-scale digital analyses. On the other hand, Sickmöller et al. (2000) argued that a pressure minimum corresponds more to a synoptic cyclone than a vorticity maximum.

To summarise, the choice of the variable to be tracked strongly depends on the purpose of the study. For instance, Bauer & Del Genio (2006) look at the influence of winter cyclones on the climatological humidity and use MSLP-based tracking with the argument that this approach is capable of detecting the cyclones important to the heat and water vapour transport in their associated conveyor belts. If one is interested in the complete life-cycle of a cyclone, though, vorticity should be used to capture the very early and very late stages of the development of a cyclone.

For this study, the use of vorticity was originally preferred. However, this proved to be inappropriate in two of the three applications presented here. For one, the comparison of the number of very deep lows detected in reanalysis and model data on the one hand and counted manually in synoptic MSLP analyses necessitated the choice of tracking MSLP minima in Chapter 3. For the other, the study of the response of cyclones to changes in greenhouse gas and aerosol concentrations (Chapter 4), the temporal resolution of the available data was not suitable for tracking vorticity maxima. Therefore, the method of tracking vorticity maxima is only used for the application described in Chapter 5.

1.4.2 The choice of a suitable tracking scheme

Cyclone algorithms have to meet certain requirements: they should produce results that are comparable to manual analyses for selected cases, be easy to use and not too computationally expensive.

A simple cyclone identification routine, such as the one introduced by Lambert (1988), fulfills these criteria and can be used to generate climatological cyclone frequency distributions. Wernli & Schwierz (2006) extend this approach of defining cyclones as local MSLP minima by considering finite areas around these minima. Their identification routine allows to capture not only the minimum itself, as is the case for other identification routines, but also the area under cyclonic influence and hence likely to experience the strong winds and precipitation associated with extratropical low pressure systems. The

motivation behind this approach arises to some extent from the requirements of the insurance industry who is not so much interested in the exact position of the pressure minimum as in the area affected by its passing.

As mentioned above, identification routines alone do not suffice to study cyclones through their growth and decay, though. This can only be achieved by tracking the cyclones through time. The challenge faced by the tracking algorithms is the correspondence problem, i.e. how to match cyclones at time step t with cyclones at time step $t-1$ or $t+1$. The majority of tracking algorithms rely on a nearest-neighbour search to meet this challenge (e.g., Alpert et al., 1990a; König et al., 1993; Serreze, 1995; Blender et al., 1997; Geng & Sugi, 2001): correspondence between two time steps is based on the first match found within a specified search region. Alternatively, preferred cyclone motion, which is computed from the geostrophic wind at the cyclone steering level, is taken into account when choosing the matching cyclone. According to Alpert et al. (1990a), the steering level is close to 700 hPa, whereas it is 500 hPa according to Terry & Atlas (1996). Nearest-neighbour searches, while computationally straight-forward, may produce inconsistent results when dealing with fast-moving features or when the time between consecutive analysis frames is large. Hence, more sophisticated matching techniques have been developed (Murray & Simmonds, 1991a; Hodges, 1994). Murray & Simmonds (1991a) apply a "prediction and matching" technique whereas Hodges (1994) adapts techniques associated with image processing and dynamical scene analysis to track features in meteorological fields.

Many tracking algorithms sample rectangular boxes distributed uniformally on a projection. This leads to the distortion of the sampling areas on the sphere so that the results are latitudinally biased. Introducing latitude-dependent area normalisation to correct for this bias may also lead to systematic bias in the analysis of cyclone frequencies (Hayden, 1981). In addition, the orientation of the cyclone tracks when passing through the sampling area can also lead to bias (Taylor, 1986).

One of the most widely used tracking algorithms, referred to as *TRACK* below, was developed by Hodges (1994), who continues to improve and update the source code. Numerous studies have established its status as a valuable research tool, e.g., for testing of the forecast skill of NWP models (Bengtsson et al., 2005; Froude et al., 2007b), determining the sensitivity of cyclone track prediction to the observing system (Froude et al., 2007a), studying the serial clustering of cyclones (Mailier et al., 2006), evaluating general circulation models (GCMs; Stratton, 2004; Greeves et al., 2006; Ringer et al., 2006) and gaining insight into tropical waves and cyclones (Hodges & Thorncroft, 1997; Thorncroft & Hodges, 2001; Bengtsson et al., 2007a,b). TRACK performs well both when examining climatological cyclone behaviour (e.g., Hoskins & Hodges, 2002; Hodges et al., 2003; Hoskins & Hodges, 2005; Bengtsson et al., 2006b) and when comparing observed and automatically detected cyclone tracks (Mailier et al., 2006). Compared to other schemes, TRACK has the advantage of being independent of the type of projection used in the analysis since the tracking is carried out directly on the unit sphere. Further-

more, TRACK includes a comprehensive statistics package (Hodges, 1996) which determines statistics of different cyclone characteristics on the unit sphere. Hence, projections are only necessary for the presentation of the results.

Two studies that directly compare different cyclone tracking schemes exist: Leonard et al. (1999) and Raible et al. (2007a). Leonard et al. (1999) assessed the schemes of Murray & Simmonds (1991a), König et al. (1993) and Terry & Atlas (1996) in the Southern Hemisphere. Both König et al. (1993) and Terry & Atlas (1996) applied a nearest-neighbour search for the tracking while Murray & Simmonds (1991a) relied on maximising the probability of association between the cyclone centres from one time step to the next. According to Leonard et al. (1999), all three schemes successfully identify large-scale depressions, although the number of the identified depressions differs from scheme to scheme. Leonard et al. (1999) also pointed out that the scheme of Terry & Atlas (1996) is more appropriate for emulating the approach of an operational forecaster while König et al. (1993) and Murray & Simmonds (1991b) are better suited for climatological studies.

Raible et al. (2007a) applied the schemes of Murray & Simmonds (1991a); Blender et al. (1997) and Wernli & Schwierz (2006) to fields of the ERA40 reanalysis data set (Uppala et al., 2005). Furthermore, they produced the cyclone climatology of the NCEP/NCAR reanalysis using the scheme of Blender et al. (1997), which relies on a nearest-neighbour tracking routine. Wernli & Schwierz (2006) also used a nearest-neighbour tracking routine, but only after calculating a first-guess position for each cyclone from the linear continuation of its previous positions. According to Raible et al. (2007a), the agreement of cyclone trajectories between the three schemes is comparable to the agreement between the re-analyses. Regarding the interannual variability of the number of cyclones per season, the observed correlation between the schemes was again comparable to the correlation between the two re-analyses. The long-term trends in the number of cyclones depended on the choice of tracking scheme, though. The schemes showed systematic discrepancies in the geographical distribution of detected cyclone centres which can be explained by parameter settings. Altogether, structural differences between the schemes were rather small which lead Raible et al. (2007a) to the conclusion that all schemes are suitable to study cyclonic activity in model data.

To summarise, the existing cyclone tracking schemes are capable of identifying cyclones and tracking them in time. The choice of the tracking scheme, as the choice of the tracking variable, depends on the purpose of the study, i.e. its application and the type of low that the user is most interested in. Some schemes are more applicable when trying to mirror the actions of an operational forecaster. Other schemes are more appropriate for research applications. Secondary considerations, such as the spatial and temporal resolution of the data to be studied, may also play a role in choosing the scheme.

For this dissertation, a scheme was needed that performs satisfactorily both for determining a long-term cyclone climatology and for studying individual cyclone trajectories. In addition, the scheme has

to do so at the resolution of the data used here, in particular data from experiments conducted with the coupled atmosphere-ocean GCM (AOGCM) ECHAM4/OPYC3 (European Centre Hamburg Model / Ocean in isopynal Coordinates). The scheme adopted that met these conditions was TRACK, which is described in detail in Section 2.6.

1.5 Cyclone activity under climate change conditions

The 4th Assessment Report of the Intergovernmental Panel on Climate Change (AR4; IPCC, 2007) states that the human-induced warming of the climate system is unequivocal and is now evident from observations of, e.g., global air and ocean temperatures. This warming represents one aspect of *climate change*, i.e., a change in the state of the climate that can be identified by changes in the mean and/or the variability of its properties, and that persists for an extended period, typically decades or longer.

In order to assess the future development of the climate, GCMs require projections of future emissions of greenhouse gases and aerosols. For this purpose, so-called scenarios are used. According to the definition of the IPCC (1994), a scenario is the coherent, internally consistent, and plausible description of a possible future state of the world. The IS92 scenarios were used in the second IPCC report (IPCC, 1996). One of them, the IS92a scenario, constitutes the basis for the climate change experiments analysed in Chapter 4. It is a business-as-usual scenario with high emissions of greenhouse gases. It assumes a world population of 11.3 billion by 2100, controls on SO_x, NO_x and non-methane volatile organic compounds as well as efforts to reduce SO_x, NO_x and CO in developing countries by the middle of the 21st century.

As mentioned above, the troposphere is expected to warm disproportionately between the North Pole and the Equator with the high latitudes of the Northern Hemisphere warming the most. There is still uncertainty about how the changes in atmospheric energetics associated with this warming will influence the number, intensity and locations of extratropical cyclones.

To gain more insight, automated cyclone algorithms have been applied to data obtained from GCM simulations of the future climate. For this type of application, the number of possible data sources is considerably larger than for the purpose of deriving a climatology from observational or reanalysis data sets. Not only is a variety of GCMs used to simulate how the earth's climate may develop in the future, but these GCMs employ many different emission scenarios. Table 1.2 summarises previous modelling studies investigating the impact of climate change on cyclonic activity. For the majority of these studies, the emission scenarios taken as basis for the future climate simulations are restricted to changes in the emissions of greenhouse gases. And even if the chosen emission scenario does include changes in anthropogenic aerosol emissions, not all GCMs can make use of that information in the simulations. Therefore, future changes in cyclone characteristics, such as intensity, are still controversial.

There is a broad agreement concerning the decrease in the total number of cyclones almost regardless of the area for which this number is calculated. However, the impact of climate change on the number of strong cyclones remains inconclusive. While there seemed to be an indication for an increase in such strong events some years ago (e.g., Carnell & Senior, 1998; Knippertz et al., 2000; Geng & Sugi, 2003; Lambert, 2004), more recent studies (Bengtsson et al., 2006a; Löptien et al., 2007) found no such evidence on the large scale. Nevertheless, the picture may be different on a regional scale: Bengtsson et al. (2006a), Leckebusch et al. (2006) and Pinto et al. (2007) report a strengthening of the storm track north of or over the British Isles.

The results of the pertinent modelling studies will be discussed in detail in relation to the results of a similar study carried out as part of this dissertation in Chapter 4.

1.6 Objectives and outline of this thesis

Given the importance of extratropical cyclones in the North Atlantic and Europe and the uncertainty associated with changes in the cyclonic activity in the future, the aims of this work are to examine the questions below:

- Is there an aerosol signal in the changes of extratropical cyclones caused by changes in anthropogenic sulphur emissions between the 1960s and the 1990s?
- How do aerosols affect the distribution and intensity of cyclones in the future?
- Do aerosols change the track of an individual cyclone?

The structure of the thesis is as follows. Chapter 2 introduces the data sets and methods that this work uses. Chapter 3 investigates changes in cyclone activity between the 1960s and the 1990s. Chapter 4 studies the influence of the direct sulphate aerosol effect on cyclones in a future climate. Chapter 5 represents a case study evaluating the influence of aerosols on an individual cyclone. Finally, Chapter 6 provides conclusions and an outlook for future research.

Table 1.2: Summary of previous modelling studies of future cyclonic activity. Extended from Geng & Sugi (2003). For abbreviations see Appendix B. "Total cyclone" refers to changes in the total number of cyclones with climate change, "strong cyclone" to changes in the number of strong or intense cyclones.

									Impact of global warming	
Author(s)	Model	Horizontal resolution	Sampling time interval [h]	Integration type	Analysis period [yr]	Tracking done?	Area	Season	Total cyclone	Strong cyclone	Position shift
König et al. (1993)	ECHAM2	T21	12	Transient	10	Yes	NH, SH	Seasonal	↓		NH: Atlantic northward, Pacific eastward
Lambert (1995)	CCC GCM	T32	24	Equilibrium	5	No	NH, SH	NH: DJF, SH: JJA	↓	↑	No shift
Carnell et al. (1996)	UKMO AOGCM	2.5° × 3.75°	24	Transient	10	Yes	NH	DJF	Slight ↑	↑	Northward shift of storm source regions
Beersma et al. (1997)	ECHAM3	T106	12	Time Slice	5	No	NA	DJF	↓	↓, but ↑ in North Sea and Bay of Biscay areas	
Zhang & Wang (1997)	NCAR CCM1	R15	12	Equilibrium	10	No	NH	DJF	↓		
Carnell & Senior (1998)	HadCM2	2.5° × 3.75°	24	Transient	4 × 30	Yes	NH	DJF	↓	↑	No shift
Schubert et al. (1998)	ECHAM3	T42	12	Time slice	10	Yes	NA	DJF			Northeastward
Sinclair & Watterson (1999)	CSIRO9 Mark2	R21	8	Equilibrium	30	Yes	NH, SH	Annual		↓	No shift
Knippertz et al. (2000)	ECHAM4/ OPYC3	T42	12	Transient	50	No	NA	DJF	Negligible changes	↑	Northeastward
Lionello et al. (2002)	ECHAM4	T106	6	Time slice	30	Yes	Med	Annual	↓	↑	
Fyfe (2003)	CCCma CGCM1	T32	24	Transient	1900–2100	No	SH	Decadal			Poleward
Geng & Sugi (2003)	JMA8911	T106	6	Time slice	20	Yes	NH, SH	DJF	↓	↑	Poleward and eastward
								JJA			
Lambert (2004)	CCCma CGCM1 & CGCM2	T32	12	Transient	10	No	NH, SH	NH: 15/11-15/02, SH: 15/05-15/08	↓	↑	
Leckebusch & Ulbrich (2004)	HadCM3	2.5° × 3.75°	24	Transient	30	Yes	NA	ONDFJM	↓	↑ between 55° and 60°N, ↓ further north	No shift
Lozano et al. (2004)	ECHAM4	T106	6	Time slice	30	Yes	NA	Seasonal			Downstream

Table 1.2: Continued from previous page.

Author(s)	Model	Horizontal resolution	Sampling time interval [h]	Integration type	Analysis period [yr]	Tracking done?	Area	Season	Impact of global warming: Total cyclone	Impact of global warming: Strong cyclone	Impact of global warming: Position shift
Wang et al. (2004)	CCCma CGCM2	T32	6	Transient	20	Yes	NH, SH	Seasonal	↓	↑ in Northern Europe in OND, JFM, AMJ, ↓ in JAS	Winter: northward shift of intense events
Muskulus & Jacob (2005)	REMO	0.5°	1	Transient	35	Yes	Med	DJF, JJA	↑	↓ in Northern Europe in OND, JFM, AMJ	
Bengtsson et al. (2006a)	ECHAM5/ MPIOM	T63	6	Transient	30	Yes	NH, SH	Seasonal	Minor ↓	No apparent change, some local ↑	DJF: poleward shift in both NH ocean basins
Lambert & Fyfe (2006)	IPCC AR4 models	Various	24	Transient	20	No	NH, SH	NH: 15/11-15/02, SH: 15/05-15/08	↓	↑	No obvious shift
Leckebusch et al. (2006)	HadAM3	2.5° × 3.75°	24	Transient	30	Yes	Europe	ONDJFM	↓	↑ over British Isles and adjacent NE Atlantic, ↓ over Iceland and Norwegian Sea	
	HadCM3	2.5° × 3.75°	24		30						
	ECHAM4/ OPYC3	T42	12		49				↓	↑ over Iceland and NE Scandinavia	
	ECHAM5/ MPIOM	T63	6		30				↓	↑ west of British Isles and central Europe, ↓ over Norwegian Sea	
Pinto et al. (2006)	ECHAM4/ OPYC3	T42	12	Transient	50	Yes	NH	ONDJFM			Poleward for cyclones deepening to < 990 hPa
Wile (2006)	GFDL-CM2.0	2.5° × 2°	24	Transient	20	Yes	NH	ONDJFM		No apparent change	
Löptien et al. (2007)	ECHAM5/ MPIOM	T63	6	Transient	20	Yes	NH	JFM	No apparent changes	No intensification of cyclones	Pacific: northeastward, Atlantic: no shift
								JAS			Pacific: southward, Atlantic: northward
Pinto et al. (2007)	ECHAM5/ MPIOM	T63	6	Transient	40	Yes	NH	ONDJFM	↓	↓ in Central North Atlantic & Central North Pacific, ↑ in West Europe	Poleward (downstream shift of storm track activity)

Chapter 2

Data, models and tools

In this chapter, the different data sources and models used for analyses in the thesis are presented. Furthermore, the analysis tools and techniques are introduced.

2.1 ECHAM4/OPYC3: an atmosphere-ocean general circulation model

The examination of the long-term response of cyclonic activity to increasing concentrations in greenhouse gases and the direct radiative effect of sulphate aerosols comprises one part of this PhD thesis. For this analysis, a set of transient climate change simulations conducted with the fully coupled AOGCM ECHAM4/OPYC3 of the Max Planck Institute for Meteorology (MPI Met) (Roeckner et al., 1999) is used. Below follows a description of the model.

The atmospheric component ECHAM4. The roots of the atmospheric component of the coupled model, ECHAM4 (Roeckner et al., 1996a), go back to the global ECMWF weather prediction model (Simmons et al., 1989), which was adapted to make it suitable for climate research at the MPI Met and the German Climate Computing Centre (Deutsches Klimarechenzentrum, DKRZ). The simulations are carried out using the standard 19-level hybrid sigma-pressure coordinate system, although the model allows other vertical discretisations. The pressure layers extend from the surface to the pressure level of 10 hPa (≈30 km). Horizontally, the spherical harmonics of the prognostic variables vorticity, divergence, logarithm of surface pressure and temperature are truncated at wavenumber 42 (T42). For the physical parametrisations, ECHAM4 uses a 128×64 longitude-latitude Gaussian grid with a horizontal resolution of ≈2.8° (≈310 km at the Equator). A semi-implicit time stepping scheme is used with time steps of 24 minutes for dynamics and physics and 2 hours for the radiation. The data are stored every 12 hours.

The advection of water vapour, cloud water and the chemical constituents, e.g., sulphate (SO_4^{2-}), dimethylsulphide (DMS) and sulphur dioxide (SO_2), is computed with a semi-Lagrangian scheme (Williamson & Rasch, 1994). The Monin-Obukhov similarity theory (Louis, 1979) provides the basis for

calculating the turbulent surface fluxes. A higher order closure scheme (Brinkop & Roeckner, 1995) is used to compute the turbulent transfer of momentum, heat, moisture, cloud water, sulphate aerosol and gaseous sulphur compounds within and above the planetary boundary layer.

Stably stratified flow over irregular terrain excites gravity waves which cause surface stress. This drag is parameterised according to Miller et al. (1989). The soil model comprises the budgets of heat and water in the soil, the snowpack over land and the heat budget of land ice. The local run-off scheme takes catchment characteristics and subgrid-scale variations of field capacity over inhomogeneous terrain into account. Land surface parameters such as background albedo, roughness length, vegetation type, leaf area index and soil parameters are taken from the global data set compiled by Claussen et al. (1994). This data set is consistent with the ecosystem complexes defined by Olson et al. (1983).

The model distinguishes between stratiform and convective clouds. The bulk mass flux concept of Tiedtke (1989) is the basis for the parameterisation of cumulus convection. The modifications of Nordeng (1994) concerning entrainment and the closure for deep convection are implemented in the ECHAM4 cumulus parameterisation as well. The stratiform cloud water content is calculated from the respective budget equation which includes sources and sinks due to phase changes, detrainment of convectively generated cloud water, and precipitation formation by coalescence of cloud droplets and gravitational settling of ice crystals (Roeckner, 1995). Fractional cloud cover in each grid cell is determined as a non-linear function of grid-mean relative humidity according to Sundqvist et al. (1989).

The solar forcing in the simulations follows both seasonal and diurnal cycles. The transfer of solar radiation is parameterized according to Fouquart & Bonnel (1980) while the transfer of longwave radiation follows the parameterisation of Morcrette et al. (1986). The modified radiation scheme additionally accounts for the influence of several greenhouse gases (carbon dioxide—CO_2, methane—CH_4, nitrous oxide—N_2O and industrial gases, such as certain chlorofluorocarbons—CFCs, hydrochlorofluorocarbons—HCFCs and hydrofluorocarbons—HFCs). Optionally, absorption by ozone (in the 14.6μm band) and various types of aerosols (Tanré et al., 1984) can be taken into account in the radiation scheme as well. The single scattering properties of cloud droplets and ice crystals, whose effective radii are parameterised in terms of liquid and ice water content (Roeckner, 1995), are derived from Mie theory and adjusted for use in the broad-band model (Rockel et al., 1991).

The tropospheric sulphur cycle in ECHAM4. In order to include the direct sulphate aerosol effect in the simulations, a model of the tropospheric sulphur cycle (Feichter et al., 1996, 1997) is incorporated into ECHAM4. It interactively calculates transport, dry and wet deposition as well as chemical interactions of the sulphuric constituents. Three sulphur species—the gaseous DMS and SO_2 as well as SO_4^{2-}, which predominantly exists in a dissolved state—are the prognostic variables. The advective transport of these species and their vertical exchange in the boundary layer as well as in convective clouds are treated

analogously to the transport of water vapour. The dry deposition flux to the ground is proportional to the respective concentration in the lowest model layer (≈30m) and a prescribed deposition velocity, which is constant for SO_4^{2-} and depends on the surface type (land, water, snow) for SO_2. Precipitation scavenging of both SO_2 and SO_4^{2-} is computed from the model's local precipitation formation rate (Giorgi & Chameides, 1986). The gaseous species DMS and SO_2 react with hydroxyl radicals ($OH\cdot$) by day. By night, DMS reacts with nitrate radicals ($NO_3\cdot$). In the model, SO_2 is the only end product of the DMS oxidisation. SO_2 dissolves in cloud water according to Henry's law. Oxidants for SO_2 in the aqueous phase are hydrogen peroxide (H_2O_2) and ozone (O_3). The concentrations of these oxidants are prescribed as three-dimensional monthly means from calculations of ECHAM4 coupled to a more comprehensive chemistry model (Roelofs & Lelieveld, 1995). The concentrations of SO_4^{2-} are calculated from the oxidisation of SO_2 in the gaseous and aqueous phases and serve as input for the calculation of the radiative aerosol forcing.

The oceanic component OPYC3. The 11-layer OPYC3 is an extended version of the model introduced by Oberhuber (1993). Poleward of 36°, the employed Arakawa B-grid coincides with the T42 Gaussian grid. Equatorward of 36°, the meridional grid spacing is gradually decreased to 0.5° to resolve the equatorial waveguide.

There are three model subdomains: the interior ocean, the surface mixed layer and sea ice. In the interior ocean, the model solves the primitive equations in the form of conservation laws for momentum, mass, heat and salt on isopycnal layers. Together with the variable sea level, these quantities constitute the prognostic variables. For momentum, the horizontal mixing depends on the local Rossby deformation radius. For temperature and salinity, the horizontal diffusion depends on the local deformation of the flow field. The concept of entrainment/detrainment with budget calculations for turbulent and mean potential energy is applied for vertical mixing. The employed convective adjustment instantaneously removes vertical instabilities.

The mixed layer is required since the concept of isopycnal coordinates does not hold near the surface when strong turbulence is present. In this model domain, the same governing equations as in the interior ocean are solved, but with a detailed calculation of turbulent entrainment and detrainment based on the turbulent kinetic energy input, which is a function of wind stirring, buoyancy flux due to heat and freshwater, and local shear.

Sea ice and snow cover are predicted in the form of ice momentum, ice concentration and grid-cell averaged thicknesses of ice and snow. The employed equation of motion neglects momentum advection and uses a viscous-plastic rheology parameterisation for the stress term (Hibler, 1979).

The coupling of ECHAM4 and OPYC3. The atmospheric and oceanic model components are coupled quasi-synchronously. Once a day, ECHAM4 receives the daily-averaged sea surface temperature and scalar sea-ice variables without any adjustment. OPYC3 receives daily-averaged surface fluxes of downward solar radiation, river discharge and wind stress without adjustment. In the case of the daily-averaged heat and freshwater fluxes, however, a flux adjustment is applied. The flux adjustment reflects the difference of flux delivered by ECHAM4 and flux requested by OPYC3 in the long-term annual mean and is estimated from a 100-yr coupled model spinup. Roeckner et al. (1996b) give details on the coupled model.

2.2 ECHAM5-HAM and MPIOM-HAMOCC5: the next model generation

Results of model simulations performed with the subsequent version of the atmospheric model component, ECHAM5, as well as with the subsequent coupled AOGCM are also used in this study. The version of the coupled AOGCM consists of the atmospheric model ECHAM5 (Roeckner et al., 2003), which includes a microphysical aerosol module (HAM—Hamburg Aerosol Model; Stier et al., 2005), and the oceanic model MPIOM (MPI Ocean Model; Marsland et al., 2003) with an embedded marine biogeochemistry model (HAMOCC5—HAMburg Ocean Carbon Cycle Model; Maier-Reimer et al., 2005). The coupled ECHAM5-HAM/MPIOM-HAMOCC5 system constitutes the major part of the emerging MPI Earth System Model (MPI-ESM) and is evaluated in Kloster et al. (2006).

The atmospheric component ECHAM5. ECHAM4 and ECHAM5 differ in a variety of aspects. ECHAM5 contains a new semi-Lagrangian transport scheme for the advection of water vapour, cloud water and chemical tracers (Lin & Rood, 1996). The new cloud scheme (Lohmann & Roeckner, 1996) separates between cloud water and cloud ice in the prognostic equations and introduces new parameterisations for cloud microphysical processes. In the model versions employed in this study, no changes were made to the calculation of cloud cover compared to ECHAM4. The solar radiation code is changed by adding 2 spectral bands. The longwave radiation code used in ECHAM4 is replaced by the Rapid Radiation Transfer Model (RRTM; Mlawer et al., 1997). Further changes concern the treatment of subgrid-scale orographic effects (Lott & Miller, 1997; Lott, 1999), the representation of land surface processes and the introduction of a new land surface data set (Hagemann, 2002). Furthermore, ECHAM5 can perform nudged simulations in which the prognostic variables are relaxed towards an atmospheric reference state provided, for example, by reanalysis data. This capability is exploited in Chapter 5 to set up an ensemble of simulations for a case study experiment.

The standard resolution of ECHAM5 is 31 vertical levels on a hybrid sigma-pressure coordinate sys-

tem. The pressure layers extend from the surface to a pressure level of 10 hPa. The horizontal resolution is T63 in spectral space. Physical processes and nonlinear terms are calculated on a Gaussian grid with a nominal resolution of 1.8° (≈200 km at the Equator). The integration time step of the semi-implicit scheme used in the simulations is 15 minutes.

The aerosol module HAM. In order to account for the radiative impact of aerosols, the complex microphysical aerosol module HAM, described in detail in Stier et al. (2005), is interactively coupled to ECHAM5. HAM predicts the evolution of an ensemble of seven superpositioned aerosol modes which are represented by log-normal distributions and cover the major global aerosol compounds—sulphate, black carbon, particulate organic mass, sea salt and mineral dust. Four geometrical size classes are considered: the nucleation mode (particle radius $\overline{r} \leq 0.005\mu\mathrm{m}$), the Aitken mode ($0.005\mu\mathrm{m} < \overline{r} \leq 0.05\mu\mathrm{m}$), the accumulation mode ($0.05\mu\mathrm{m} < \overline{r} \leq 0.5\mu\mathrm{m}$) and the coarse mode ($0.5\mu\mathrm{m} < \overline{r}$). The nucleation mode only contains one soluble compound, sulphate, while the other size modes contain both soluble and insoluble compounds. The aerosol compounds can be internally and externally mixed. The main components of HAM are its microphysical core M7 (Vignati et al., 2004), an emission module, the sulphur chemistry scheme of Feichter et al. (1996), a deposition module and a module which calculates the aerosol radiative properties. The sulphur chemistry scheme is described in Section 2.1, the other components are described below.

The microphysical processes calculated by the M7 module are the coagulation among the modes, the condensation of gas-phase sulphuric acid onto the aerosol surface, the binary nucleation of sulphate, and the water uptake. Each mode is represented by the three moments aerosol number, number mean radius and standard mean radius. The integration of the aerosol dynamics equation yields updated aerosol numbers and the transfer between the modes.

The emission module assumes that all but the sulphur compounds are emitted as particulate matter, i.e. that they are primary emissions. Dust emissions depend on the ECHAM5 10m wind speed, soil moisture and snow cover and are calculated interactively according to Tegen et al. (2002). Sea salt emissions are also calculated interactively, as a function of the 10m wind speed and the sea ice cover (Schulz et al., 2004). The emissions of DMS are derived from the simulated DMS seawater concentrations of the HAMOCC5 ocean biogeochemistry. For the remaining aerosol compounds, emission strengths, emission size distribution and emission height are prescribed from an emission inventory, e.g., the AeroCom emission inventory (Dentener et al., 2006). Anthropogenic emission sources are industry, fuel use and biomass burning; natural emission sources are volcanoes.

The aerosol sink processes wet deposition, dry deposition and sedimentation are calculated online as functions of aerosol size distribution, composition and mixing state in conjunction with the model meteorology. Aerosol size distribution, composition and mixing state also determine the aerosol radiative

properties whose calculation is based on Mie theory. These radiative properties serve as input for the ECHAM5 radiation scheme. Only the effects of aerosols on the shortwave part of the spectrum are considered.

Indirect aerosol effects, i.e. the cloud albedo and the cloud lifetime effects, are accounted for in the extended stratiform cloud scheme. This scheme introduces a prognostic equation for the cloud droplet number concentration (CDNC; Lohmann et al., 1999). The nucleation of cloud droplets is parameterised semi-empirically in terms of the aerosol number size distribution and vertical velocity (Lin & Leaitch, 1997). On the subgrid scale, vertical velocity is derived from the turbulent kinetic energy (Lohmann & Kärcher, 2002). Sink processes are treated analogously to those formulated in ECHAM5 for the in-cloud liquid water content. The cloud optical properties depend on the droplet effective radius, which in turn is a function of the in-cloud liquid water content and CDNC. These parameters govern the auto-conversion rate which is calculated according to Khairoutdinov & Kogan (2000).

The oceanic component MPIOM. MPIOM evolved from the Hamburg Ocean Primitive Equation model (HOPE; Wolff et al., 1997). It employs a curvilinear orthogonal C-grid (Arakawa & Lamb, 1977) with a horizontal resolution of 1.5° and a z-coordinate system in the vertical. The poles of the grid are located over Greenland and inland of the Wedell Sea, although the grid allows for their arbitrary placement. MPIOM is based on the primitive equations for a Boussinesq-fluid on a rotating sphere with a free surface. Subgrid-scale processes such as isopycnal diffusion, horizontal tracer mixing by advection with unresolved eddies, vertical eddy mixing, near-surface wind stirring, convective overturning and slope convection are parameterised. The embedded sea ice model calculates the concentration and thickness of sea ice accounting for snow accumulation on the ice, snow to ice transformation and ice melting. Its dynamics are formulated using the same viscous-plastic rheology as in OPYC3. Also embedded in MPIOM is the marine biogeochemistry model HAMOCC5 which interactively simulates biological and biogeochemical tracers in the oceanic water column and the sediment. Its ecosystem model is of the NPZD type (nutrients, phytoplankton, zooplankton and detritus; Six & Maier-Reimer, 1996). Furthermore, the model accounts for several new elements—nitrogen, dissolved iron and dust—and incorporates new processes such as denitrification and nitrogen-fixation, formation of calcium carbonate and opaline shells, DMS production and consumption processes, dissolved iron uptake and release by biogenic particles as well as dust deposition and sinking. Iron fertilisation of the ocean occurs by dust deposition as calculated by HAM under the assumption of a dust iron content of 3.5%. DMS production depends on the degradation of phytoplankton by senescence and grazing processes. DMS sinks are bacterial consumption, chemical oxidation and flux to the atmosphere. The latter is passed as emission flux to HAM.

The coupling of ECHAM5-HAM and MPIOM-HAMOCC5. The Ocean-Atmosphere-Sea Ice-Soil (OASIS) coupler (Valcke et al., 2003) performs the coupling of the atmospheric and oceanic components of the AOGCM. The atmosphere receives sea surface temperature, sea ice concentration, sea ice thickness, snow depth on ice, and the ocean surface velocities from the ocean. With these values as boundary condition, the atmosphere model accumulates the forcing fluxes during the coupling time step of one day. Flux adjustment is not required.

2.3 The nudging technique in ECHAM5

In principle, an atmospheric GCM simulates the atmospheric variability on all time scales. Due to the strong nonlinear behaviour of the atmosphere, a single transient model simulation performed with such an atmospheric model represents only one realisation of the possible atmospheric development over a certain period of time. Hence, the state of the model atmosphere for a specific day in a specific year does not correspond to the state of the real atmosphere and cannot be directly compared to observations. Instead, only the statistical behaviour of model data and observational data can be compared. To compare model output with observations for short periods of time, an adjustment of the large-scale component of the modelled circulation toward meteorological analyses is needed (Jeuken et al., 1996). This can be achieved by "nudging" or Newtonian relaxation, which was introduced in the 1970s (e.g., Anthes, 1974) as a tool for four-dimensional data assimilation to insert asynoptic data, such as satellite and aircraft observations, into NWP systems. In climate modelling, nudging serves as a tool for model validation and for keeping the model close to the observed meteorology (Jeuken et al., 1996).

The nudging method relaxes the model state towards the observed data by adding a non-physical relaxation term to the model equations:

$$\frac{\partial X}{\partial t} = \underbrace{F_m(X)}_{\text{Model forcing}} + \underbrace{G(X) \times (X_{\text{obs}} - X)}_{\text{Relaxation}} \tag{2.1}$$

X represents any prognostic model variable. In the standard version of ECHAM5, nudging is implemented for surface pressure, divergence, vorticity or temperature and can easily be invoked. The forcing term, $F_m(X)$, represents the model forcing which describes the dynamical and physical processes governing the evolution of X. The relaxation term is the product of the relaxation coefficient G and the difference between the observational and the model-calculated value of X. G has the unit s^{-1} and is the inverse of the relaxation time τ which defines the strength of the nudging.

The choice of the relaxation time is crucial. If τ is chosen too large, though, the influence of the reference data set on the model will be negligible. If τ is chosen too small, noise and spinup problems will cause the model to deviate too far from its own balanced state which leads to artificial responses to

these unbalanced tendencies (Guldberg et al., 2005). Longer relaxation times substantially reduce these artificial responses while keeping the model close to the actual meteorology. The standard relaxation times and their corresponding nudging coefficients implemented in ECHAM5 following Guldberg et al. (2005) are given in Table 2.1.

Table 2.1: Standard nudging coefficients and relaxation times for different prognostic variables in ECHAM5

X	Relaxation time [h]	Nudging coefficient [10^{-5}s^{-1}]
log surface pressure	24	1.16
Divergence	48	0.579
Vorticity	6	4.63
Temperature	24	1.16

2.4 The ERA40 reanalysis data set

ERA40 (ECMWF re-analysis, Uppala et al., 2005) represents the latest reanalysis product of ECMWF and covers a period of 45 years (September 1957 to August 2002). It uses a three-dimensional variational (3D-Var) scheme for the assimilation of surface, upper air, and satellite observations and combines these disparate and inhomogeneous observations with a modified version of the NWP model operational at the ECMWF from June 2001 to January 2002. White (2003) provides a complete documentation of the used system.

When using ERA40 for a comparison with model data, it has to be taken into account that considerable changes in the observing system occurred during the reanalysis period. Increasing numbers of observations from aircraft, ocean-buoys and other surface platforms became available during the later years, but the number of radiosonde ascents declined starting in the late 1980s. Satellite observations are used from 1973 onward. Their amount substantially increases with time. Contrary to the approach used in previous re-analyses, in which satellite data are assimilated in the form of variables retrieved from the radiances, satellite data for temperature and humidity are predominately assimilated directly from the radiances measured in space in the ERA40 reanalysis. The changes in the observing system during the reanalysis period may be reflected in the diagnostics derived from ERA40. This is particularly relevant for the Southern Hemisphere, where analyses in the pre-satellite period depend much more on the assimilating GCM than on the observations themselves. However, due to better data coverage, the analyses in the Northern Hemisphere are much less affected by changes in the observing system and are considered consistent regarding the diagnostics employed in this thesis (Wang et al., 2006).

The ERA40 data are provided at the spectral resolution T106 resolution and temporal resolution of 6 hours by the DKRZ.

2.5 Synoptic weather charts

For the analysis of decadal changes in cyclone activity in the North Atlantic (Chapter 3), a manually derived time series of strong winter storms, i.e. cyclones with a core pressure of 950 hPa or less, is used for comparison (Franke, 1994). The time series starts in 1956 and is regularly updated (R. Franke, pers. comm.). The storms are identified and tracked in 3-hourly synoptic weather charts. They occur between September and April, although more than 90% occur during the extended winter season from November to March.

For the case study presented in Chapter 5, cyclone tracks of the year 2000 were constructed from three different sets of synoptic weather charts: the Berliner Wetterkarte (2000), the Wetterkarte of the DWD (2000, Deutscher Wetterdienst, German Meteorological Service) and the operational weather charts archived in the Deutsches Seewetteramt, Hamburg.

2.6 Cyclone tracking: TRACK

As mentioned in Section 1.4.2, Hodges (1994) adapts techniques associated with image processing and dynamical scene analysis for the tracking of characteristic features in meteorological data. TRACK has been tested for many different variables, not only cyclones. Hence, it is often referred to as a "feature tracking algorithm". Further developments of the algorithm include the extension to the unit sphere obviating its reliance on the projection of the field (Hodges, 1995), the inclusion of spherical nonparametric estimators to determine statistical diagnostic fields from ensembles of feature tracks (Hodges, 1996) and the introduction of adaptive constraints for feature tracking (Hodges, 1999a).

Cyclone identification. The first step in the identification algorithm consists of removing the spherical harmonics with wavenumber $n \leq 5$ from the original fields. This spatial filtering is in particular recommended for fields such as MSLP that are strongly influenced by large spatial scales and strong background flows (Hoskins & Hodges, 2002). While the filtering does not have a strong influence on the feature tracking in the 850 hPa relative vorticity field ($\xi_{850\,\mathrm{hPa}}$), it does ensure that the local minima or maxima to be tracked are not confounded by planetary wave factors (Anderson et al., 2003). To ensure that only synoptic-scale features are identified, the data are also truncated at wavenumber 42 (T42). This is in particular necessary for tracking $\xi_{850\,\mathrm{hPa}}$ features as these can also be associated with fronts in higher-resolution data. Additionally, the Hoskins filter (Sardeshmukh & Hoskins, 1984) tapers the spectral coefficients to diminish the Gibbs effect, which arises when applying Fourier series expansions

to functions with sharp gradients and causes unrealistic spectral ripples in the model orography over the oceans or flat land close to mountain ranges.

In a second step, the field is divided into objects and background by applying a threshold criterion. Only the objects, i.e. regions around extrema in the filtered field, are retained for further analysis which reduces the amount of data to be stored. All object points are partitioned into distinct sets by labelling connected points with the help of a quad tree data structure.

The third step involves the identification of features, i.e. minima or maxima in the field. Due to the relatively coarse resolution of T42, B-spline techniques of Dierckx (1981, 1984) are used to interpolate the data so that extrema can be located within the grid boxes. This method provides surface fits with continuity constraints so that the surface is periodic in longitude and continuous at the poles. Taking the grid point extrema as starting points, the off-grid position and field value of the local extremum, or feature point, are then found by means of a constrained conjugate gradient method (Goldfarb, 1969; Hodges, 1995).

Cyclone tracking. The tracking is based on the method of Sethi & Jain (1987) and Salari & Sethi (1990). Hodges (1995) extends this method for application on a spherical domain to overcome the problems caused by the unavoidable distortion errors that arise when using projections. At first, feature points in consecutive time frames are connected using a nearest neighbour search. The search region is constrained by the upper bound displacement distance, d_{max}. This constraint is relaxed over oceanic regions in order to capture extreme cases of exceptionally fast features. Incomplete tracks, i.e. those not lasting the full length of the time series, are padded out with phantom feature points to deal with the appearance and disappearance of features—cyclogenesis and cyclolysis in the case of cyclones—during the time series. The correspondence between the feature points in successive frames is then determined by minimising a cost function. This cost function is constructed from the local smoothness of the tracks and expresses their local deviations. The local smoothness—or path coherence—is a measure of the change of speed and direction of the features and is calculated from the position of the feature points over three consecutive time steps. It represents the weighted sum of the local deviation in direction and the local deviation in displacement distance (speed). There are two constraints on the cost function: the local smoothness of each track must be less than or equal to the upper bound track smoothness ϕ_{max} and the displacement distance between any two consecutive feature points, calculated using a geodesic norm to avoid projection-based biases, must be less than or equal to d_{max}. ϕ_{max} and d_{max} are applied adaptively (Hodges, 1999a). The cost to be minimized is then the sum of the local deviations over all the tracks in order to produce the smoothest possible set of tracks.

Once the tracks are computed, they can be filtered to retain only those tracks with a specific minimum lifetime and/or a specific minimum distance travelled. In this thesis, only cyclones that last longer than

2 days and travel more than 1000 km during their lifetime are considered.

With the help of spherical nonparametric estimators (Hodges, 1996), a set of statistical quantities such as track density, feature density, cyclogenesis density, cyclolysis density, speed and lifetime can be produced from the subset of tracks for further analysis. Since many feature points do not coincide with the gridpoints used in plotting the data (estimation points), each feature point is assigned a probability density function or kernel. Each feature point then contributes to the statistics at the estimation points, with those closest to the estimation points contributing the most.

2.7 Baroclinicity

Cyclonic activity is closely related to the baroclinic instability of the time-mean flow. Charney (1947) and Eady (1949) revealed the basic mechanism of large-scale instability of a geostrophically balanced baroclinic jet in their theoretical work. Lindzen & Farrell (1980) simplified the Eady-wave theory and provided a measure of baroclinic instability: the baroclinicity σ_{BI} as given by the e-folding time of the fastest growing Eady wave. It is proportional to the ratio of thermal wind to static stability:

$$\sigma_{\mathrm{BI}} = 0.31 \frac{|f|}{N} \left| \frac{\partial \vec{V}}{\partial z} \right| \tag{2.2}$$

where f is the Coriolis parameter, N the Brunt-Vaisala frequency, $\vec{V}$ the horizontal wind speed and z the vertical coordinate.

2.8 Non-parametric testing of statistical significance

Statistical tests are a common tool to determine whether averages derived from climatological data sets are significantly different from each other. The widely-used conventional Student's t-test, a parametric hypothesis test, requires that the data sets under consideration are statistically independent and that the data samples are normally distributed and the variances of the two populations can be considered equal. The first assumption is often violated in climatological applications since the data are serially correlated (von Storch & Zwiers, 2002).

The effect of serial correlation will not be addressed in the following. To avoid the parametric assumptions of normality and equal variances, though, a non-parametric significance test (Fischer-Bruns et al., 2007) is used in Chapter 4. In this chapter, differences between the 30-year averages from two transient climate simulations are discussed. The test is based on the null hypothesis that the difference $\Delta\bar{x} = \bar{x}_1 - \bar{x}_2$, where x is an arbitrary variable and the subscripts 1 and 2 denote the 30-year averages of two different simulations, does not exceed the range of differences between randomly chosen 30-year averages of the same variable in the undisturbed control simulation CTL. The testing procedure for prov-

ing statistical significance at the 95%-level, as used here, first determines m 30-year averages from the 300-year CTL simulation, i.e. $m = 10$. All averages are substracted from each other, so that a frequency distribution of $\frac{m \times (m-1)}{2} = 45$ differences is obtained. This frequency distribution is assumed to be an unbiased and robust estimation of the true frequency distribution. If $\Delta\bar{x}$ is larger than 95th percentile of the frequency distribution, the null hypothesis is rejected and $\Delta\bar{x}$ is taken to be significant at the 95% level.

Chapter 3

Decadal changes of cyclone track statistics over the North Atlantic

3.1 Introductory remarks

An intermediate step in studying the influence of aerosols on North Atlantic cyclones was to become familiar with the tracking algorithm and to evaluate the performance of the model to reproduce the major cyclone tracks. In order to achieve these goals, characteristics of the behaviour of cyclones were analysed in ERA40 and model data. Here, average characteristics of the extended winter season November to March for the period 1991–2000 are discussed and compared to the period 1961–1970. The year corresponds to January, i.e. the winter of 1991 covers the period November 1990 to March 1991. The two decades 1991–2000 and 1961–1970 were chosen because of their difference in aerosol emission strengths: in Europe and the United States a decrease in emissions was observed from the 1960s to the 1990s whereas emissions increased in South East Asia. The objective of the comparison is to isolate a possible aerosol signal in the cyclonic activity.

In addition to the cyclone characteristics, the NAO index is determined for the period 1961–2000. The index is also correlated to time series of deep cyclones (core pressure below 950 hPa at least once during the lifetime of the cyclone) derived from reanalysis, model and manually-analysed synoptic weather maps.

The model data are from an ECHAM5-HAM/MPIOM-HAMOCC5 simulation, henceforth designated as "E65". This simulation (Stier et al., 2006) is set up according to the standard procedure in coupled atmosphere-ocean climate simulations. A preindustrial control simulation serves as starting point for a transient simulation from the year 1860. The greenhouse gas forcing for the control simulation is based on the 1860 concentrations of the following gases: $[CO_2] = 286.2\,\mathrm{ppmv}$, $[CH_4] = 805.6\,\mathrm{ppbv}$, $[N_2O] = 276.7\,\mathrm{pptv}$, [CFC-11*] $= 12.5\,\mathrm{pptv}$. CFC-11* accounts for the radiative effect of minor

CFC species and includes a small contribution from natural sources. O_3 is prescribed monthly in latitude-height distributions (Kiehl et al., 1999). For the so-called "20th century integration" (1860–2000) the greenhouse gas concentrations are prescribed annually from direct observations and indirectly inferred from smoothed fits to ice core data. The optical depths of stratospheric aerosol due to volcanic eruptions are based on an updated data set of Sato et al. (1993) which is available online at http://www.giss.nasa.gov/data/strataer. Variations in solar irradiance are specified as suggested by Solanki & Krivova (2003). For the scenario time period (2001–2100), the emissions are based on the SRES A1B storyline (SRES: Special Report on Emission Scenarios; IPCC, 2000). A compilation of the Japanese National Institute for Environmental Studies (NIES) provides transient emission fluxes from 1860 to 2100 of SO_2 as well as black carbon (BC) from fossil fuel combustion, domestic fuel-wood consumption, agricultural waste burning, and forest fires. This compilation relies on data and scaling assumptions drawn from a variety of sources, in particular Lefohn et al. (1999) and the GEIA database (http://www.geiacenter.org), and is described in detail in Stier et al. (2006).

3.2 Results

3.2.1 Comparison of cyclonic parameters

In this section, the cyclonic parameters track density, genesis density, lysis density, mean intensity and mean lifetime are discussed. These parameters represent the following:

Track density. This statistic measures the number of tracks passing through a specified region in a certain time period. In this chapter, the extended winter season (November through March) comprises this time period. The specified region is scaled as a unit area equivalent to a 5° circle or about 10^6 km^2. Each track is counted only once in this region even though its corresponding cyclone may take more than one time step to travel through the region. In contrast to the track density, the *feature density* gives the number of occurrences of cyclones per season per 10^6 km^2 so that each cyclone occurrence contributes to this statistic. In particular, slow-moving cyclones may be counted repeatedly within any one region so that the feature density is biased towards these systems.

Genesis density. This statistic shows the locations at which features are first identified unless they coincide with the start of the data record.

Lysis density. This statistic is defined in analogy to the genesis density. It shows locations at which features appear for the last time unless they coincide with the end of the record.

Mean intensity. This is the average intensity of all the systems as they pass the estimation point. A

large number of weak systems hence produces a low value of this statistic.

Mean lifetime. This measure represents the average age that all the tracks passing through one region defined as above reach.

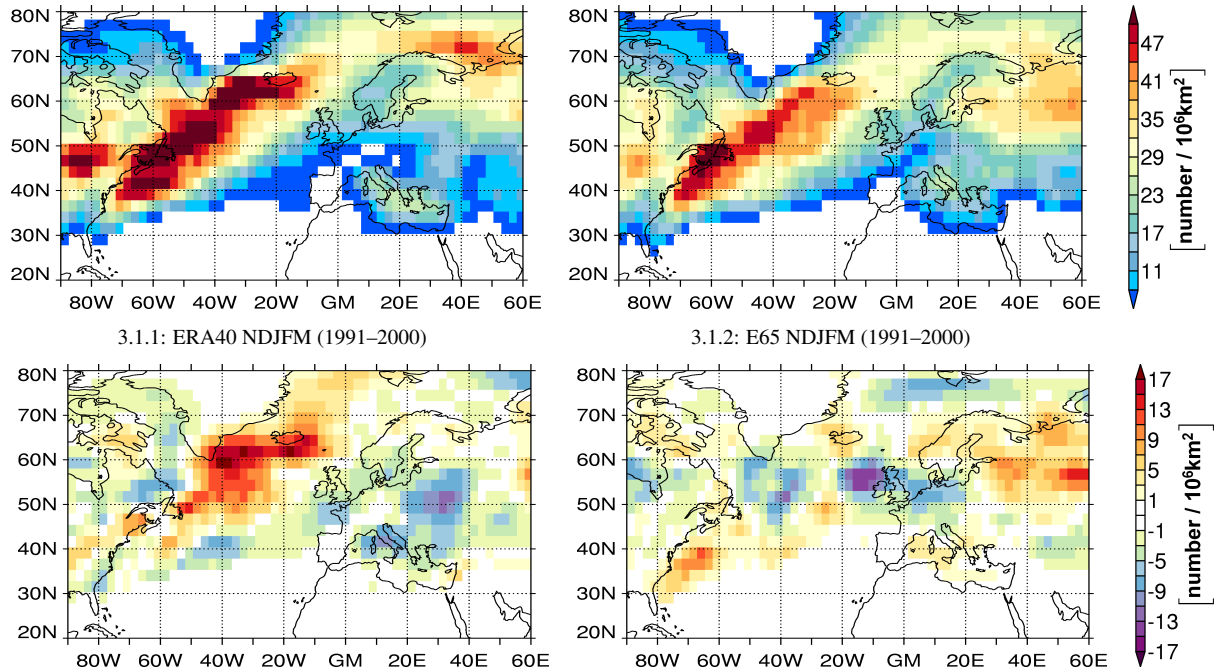

3.1.1: ERA40 NDJFM (1991–2000)

3.1.2: E65 NDJFM (1991–2000)

3.1.3: ERA40 NDJFM (1991–2000)–(1961–1970)

3.1.4: E65 NDJFM (1991–2000)–(1961–1970)

Figure 3.1: Track density in winter (Nov–Mar) [number of tracks per 10^6 km^2 per winter]. Top panels: 10-year average 1991–2000, bottom panels: difference in track density (1991–2000)–(1961–1970). Left column: ERA40, right column: model simulation E65. Areas with track densities below 5 are masked.

Fig. 3.1 shows the average track density in winter (November to March) for the period 1991–2000 and the difference between the two periods (1991–2000)–(1961–1970). Both ERA40 and E65 capture the regions of enhanced cyclonic activity in the North Atlantic and the Mediterranean. However, compared to ERA40, E65 underestimates the track density near the Great Lakes, southwest of Iceland and to the north/northeast of Scandinavia (Fig. 3.1.1 and 3.1.2). On the other hand, E65 has a higher track density over western Russia. This is caused by stronger lee cyclogenesis between Sweden and Finland and longer lifetimes—and hence longer tracks—of cyclones in that area when comparing to ERA40 (cf. Fig. 3.2.1 and 3.2.2 for cyclogenesis and Fig. 3.5.1 and 3.5.2 for lifetime). Altogether, about the same number of cyclone trajectories are detected in the 10 winters 1991–2000: 14477 in ERA40 and 14456 in E65.

The ERA40 track density pattern is very similar to the one shown by Hoskins & Hodges (2002) which was derived from the three-month period December to February of an extended ERA15 data set (1979–2000). A quantitative comparison with other studies (Sickmöller et al., 2000; Hanson et al., 2004; Bartholy et al., 2006; Benestad & Chen, 2006; Wernli & Schwierz, 2006; Löptien et al., 2007; Schneidereit et al., 2007) is only possible for feature density (not shown). This parameter shows a clear

maximum between Greenland and Iceland in all the studies as well as the current analysis, the Icelandic Low. Its location varies slightly from study to study, though. An explanation can be found in the varying analysis techniques as well as the different time periods chosen for the analyses. On the whole, the different analysis techniques produce comparable results.

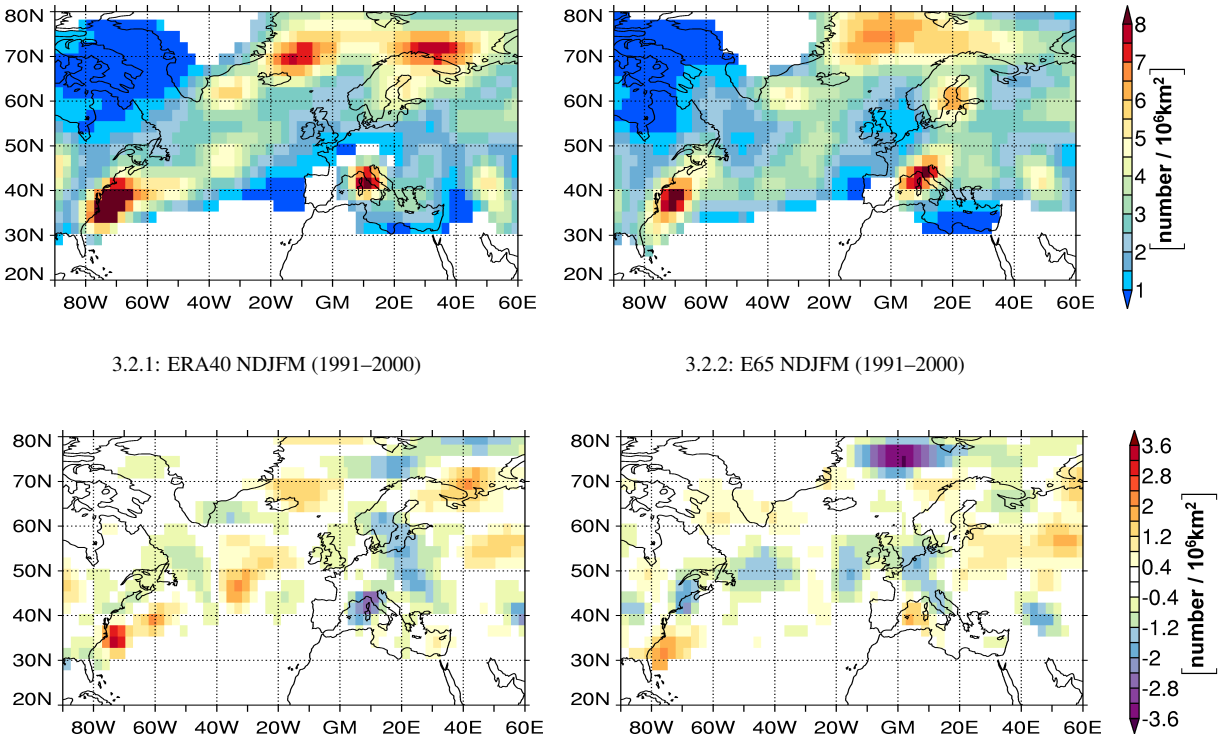

3.2.1: ERA40 NDJFM (1991–2000)

3.2.2: E65 NDJFM (1991–2000)

3.2.3: ERA40 NDJFM (1991–2000)–(1961–1970)

3.2.4: E65 NDJFM (1991–2000)–(1961–1970)

Figure 3.2: As Fig. 3.1, but for cyclogenesis density [number of genesis events per 10^6 km^2 per winter].

With regard to the changes in track density between the 1960s and the 1990s in ERA40 (Fig. 3.1.3), the track density increases in a band from Nova Scotia to the Greenland Sea and decreases to the southeast of that band and over Europe. This pattern indicates a systematic northwestward shift in track density in ERA40. In E65, the pattern of the change in track density is not as uniform as in ERA40 (Fig. 3.1.4). Here, decreases in track densities dominate in the North Atlantic from Newfoundland into western Europe while the track density increases over Scandinavia and western Russia and off the US east coast. This discrepancy manifests itself also in other aspects of cyclonic activity as will be shown below.

Track density is closely related to the densities of cyclogenesis and cyclolysis (Fig. 3.2 and 3.3). In ERA40, cyclogenesis regions are off the east coast of the United States between about 30° and 40°N, southwest and northeast of Iceland, north of Scandinavia and in a region centred over northern Italy (Fig. 3.2.1). E65 shows corresponding cyclogenesis maxima, though on a smaller order of magnitude (Fig. 3.2.2). This is particularly evident north of Iceland and Scandinavia. However, lee cyclogenesis

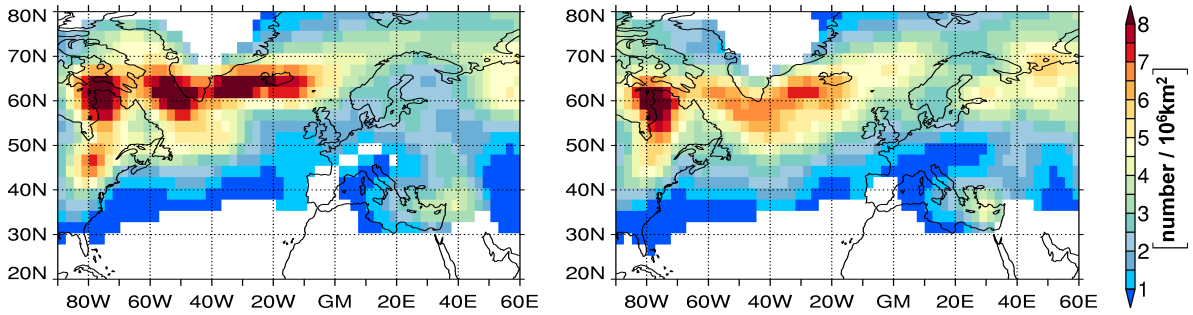

3.3.1: ERA40 NDJFM (1991–2000)

3.3.2: E65 NDJFM (1991–2000)

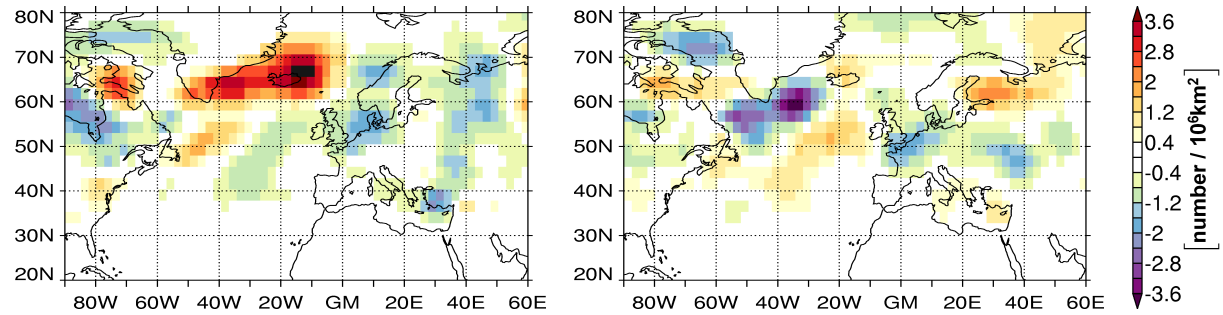

3.3.3: ERA40 NDJFM (1991–2000)–(1961–1970)

3.3.4: E65 NDJFM (1991–2000)–(1961–1970)

Figure 3.3: As Fig. 3.1, but for cyclolysis density [number of lysis events per 10^6 km^2 per winter].

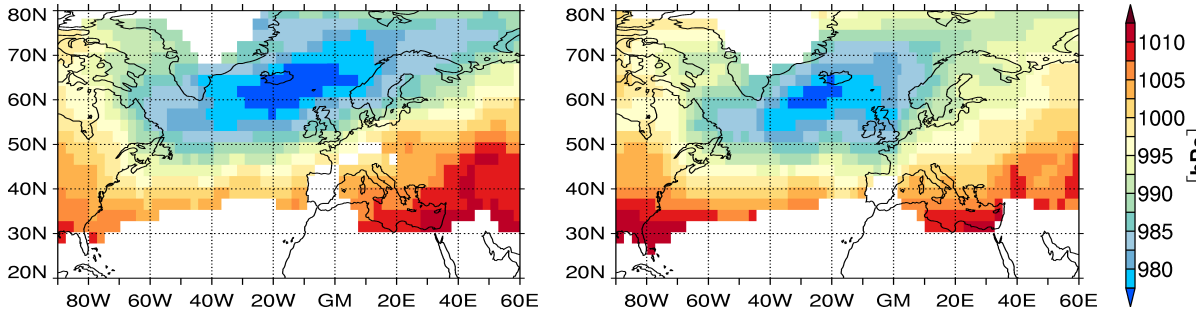

3.4.1: ERA40 NDJFM (1991–2000)

3.4.2: E65 NDJFM (1991–2000)

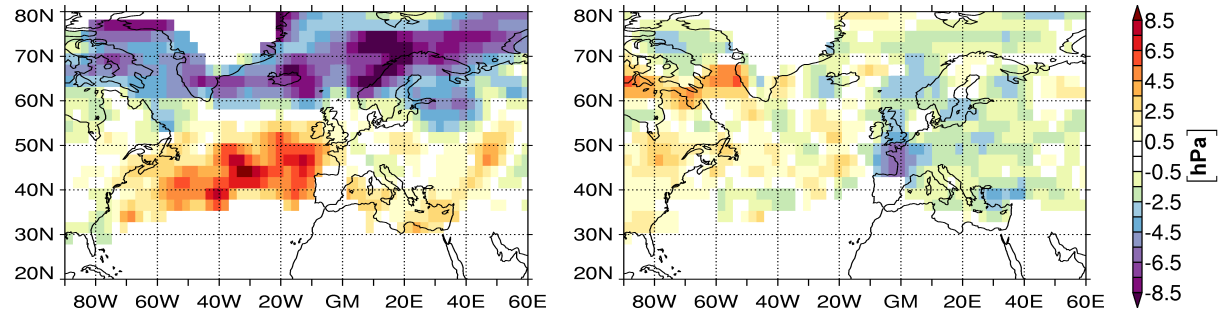

3.4.3: ERA40 NDJFM (1991–2000)–(1961–1970)

3.4.4: E65 NDJFM (1991–2000)–(1961–1970)

Figure 3.4: As Fig. 3.1, but for mean intensity [hPa].

east of the Scandinavian peninsula is enhanced in E65 compared to ERA40.

Cyclolysis occurs predominantly in the Baffin and Denmark Straits and over the Norwegian Sea. The cyclolysis maximum south of Baffin Island is the result of decaying cyclones from outside of the analysis region. Again, the magnitude of the E65 cyclolysis is reduced compared to ERA40, especially near southern Greenland.

The increase in cyclogenesis events near Cape Hatteras is not sufficient to explain the increases track density south of Greenland in ERA40 from 1961–1970 to 1991–2000 (Fig. 3.2.3). The explanation is found in the changes in cyclonic activity over the North American continent: decreased lysis density in an area centred over the Hudson Bay in conjuction with longer cyclone lifetimes in the northern Great Plains and extending from there to the east ensures that more cyclones originating in continental North America contribute to the track density increase south of Greenland (Fig. 3.1.3). For E65, the changes in track density are more closely linked to nearby changes in cyclogenesis and cyclolysis. For example, fewer cyclones are generated along the US east coast and east of Nova Scotia (Fig. 3.2.4). Combined with an increase in cyclolysis near Nova Scotia (Fig. 3.3.4), this leads to the reduction in track density seen south of Greenland in Fig. 3.1.4.

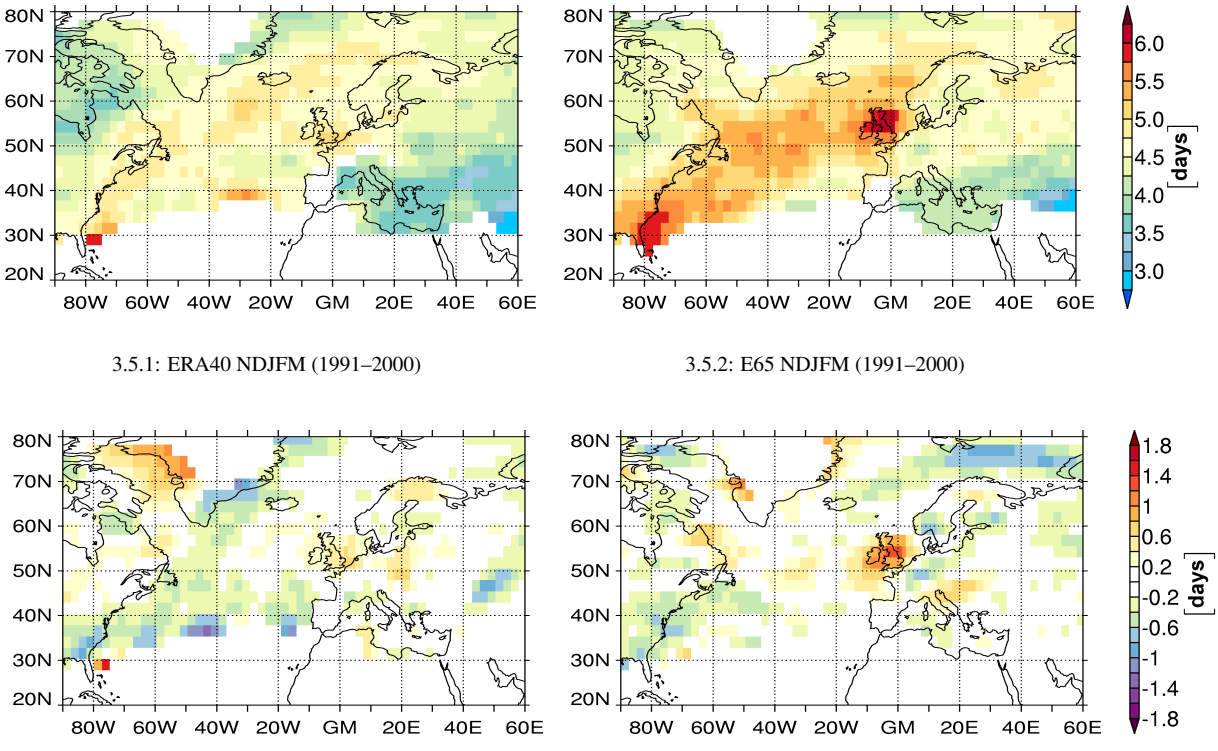

3.5.1: ERA40 NDJFM (1991–2000)

3.5.2: E65 NDJFM (1991–2000)

3.5.3: ERA40 NDJFM (1991–2000)–(1961–1970)

3.5.4: E65 NDJFM (1991–2000)–(1961–1970)

Figure 3.5: As Fig. 3.1, but for average lifetime [days].

To complement the picture of cyclonic activity and its changes from the 1960s to the 1990s, the mean cyclone intensity and lifetime are presented. The Icelandic Low is clearly discernible in both ERA40 and E65 (Fig. 3.4.1 and 3.4.2), but its extent is larger in the reanalysis. And while there is a widespread decrease in mean intensities north of about 60°N and an increase between about 40° and 50°N in ERA40 (Fig. 3.4.3), the changes in E65 are by far not as uniform (Fig. 3.4.4): the cyclones in the US became slightly weaker whereas the cyclones in western Europe gained strength. Over the North Atlantic, neither increases nor decreases dominate. This discrepancy between ERA40 and E65 has already been alluded to above. It is connected to the large-scale mode of circulation dominating the North Atlantic region, the North Atlantic Oscillation.

Average lifetimes of cyclones in the North Atlantic are 4.5 to 6 days in ERA40 (Fig. 3.5.1). In E65, maritime cyclones live about 0.5 to 1 day longer than their counterparts in ERA40 (Fig. 3.5.2). Over the continents, the mean lifetime is less than about 5 days in both ERA40 and E65. Again, continental cyclones in E65 exhibit longer lifetimes than in ERA40. Blender et al. (1997), Sinclair & Watterson (1999) and Hoskins & Hodges (2002) find comparable lifetimes for ECMWF data. Differences between the 1960s and 1990s are not uniform in either ERA40 or in E65. ERA40 seems to be dominated by a decrease in lifetime, especially in the western North Atlantic and west of Spain. In E65, cyclones are shorter-lived along the US east coast and north and west of Scandinavia while the British Isles experience the strongest increase in cyclone lifetime.

3.2.2 The North Atlantic Oscillation and its influence on deep cyclones

The cyclonic activity in the North Atlantic/European region is closely related to the recurring pressure anomaly pattern known as the North Atlantic Oscillation (NAO). It arises from the pressure see-saw between the Icelandic Low and the Azores High which tend to strengthen or weaken simultaneously (Walker, 1923). This see-saw is equivalent to a redistribution of amospheric mass between the Arctic and the subtropical Atlantic. The NAO is the dominant mode of atmospheric variability in this region and one of the most prominent patterns of atmospheric circulation variability. It is most pronounced during boreal winter and plays an important role in Europe where it controls numerous meteorological variables such as temperature, precipitation and surface wind speed (e.g., Hurrell et al., 2003). During a positive NAO phase (NAO+), the Icelandic Low is deeper and the Azores High stronger than normal and both tend to be located north of their average positions. The negative NAO phase (NAO−) is characterised by the opposite pattern of pressure anomalies. Both phases of the NAO are associated with basin-wide changes in the intensity and location of the North Atlantic jet stream and storm track, and in large-scale modulations of the normal patterns of zonal and meridional heat and moisture transport. These modulations result in changes in temperature and precipitation patterns often extending from eastern North America to western and central Europe: for strong positive NAO phases, enhanced westerly flow

results in above-average temperatures and precipitation in northern Europe whereas central and southern Europe tends to be cooler and drier than normal. For negative NAO phases, the mean surface westerlies are weaker and the Siberian High extends its influence westward with corresponding cold and dry winters in western and northern Europe. In southern Europe, winters are warmer and wetter than normal.

From gridded data, the NAO pattern is often determined by the empirical orthogonal function (EOF) analysis (e.g., von Storch & Zwiers, 2002). The EOFs are defined as the eigenvectors of the covariance matrix that is calculated from the time variations of the grid point values of MSLP for the North Atlantic/ European region (here: 20°–80°N, 80°W–60°E). The leading EOF describes the spatially coherent pattern maximising its variance. The principal component (PC) time series of this first EOF defines the NAO index as a measure of the difference in MSLP between the low pressure centre south of Iceland and the high pressure centre near the Azores. It thus gives an indication of the strength of the westerlies over the eastern North Atlantic over time.

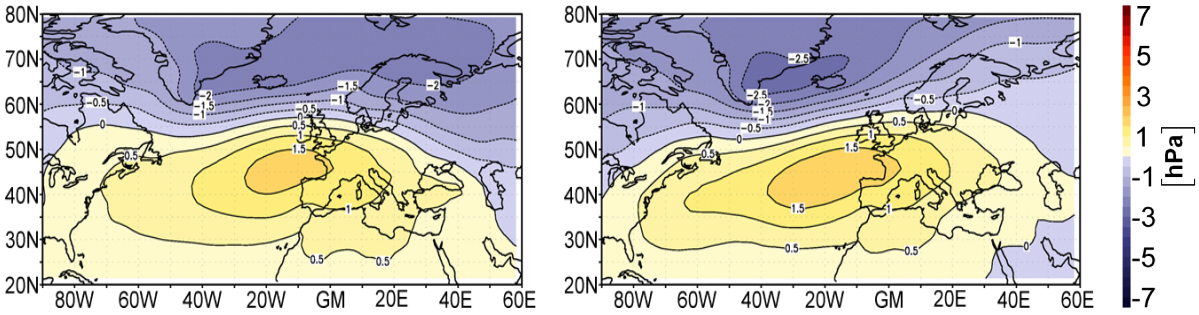

3.6.1: ERA40 NAO

3.6.2: E65 NAO

Figure 3.6: NAO (leading EOF) using monthly mean MSLP data for the winters (Nov–Mar) 1961–2000.

For both ERA40 and E65, the typical NAO pattern is derived from the EOF analysis of monthly mean MSLP data for the extended winters 1961–2000 (Fig. 3.6). It exhibits two distinct centres of action: (1) a negative maximum near Iceland and (2) a positive maximum between the Azores and the Bay of Biscaye. The characteristic features of the pattern are similar in both data sets. However, E65 exhibits a larger amplitude than ERA40 near Iceland. Furthermore, the positive maximum is of a larger spatial extent in E65 than in ERA40. The first EOF explains a large amount of the total variance (53.1%) in the ERA40 data; for the E65 data it explains 40.3% of the total variance.

The corresponding PC time series, i.e., the NAO indices, are shown in Fig. 3.7. The simulated NAO index exhibits a stronger interannual variability than the NAO index inferred from ERA40 which shows a strong variance on interdecadal time scales. For example, the NAO index is predominantly negative in ERA40 between 1977 and 1988 (Fig. 3.7.1), but alternates between positive and negative values almost every other year in E65 (Fig. 3.7.2). The predominantly positive NAO phase in the early 1990s in ERA40 is not captured by E65, either. This discrepant behaviour of the NAO in the 1960s and the

1990s in ERA40 and E65 explains the discrepancies seen earlier in the track densities and mean cyclone intensities in both data sets.

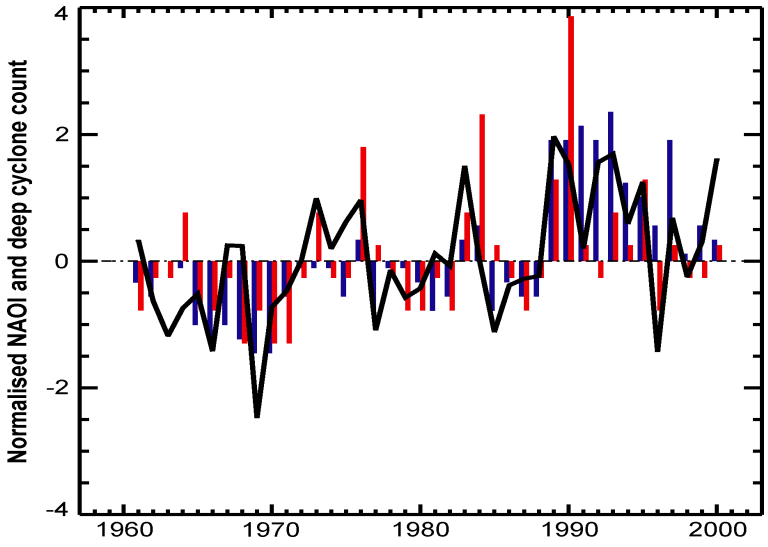

3.7.1: ERA40 NAO index

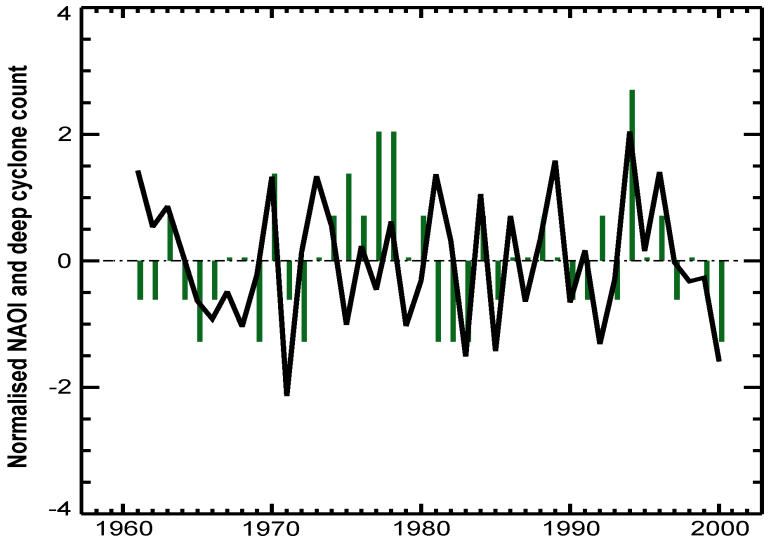

3.7.2: E65 NAO index

Figure 3.7: Comparison of NAO Index (NAOI) and normalised counts of very deep cyclones (core pressures < 950 hPa). Top panel: DWD cyclone count (blue), ERA40 cyclone count (red), ERA40 NAO index (black). Bottom panel: simulated (E65) cyclone count (green), simulated NAO index (black).

Fig. 3.7 also shows the normalised counts of very deep cyclones as derived from different data sets. Cyclones whose core pressure falls below 950 hPa at least once during their lifetime contribute to this count. One of the time series represents the normalised cyclone counts from manually-analysed synoptic weather charts of the DWD (Franke, 1994), it will henceforth be designated as DWD time series. On average, about 6.6 such storms occur in the extended winter season November to March in the DWD data. However, in two consecutive winters (1969, 1970) no such deep cyclone occurred. On the other hand,

the average number of deep cyclones was 15 for the winters 1989 to 1994. Several studies indicate that the strength and frequency of intense cyclones (Schinke, 1993; Stein & Hense, 1994) and waves (Carter & Draper, 1988; Bacon & Carter, 1991) were already enhanced in the years prior to this sequence of very stormy winters, even going back as far as the 1950s. Considering these occurrences together, and in particular their apparent long-term trend, an intense public debate ensued about whether the increased storminess was anthropogenic or natural in origin.

However, NAO-like atmospheric variability and the associated North Atlantic storm climate can occur also on decadal and possibly also on even longer time scales. Therefore, great care has to be taken when examining trends on time scales of about two or three decades only. When considering longer time series, though, changes in the observation process may introduce an artificial trend in the data. The introduction of proxies, especially within the EU project WASA (WASA, 1998), helped to address these issues. From the extensive data set containing station pressure values, which was compiled by the WASA group, Alexandersson et al. (1998) calculated geostrophic winds and used them to assess storminess in northwestern Europe. They showed that the increase in storm activity starting in the 1960s was actually the turning point for a decreasing trend in storm activity prior to that, at least since 1880. Thus, the enhanced storminess in the early 1990s can not unequivocally be attributed to human-induced climate change. The reduction in storm counts since the mid 1990s can be taken as further evidence that the enhanced storminess in the early 1990s is part of the natural variability.

When comparing the DWD time series to an objective time series derived from the cyclone tracking analyses of ERA40 and E65, one notices that significantly fewer deep cyclones occur in both of the data sets compared to the DWD time series: for the 40 winters 1961–2000, the DWD time series sums up to a total number of 266 strong cyclones while 102 of such events occur in the ERA40 data and 77 in E65.

The DWD deep cyclone counts are correlated to the ERA40 counts (correlation coefficient of 0.59), but not to the E65 counts. The correlation coefficient of the ERA40 NAO index and the ERA40 cyclone count is 0.53, while it is 0.69 for the correlation between the ERA40 NAO index and the DWD cyclone count. The E65 NAO index and the E65 cyclone count are not well correlated (correlation coefficient 0.33). All these correlation coefficients are statistically significant at the 95% level according to the Student's t-test.

3.3 Conclusions

The comparison of ERA40 and E65 shows that the general patterns of cyclone characteristics, for example track density and mean intensity, are reproduced in the GCM which gives confidence in the performance of both the GCM and the tracking algorithm.

The reduced number of very deep cyclones in ERA40 and E65 compared to the DWD data is related

to the horizontal resolution of the gridded data sets which is consistent with results of Haak & Ulbrich (1996). However, it must be kept in mind that the DWD time series is a manual, and hence subjective, analysis. The experience of the analysist plays a large role in deriving the time series, especially given the scarcity of synoptic data over oceanic regions at the beginning of the time series. Additionally, the threshold of 950 hPa is very restrictive and does not allow for a large sample. With a higher threshold value, more reliable statistics on the behaviour of deep cyclones can be determined due to the larger sample size.

The discrepancy of the NAO index between ERA40 and E65 can be attributed to the fact that E65 comprises only a single model simulation. A comparison of the wavelet spectrum of observations (Monthly Northern Hemisphere Sea-Level Pressure Grids, ds010.1 data set, available online at http://dss.ucar.edu/data sets/ds010.1) and ECHAM5 shows coherence between the observational and the model data, particularly on interdecadal time scales. Moreover, the NAO appears as the leading mode of climate varability in the North Atlantic region in both observations and ECHAM5 (W. Mueller, pers. comm.). Thus, it can be concluded with some confidence that the atmospheric circulation on interannual time scales is well represented by the model.

The changes in track density and mean cyclone intensities from the 1960s to the 1990s in ERA40 reflect the change from a predominantly negative to a predominantly positive NAO phase as shown by the ERA40 NAO index. Since E65 does not exhibit such an obvious change, the inconsistent change in track density and mean cyclone intensities between the two decades is reasonable.

There are no indications that the decrease in aerosol emissions from the 1960s to the 1990s, for which reason these two decades had been chosen, influences the large-scale circulation in the North Atlantic/European region on a decadal time scale.

Chapter 4

The influence of the direct sulphate aerosol effect on North Atlantic cyclones in a global climate change scenario

4.1 Introductory remarks

In order to explore the long-term response of cyclonic activity to increasing concentrations in greenhouse gases and the direct radiative effect of sulphate aerosols, a set of transient climate simulations (Roeckner et al., 1999) performed with the AOGCM ECHAM4/OPYC3 (Section 2.1) is analysed. The simulations are the 300-year control run "CTL" and the two transient experiments "GHG" (greenhouse gases) and "GSD" (greenhouse gases + sulphate direct; Table 4.1). This set of experiments is complemented by another simulation which accounts for the influences of greenhouse gases and O_3 as well as the direct and indirect sulphate aerosol effects ("GSDIO": greenhouse gases + sulphate direct + sulphate indirect + ozone). Unfortunately, the consideration of O_3 impedes the separation of greenhouse gas and aerosol effects. Therefore, this simulation is excluded from the analysis.

Table 4.1: List of experiments (from Roeckner et al. (1999)).

Experiment	Forcing	Years
CTL	1990 concentrations of CO_2, CH_4, N_2O	300a
GHG	Changing concentrations of CO_2, CH_4, N_2O, certain CFCs, HCFCs, HFCs	1860-2100
GSD	As in GHG plus sulphate aerosol (direct effect only)	1860-2050

For CTL, the atmospheric concentrations of CO_2, CH_4 and N_2O are kept constant at their 1990 values. The concentrations of O_3 and background aerosols are prescribed as climatological distributions

(Tanré et al., 1984). There are no industrial gases, such as CFCs and their replacements, and no sulphur cycle in this simulation. The CTL experiment represents climate conditions of 1990 as observations of that year were used for the ocean spin-up.

In both of the transient experiments the greenhouse gas concentrations are explicitly prescribed: from 1860 to 1990 as observed, and from 1990 onward according to the updated version of the IS92a emission scenario (IPCC, 1996) which assumes compliance with the London and Copenhagen Amendments to the Montreal Protocol for the industrial gases. Fig. 4.1 shows the assumed global emissions of CO_2, CH_4, N_2O and SO_2 between 2000 and 2100. In the GHG experiment only the greenhouse gas forcing is taken into account. The GSD experiment additionally accounts for the direct radiative effect of anthropogenic sulphate aerosol while neglecting the influence of natural biogenic and volcanic emissions.

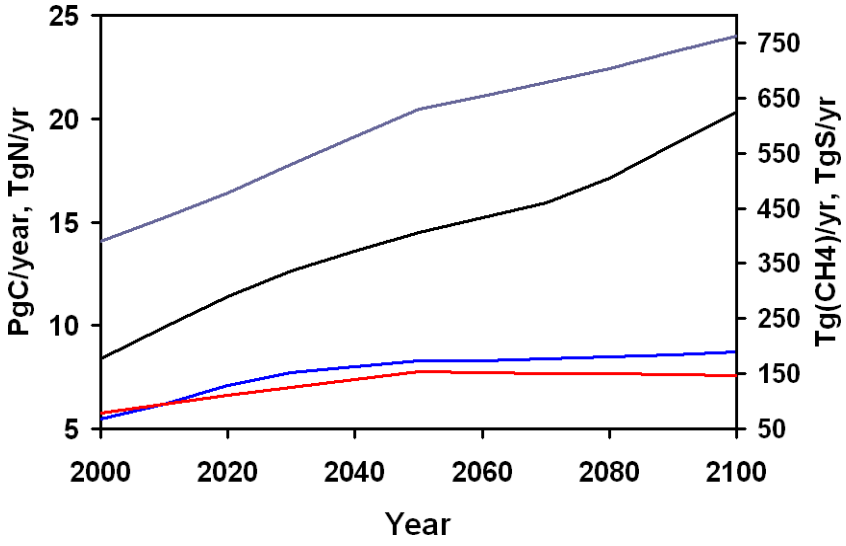

Figure 4.1: Emissions of CO_2 (PgC/yr, black, left axis), N_2O (TgN/yr, blue, left axis), CH_4 (Tg(CH_4)/yr, blue-grey, right axis) and SO_2 (TgS/y, red, right axis) from 2000 to 2100 according to the IS92a scenario (IPCC, 2001).

To determine the future influence of greenhouse gases and sulphate aerosol on the cyclonic activity in the North Atlantic region, differences between the seasonal averages of two 30-year periods ((2021–2050)−(1961–1990)) are considered. On the one hand, cyclonic activity has its maximum in winter. On the other hand, the direct aerosol effect is strongest in summer when the sun provides more energy for photochemical reactions and the sulphate yield from the oxidation of sulphur dioxide is high. Hence, winter (Dec–Feb) and summer (Jun–Aug) seasons are discussed. The winter year is defined as in Chapter 3, but without November and March. The future influence of greenhouse gases is quantified by studying the difference GHG(2021–2050)−GHG(1961–1990). The direct radiative sulphate aerosol effect is approximated by studying the difference between the GHG and GSD experiments: [GSD(2021–2050)−GSD(1961–1990)]−[GHG(2021–2050)−GHG(1961–1990)].

For the analyses, MSLP, temperature and wind speed fields are used. The temperature and wind speed fields at 600 hPa and 400 hPa serve to determine the baroclinicity σ_{BI} as defined by Equation 2.2.

4.2 Results

Similarly to Chapter 3, the statistics of cyclone parameters of ECHAM4/OPYC and ERA40 are compared. One example is given in Fig. 4.2. The tracking algorithm captures well the areas of enhanced cyclonic activity reported in the literature: a band expanding from the east coast of North America via Greenland and Iceland into the Norwegian and Barents Seas as well as a local maximum in the Mediterranean. The comparison of the winter cyclone activity reveals fewer cyclones in CTL in the region of the Great Lakes, in the Denmark Strait, to the west and north of Scandinavia and in the Mediterranean (Fig. 4.2.2 and 4.2.1). On the other hand, more cyclones than in ERA40 occur near the Black Sea and in the European part of Russia. In summer, the maximum in track density is located further north than in winter on the east coast of Newfoundland (Fig. 4.2.4 and 4.2.3). Furthermore, the area of high track density extends in a more zonal direction than in winter. Again, there are slightly fewer tracks detected in CTL than in ERA40. However, the overall agreement between CTL and ERA40, especially in the North Atlantic and Western Europe, gives confidence in the performance of the GCM and the tracking algorithm and in its applicability to investigate the influence of the direct sulphate effect on cyclonic activity in this region.

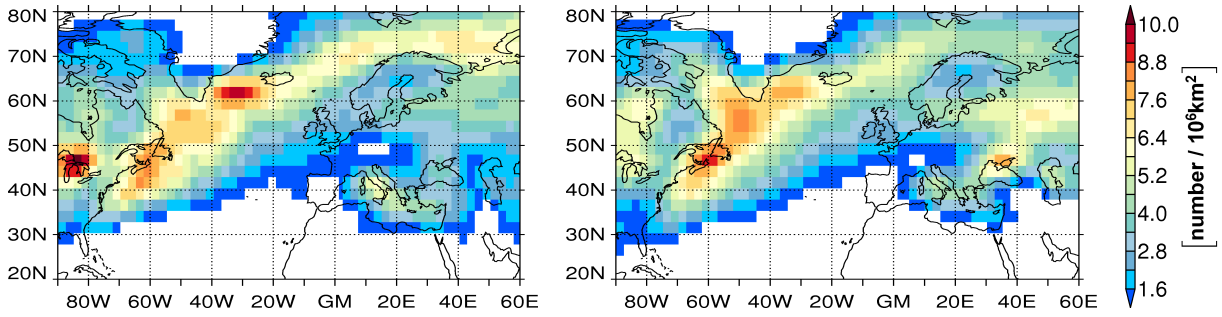

4.2.1: ERA40 DJF (averaged over 1961–1990)

4.2.2: CTL DJF (averaged over 300a)

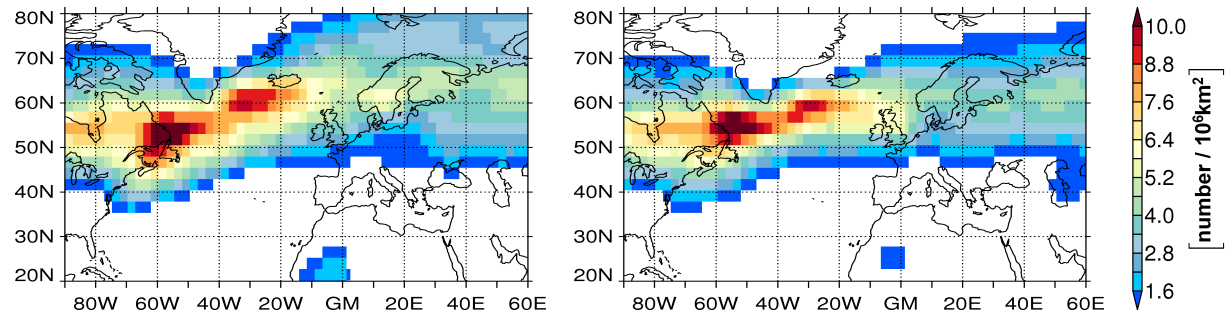

4.2.3: ERA40 JJA (averaged over 1961–1990)

4.2.4: CTL JJA (averaged over 300a)

Figure 4.2: Track density [number of tracks per 10^6 km^2 per month] for winter (DJF, top panels) and summer (JJA, bottom panels). Left column: ERA40 averaged over 1961–1990; right column: CTL averaged over 300 years. Track density suppression threshold is 0.5.

In the GSD experiment, the atmospheric burden of sulphate averaged over the North Atlantic/European

region steadily increases according to the IS92a "business-as-usual" scenario (Fig. 4.3). The increase is stronger in summer than in winter. Maps of the the sulphate burden (Fig. 4.4.1 and 4.4.2) for the period 1961–1990 reveal the highest burdens south of the Great Lakes in North America and in middle and central Europe in the vicinity of the source regions. Between 2021 and 2050 the burden increases in the whole region in winter, but in particular over the Gulf of Mexico and Saudi Arabia (Fig. 4.4.3). The pattern of the increase is similar in summer (Fig. 4.4.4) with one notable difference: the sulphate burden decreases over the Benelux countries and parts of Great Britain, Germany and Poland. The main regions of sulphate emissions shift southward in the IS92a scenario.

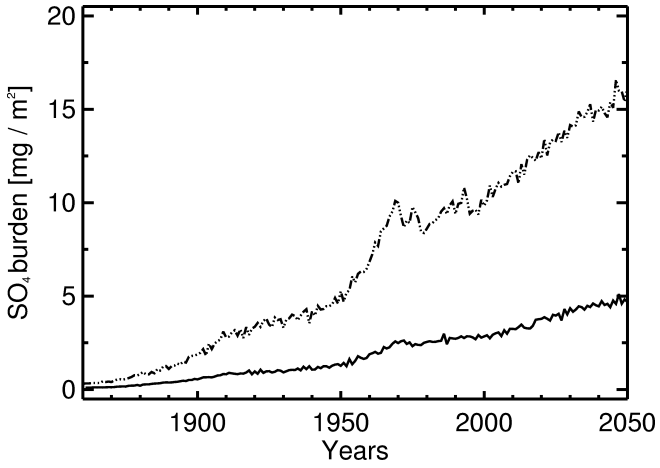

Figure 4.3: Sulphate burden in the GSD experiment for the North Atlantic/European region (20°–80°N, 90°W–60°E) for winter (DJF, solid line) and summer (JJA, dash-dotted line).

Fig. 4.5.1 and 4.5.2 show the surface temperature for winter and summer averaged over 30 seasons (1961–1990) for the GHG experiment. The warming effect of the thermohaline circulation is obvious from the positive sea surface temperature (SST) between Spitsbergen and Scandinavia whereas temperatures below the freezing point are prevalent at the same latitude in the Baffin Bay and northern Davis Strait (Fig. 4.5.1). In winter, the averaged meridional temperature gradient over the North Atlantic Ocean is stronger than in summer. The land-sea temperature difference is also larger. The mean winter and summer temperatures in GSD between 1961 and 1990 are similar to those in GHG (not shown).

The difference in winter surface temperature between 2021–2050 and 1961–1990 reveals that the warming is most pronounced over the continents north of 50°N and also in the oceanic polar regions where the sea ice recedes (Fig. 4.5.3). The weaker warming between southern Greenland and Iceland results from stronger vertical oceanic mixing in this area (P. Wetzel, pers. comm.). In summer, the polar warming is not as noticeable, though Greenland stands out as a hot spot (Fig. 4.5.4). The respective difference plots for GSD show patterns similar to Fig. 4.5.3 and 4.5.4. Hence, only the differences between GSD and GHG are presented in order to separate the direct radiative effect of sulphate aerosol. They depict a cooling over most of the domain consistent with the increasing sulphate burdens (Fig. 4.5.5

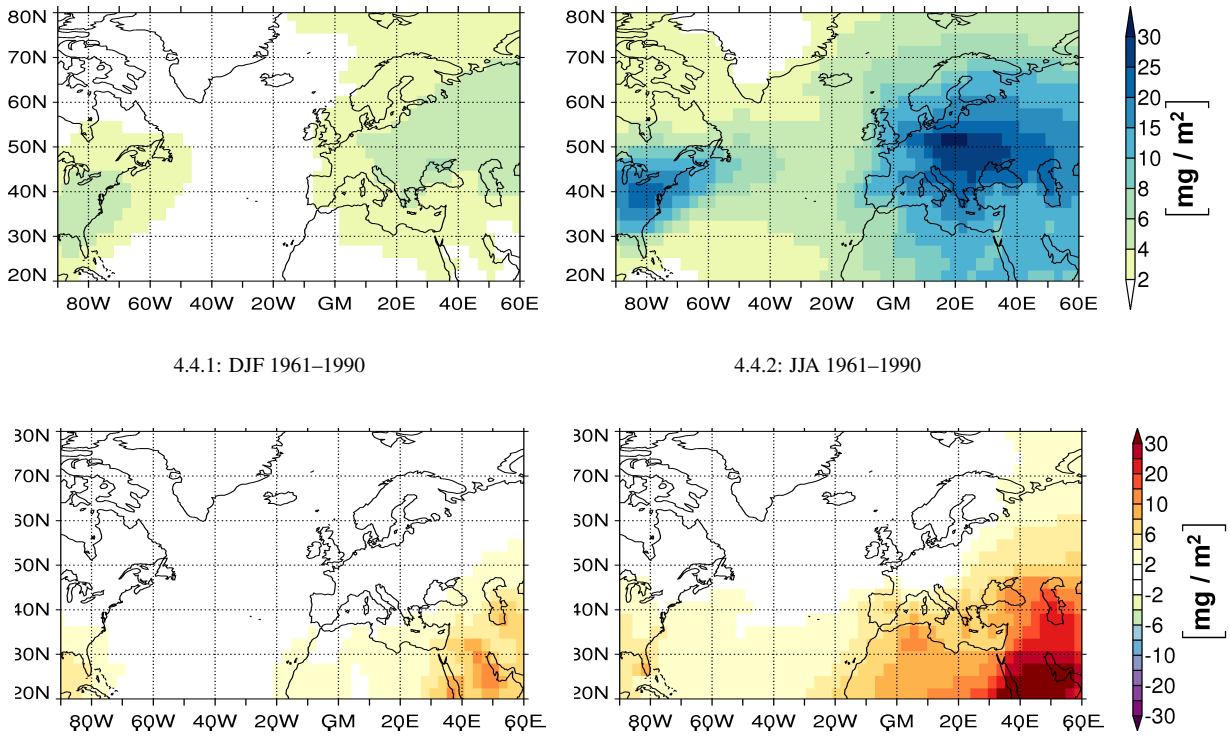

4.4.1: DJF 1961–1990

4.4.2: JJA 1961–1990

4.4.3: DJF (2021–2050)–(1961–1990)

4.4.4: JJA (2021–2050)–(1961–1990)

Figure 4.4: GSD sulphate burden. Top panels: averages over 1961–1990; bottom panels: difference between (2021–2050) and (1961–1990). Shown are winter (left column) and summer (right column)

and 4.5.6). The decrease in the sulphate burden centred over the Benelux countries has no discernible influence on the summer temperature changes. The results are statistically significant at the 95% level for most of the region.

Fig. 4.6 depicts the zonally averaged SST for the North Atlantic Ocean from the Equator to 60°N and from 80°W to the Greenwich Meridian for the two periods 1961–1990 and 2021–2050 as well as the difference between the periods. In the whole domain, the SST increases in both GHG and GSD. In summer, the strongest warming occurs at about 45°N. In winter, the largest differences in SST occur further poleward. The positive slope of the difference curve between the Equator and about 45°N in winter of the GHG simulation indicates that the mid-latitudes warm more than the tropics which is equivalent to a decrease in the meridional temperature gradient (∇_{m}SST) in 2021–2050 compared to 1961–1990. Accordingly, a negative slope corresponds to an increase in ∇_{m}SST. Poleward of about 50°N, the steep slope of the SST difference reflects the amplification of the warming caused by the sea-ice albedo feedback. In GSD, this feedback is not important south of 60°N. In summer, ∇_{m}SST decreases in both simulations from the Equator to about 45°N and increases towards the pole. The temperature difference in GSD is similar to that of GHG, but of smaller magnitude. To summarise, the sulphate aerosol weakens the decrease in ∇_{m}SST with increasing latitude.

The changes in ∇_{m}SST result in changes in the thermal wind, i.e. in the vertical shear of horizontal

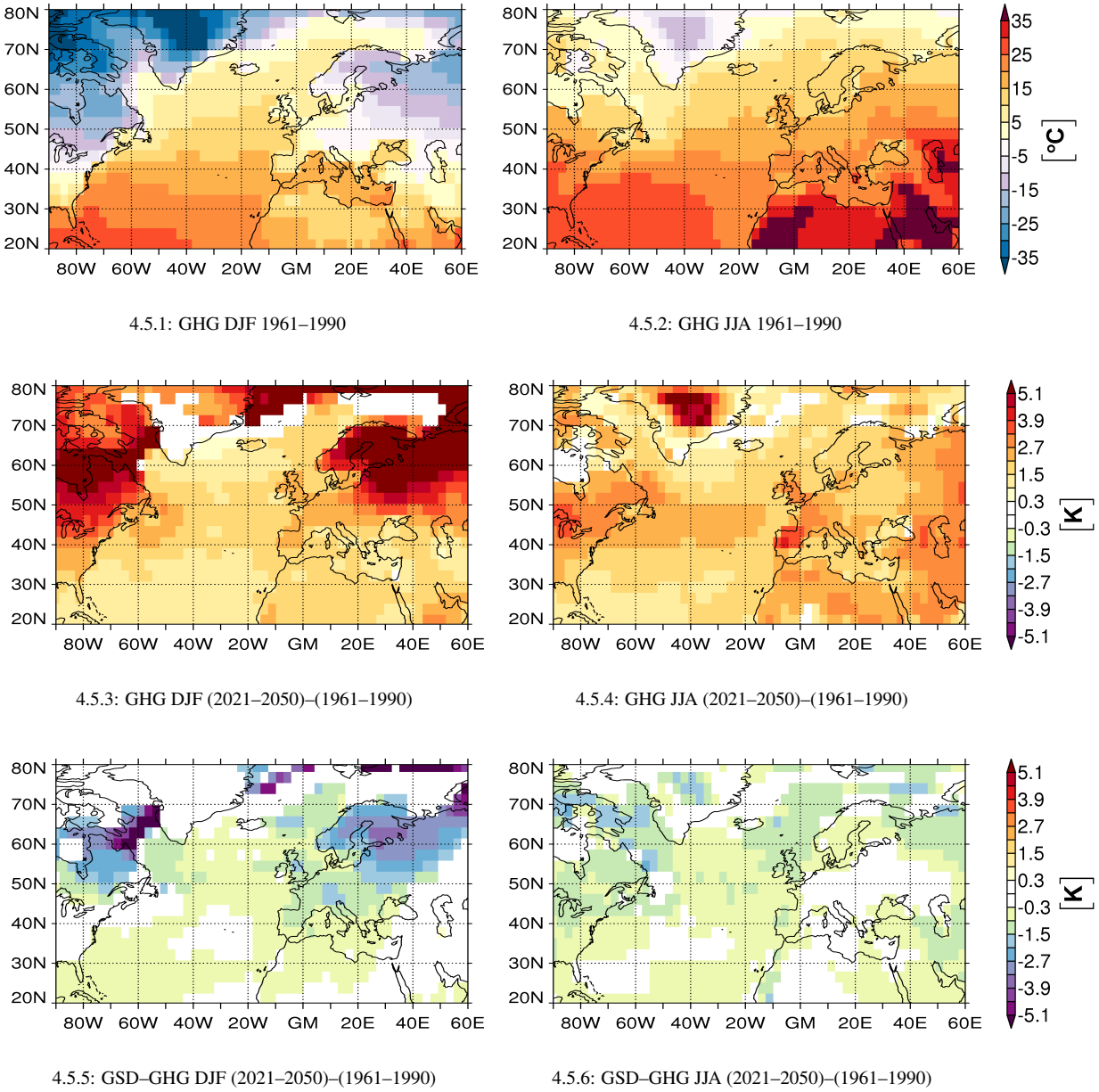

4.5.1: GHG DJF 1961–1990

4.5.2: GHG JJA 1961–1990

4.5.3: GHG DJF (2021–2050)–(1961–1990)

4.5.4: GHG JJA (2021–2050)–(1961–1990)

4.5.5: GSD–GHG DJF (2021–2050)–(1961–1990)

4.5.6: GSD–GHG JJA (2021–2050)–(1961–1990)

Figure 4.5: Surface temperature. Top panels: Averaged over 1961–1990; middle panels: difference between (2021–2050) and (1961–1990) for GHG; bottom panels: difference between (2021–2050) and (1961–1990) for GSD–GHG. Left column: winter (DJF), right column: summer (JJA). Areas where the difference is not statistically significant at the 95% level are masked white.

wind, which is, in turn, one of the factors influencing the baroclinicity σ_{BI}. Fig. 4.7.1 shows σ_{BI} between 600 hPa and 400 hPa averaged over 1961–1990 for GHG in winter. Regions of enhanced baroclinicity can be found off the American coast between ≈30°–50°N and then extending eastward to Western Europe. Over Africa and Saudi Arabia, the sub-tropical jet stream is apparent. In summer, the strongest baroclinic activity, whose magnitude is reduced by about a factor of 2 compared to winter, occurs further north extending from te Great Lakes to the Bay of Biscaye (Fig. 4.7.2). Over parts of Africa and Saudiarabia the windspeed decreases with height between 600 hPa and 400 hPa. Hence, σ_{BI} is negative there.

Fig. 4.7.3 and 4.7.4 depict the difference in baroclinicity between 2021–2050 and 1961–1990 for

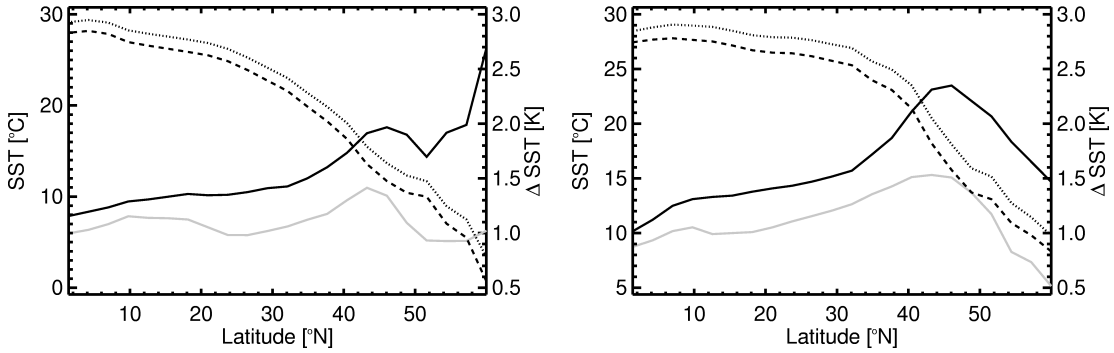

4.6.1: DJF 4.6.2: JJA

Figure 4.6: Zonally averaged SST in the North Atlantic Ocean (0–60°N and 80°W–0) for winter (4.6.1) and summer (4.6.2). Dotted line: GHG 2021-2050, dashed line: GHG 1961-1990 (left-hand y axis). Solid lines: difference between (2021–2050) and (1961–1990) for GHG (black) and GSD (grey) (right-hand y axis).

both seasons. Areas of decreasing baroclinicity, which also coincide to a large extent with the areas of statistically significant changes, dominate the pattern in winter. In summer, statistically significant decreases between 30°N and 40°N are accompanied by increased baroclinicity south of Iceland and extending via Scotland to southern Scandinavia in GHG in a warmer climate. The radiative aerosol effect has the opposite sign to the greenhouse gas effect over large areas, in particular over Europe and the Norwegian Sea in winter and the North Atlantic Ocean north of 40°N in summer (Fig. 4.7.5 and 4.7.6).

Baroclinicity denotes the tendency of the atmosphere to form cyclones. Changes in this quantity are therefore related to changes in cyclogenesis and hence to changes in track density. Baroclinicity maxima tend to occur upstream of maxima in track density as a comparison of Fig. 4.7.1 and 4.8.1 reveals for the east coast of North America. In winter (Fig. 4.8.1), the maximum track densities occur near Nova Scotia and Newfoundland, in the Davis Strait and in the Denmark Strait. The enhanced cyclonic activity north of the Black Sea is a model characteristic. The model overestimates track densities compared to ERA40. The summer track density is especially high east in the Labrador Sea and southwest of Iceland (Fig. 4.8.2). However, the systems are much shallower and slower compared to winter.

Fig. 4.8.3 shows the difference in track density between 2021–2050 and 1961–1990 for the GHG experiment in winter. A clear shift towards the north is discernible with decreasing track densities over the central and eastern North Atlantic and Europe and increasing track densities east of Greenland and north of 60°N. A significant decrease is also apparent along the American coast north of 35°N and over Baffin Island. The latter occurs in conjunction with increased lysis density over northwestern Canada and a decrease in cyclone lifetimes in that area (not shown). In summer, the GHG response is characterised by a marked decrease in cyclogenesis south of Labrador and a marked increase in the Denmark Strait (not shown). This signal is propagated downstream and results in a clear northward shift in track density

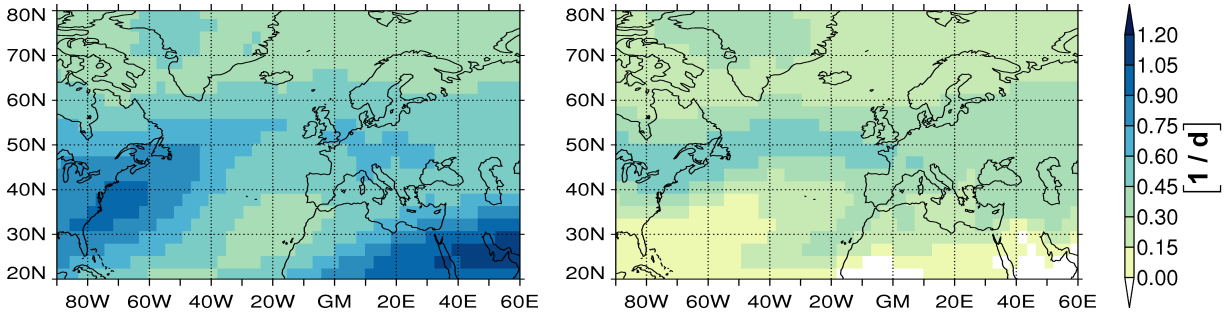

4.7.1: GHG DJF 1961–1990

4.7.2: GHG JJA 1961–1990

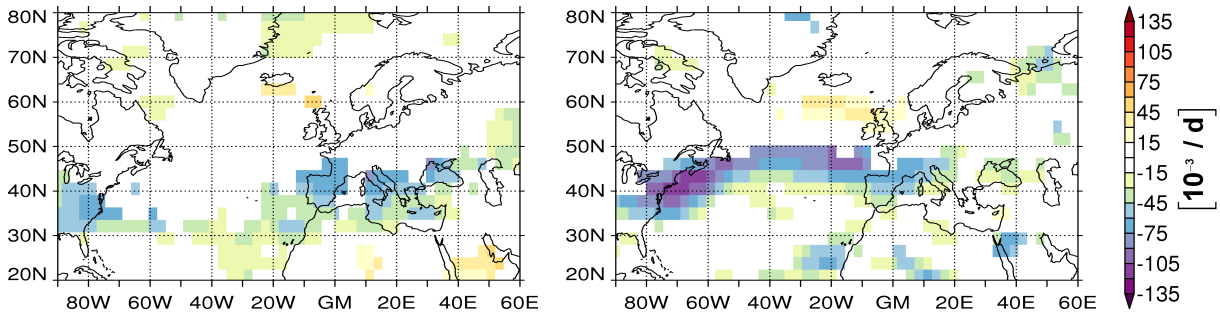

4.7.3: GHG DJF (2021–2050)–(1961–1990)

4.7.4: GHG JJA (2021–2050)–(1961–1990)

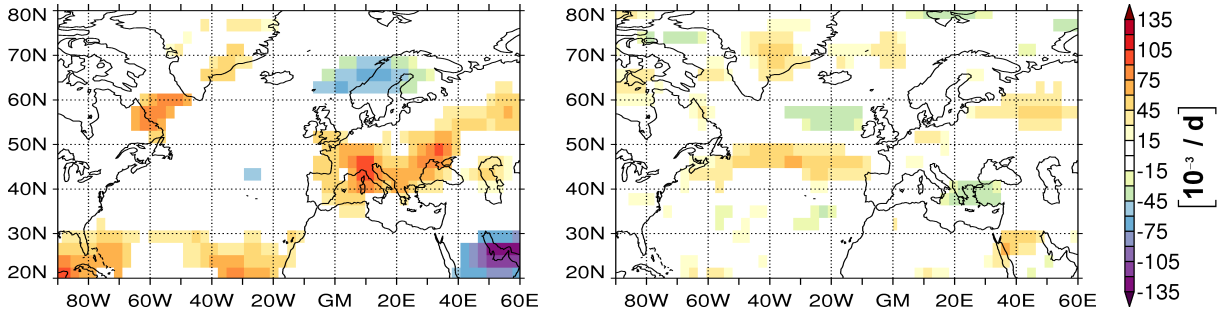

4.7.5: GSD–GHG DJF (2021–2050)–(1961–1990)

4.7.6: GSD–GHG JJA (2021–2050)–(1961–1990)

Figure 4.7: As Fig. 4.5, but for baroclinicity between 600–400 hPa.

over the whole North Atlantic accompanied by increasing track densities north of Scandinavia and in the Barents Sea (Fig. 4.8.4). The mirrorlike effect of sulphate aerosol is discernible for the track density which decreases in the central North Atlantic and from Iceland into the Barents Sea in winter. These decreases coexist with increases in track density over Baffin Island, parts of Labrador, along the east coast of North America and parts of Europe (Fig. 4.8.5). In summer, the aerosol influence leads to a southward shift of track density in the central North Atlantic (Fig. 4.8.6).

The number of all detected cyclones in the region does not change significantly from 1961–1990 to 2021–2050 for GHG, neither in winter (2113 events for 1961–1990 versus 2050 events for 2021–2050) nor in summer (1248 versus 1207 events). However, the number of deep cyclones, defined in this study as

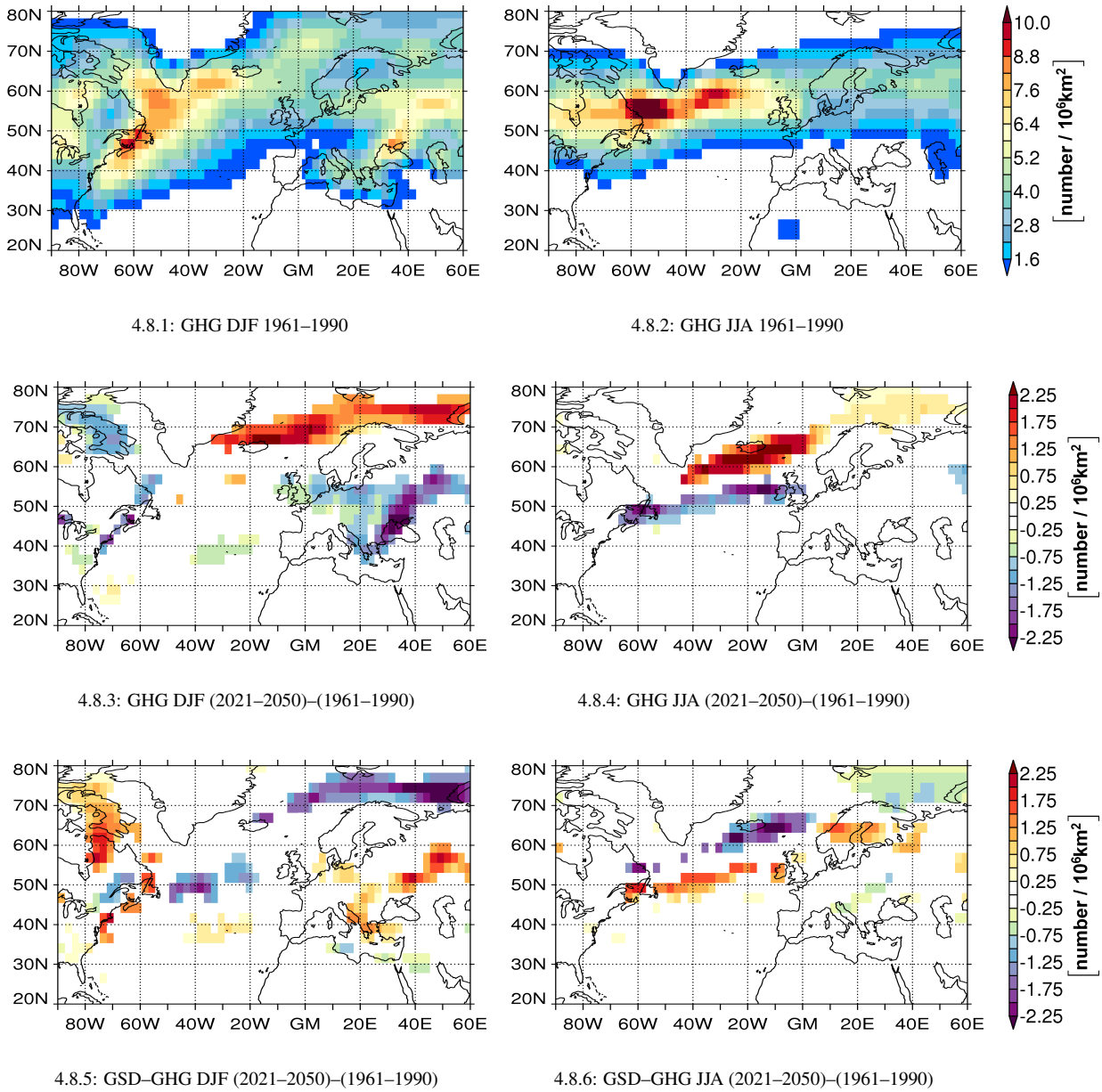

4.8.1: GHG DJF 1961–1990

4.8.2: GHG JJA 1961–1990

4.8.3: GHG DJF (2021–2050)–(1961–1990)

4.8.4: GHG JJA (2021–2050)–(1961–1990)

4.8.5: GSD–GHG DJF (2021–2050)–(1961–1990)

4.8.6: GSD–GHG JJA (2021–2050)–(1961–1990)

Figure 4.8: As Fig. 4.5, but for track density [number of tracks per 10^6 km^2 per month]. Track density suppression threshold is 1.

events whose core pressures fall below 970 hPa at least once during their lifetimes, increases significantly from 229 to 316 events in winter. In the summer season, deep cyclones are not detected in the analysed region.

Similarly to GHG, the number of all detected cyclones does not change significantly from 1961–1990 to 2021–2050 in GSD either (winter: 2148 versus 2071 events, summer: 1188 versus 1130 events). Furthermore, there is no significant increase in the number of deep cyclones in winter (246 versus 250 events).

4.3 Discussion

In order to quantify the effect of an increasing sulphate aerosol concentration on cyclonic activity in the North Atlantic region, changes in temperature, baroclinicity and track density between a reference period and a future period of two transient AOGCM simulations are presented. Table 4.2 gives a summary of the results. The main result of the analyses is that the increasing sulphate concentration leads to an increase in cyclonic activity. In particular, the direct radiative aerosol effect masks the response to the greenhouse gas forcing. Hence, the changes in track density between 2021–2050 and 1961–1990, which are statistically significant in the GHG simulation, are so no longer when including sulphate. Despite this important influence of sulphate, most studies investigating cyclonic activity in climate change scenarios have so far only focussed on the influence of greenhouse gases. Some studies considered greenhouse gas and aerosol effects conjointly, but only Carnell & Senior (1998) and Geng & Sugi (2003) explicitly allowed for the direct sulphate aerosol effect in their analyses. Carnell & Senior (1998) found qualitatively similar changes in mid-latitudinal variability for both a simulation forced by increasing greenhouse gas concentrations and a simulation that additionally included the direct radiative effect of sulphate aerosol. As the greenhouse gas forcing reaches quadruple CO_2 levels, though, the differences between the two simulations decrease. They further found a decrease in the total number of cyclones and an increase in the number of deep systems (core pressure below 970 hPa) for both simulations. Geng & Sugi (2003) analysed a simulation with increased concentrations of both greenhouse gases and sulphate aerosol. They attribute their detected decrease in total cyclone density in the mid-latitudes of the Northern Hemisphere to a decrease in baroclinicity caused by a decrease in the meridional temperature gradient.

Table 4.2: Summary of results (difference 2021–2050 – 1961–1990) for the North Atlantic/European region.

Parameter	Greenhouse gas effect	Aerosol effect
SO_4 burden		increase in the whole domain in winter, slight decrease over western Europe in summer
temperature	warming in summer and winter, especially north of 50°N in continental areas	cooling
baroclinicity	most areas show decrease	most areas show increase
track density	in winter: increase in band from the Denmark Strait to the Barents Sea, decrease over Europe, i.e. northward shift over Europe, also decrease over the Azores region and Baffin Island; in summer: northward shift over the northern North Atlantic	in winter: decrease in band extending eastward from Jan Mayen to Novaya Zemlya as well as east of Newfoundland, increase over parts of Europe, the Azores region and Baffin Island; in summer: southward shift over northern North Atlantic

The following discussion will focus on the effects of greenhouse gases and sulphate aerosol on the position and frequency of cyclones.

Concerning the position of the cyclones, the results for the GHG simulation are consistent with the results presented by Knippertz et al. (2000) and Pinto et al. (2006) who analysed the same simulation. Both studies examined differences between 1880–1930 and 2039–2089. While Knippertz et al. (2000) applied only a detection routine to identify cyclone core positions, Pinto et al. (2006) used an adapted version of the Murray & Simmonds (1991a) tracking algorithm to obtain full cyclone tracks. The simulated poleward shift in track density is related to the overall changes in the pressure field in the simulation and is robust regardless of the analysis method used. Carnell et al. (1996) and Schubert et al. (1998) also reported a poleward shift of the regions of enhanced track density under increasing greenhouse gas concentrations. On the other hand, Lambert & Fyfe (2006) found no discernible change in the mean position of the main cyclone tracks in model simulations based on the SRES A1B storyline. However, they did not exclude the occurrence of small shifts in position which might not be detected due to the coarse spatial resolution they used for the analysis. Whereas the poleward shift is no longer significant after the inclusion of sulphate aerosol in the GSD simulation, Geng & Sugi (2003), Fyfe (2003) and Bengtsson et al. (2006a), who analysed model simulations which take both the greenhouse gas and the radiative aerosol effect into account, did report a poleward shift in the activity. On the other hand, Leckebusch & Ulbrich (2004) did not detect any spatial shift in climate change simulations of the HadCM3 model based on the SRES A2 storyline.

It is difficult to identify the causes for these apparently opposing responses to similar changes in the forcing. One cause could be the forcing itself since only a few of the cited studies analyse model simulations based on the same emission scenario. Another cause are the differences between the AOGCMs used. For example, Pinto et al. (2006) attributed changes between their results and other results to a dissimilar response of the AOGCMs to changes in the large-scale variability.

Concerning the frequency of cyclones, a number of studies reported decreasing tendencies in the number of detected cyclones under climate change conditions (Lambert, 1995; Carnell et al., 1996; Zhang & Wang, 1997; Carnell & Senior, 1998; Geng & Sugi, 2003; Lambert, 2004; Leckebusch & Ulbrich, 2004; Lambert & Fyfe, 2006; Pinto et al., 2006; Leckebusch et al., 2006; Bengtsson et al., 2006a), regardless of whether the effects of sulphate aerosol are included in the experiments or not. Often, the reported decrease was small and was not tested for its statistical significance. The results presented here support Knippertz et al. (2000) who found only negligible changes in the number of detected cyclones for the GHG simulation. A possible explanation for this discrepancy in the response of the total numbers of detected cyclones to greenhouse gas forcing can be found when taking into account that these total numbers are taken from different regions. The area used here for the cyclone count (20°–80°N, 90°W–60°E) most closely resembles the one used by Knippertz et al. (2000), which was about 30°–85°N, 80°W–40°E. The

studies cited above considered either the whole hemisphere, thereby possibly introducing averaging effects between the responses in the North Atlantic and the North Pacific as pointed out by Fischer-Bruns et al. (2005), or a smaller area, thereby possibly missing trends included in the numbers presented here.

Changes in the number of deep cyclones are also analysed in several studies, although the approaches to determine such changes differ. One approach is to calculate the difference in the numbers of occurrence of lows with core pressures below a certain threshold (Lambert, 1995, 1996; Knippertz et al., 2000; Lambert & Fyfe, 2006; Pinto et al., 2006; Wile, 2006). Lambert & Fyfe (2006) reported that the value chosen for the threshold only slightly influences the qualitative results of the counting. Other approaches are based on the strength of the gradient in pressure or geopotential height (Sickmöller et al., 2000; Schubert et al., 1998; Geng & Sugi, 2003), the shift in a certain percentile (Leckebusch & Ulbrich, 2004), partitioning the cyclones into bins according to their strength (Sinclair & Watterson, 1999; Beersma et al., 1997; Carnell et al., 1996; Carnell & Senior, 1998) or classification schemes involving several cyclone characteristics (Paciorek et al., 2002; Zhang et al., 2004; Bauer & Del Genio, 2006). Sinclair (1997) pointed out that an increase in the number of extreme events defined by a certain threshold in pressure does not necessarily correspond to increased cyclone intensities, in particular if there is a simultaneous overall decrease in MSLP. He suggested using a measure of intensity that involves the strength of the vortex, e.g., vorticity. Bengtsson et al. (2006a) compare the distribution of cyclones as a function of intensity based on vorticity as well as filtered MSLP data (i.e., without the planetary background) and obtain largely similar results with only negligible changes in the tails of both distributions under climate change conditions. When the tracks based on the filtered MSLP data were referenced back to the unfiltered pressure field, though, a shift towards stronger cyclones occurs from the present to the future. However, Pinto et al. (2006) found that the increasing numbers of cyclones with deeper core pressures coincide with increasing numbers of intense cyclones when they applied a threshold criterion to their measure of intensity, the Laplacian of the pressure, which is related to vorticity. To study this phenomenon in the current simulations, an analysis similar to the one described by Bengtsson et al. (2006a) was carried out for the GHG experiment (Fig. 4.9). This analysis shows a shift towards stronger cyclones both for the filtered and the unfiltered MSLP data which indicates that the increase in strong cyclones is not only caused by changes in the large-scale background pressure field.

The significant increase in deep cyclones found in the GHG simulation in this study agrees well with Knippertz et al. (2000), Carnell et al. (1996), Carnell & Senior (1998), Lambert (1995) and Lambert (2004). In contrast, Sinclair & Watterson (1999) found a decrease in deep events when comparing two equilibrium simulations with 1x and 2x CO_2 concentrations. Since Lambert (1995) also analysed a set of equilibrium simulations, this discrepancy in results can not be attributed to the type of simulation, i.e. transient or equilibrium or time-slice, used for the analysis.

The insignificant change in the number of deep cyclones found in GSD is in contrast to Carnell &

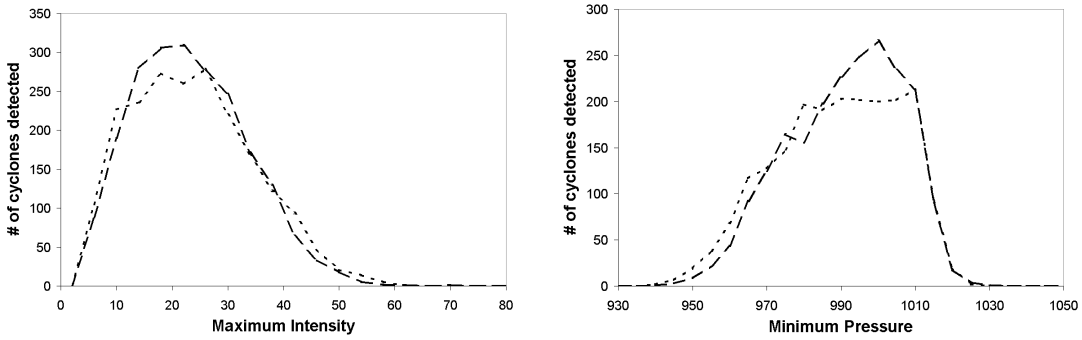

4.9.1: Data with planetary scales removed.

4.9.2: Unfiltered data

Figure 4.9: Distributions of number of low pressure systems detected in winter (DJF) versus their maximum intensity for the North Atlantic/European region for GHG. Short-dashed line: 2021-2050, long-dashed line: 1961-1990. Intensities are given in hPa, bin widths are 4 hPa and 5 hPa, respectively.

Senior (1998) and Bengtsson et al. (2006a) who reported increases in the number of deep cyclones even in the presence of sulphate aerosol in the North Atlantic/European region. A possible explanation for these contrasting results are the higher sulphate concentrations in the IS92a emission scenario (IPCC, 2001) used for GSD compared to other scenarios such as the SRES A1B used in Bengtsson et al. (2006a).

4.4 Conclusions

In general, the presented analyses show that the response of the atmospheric circulation to the sulphate aerosol forcing is not restricted to changes in the vicinity of the emission sources in the North Atlantic/ European region. Rather, the strongest response to the aerosol forcing often coincides spatially with the region of strongest response to the greenhouse gas forcing. The separation between the effects of the two forcings on cyclonic behaviour is an aspect not considered previously.

To conclude, the direct aerosol effect as presented in this study dampens the response of the climate system to the increase in greenhouse gas concentrations, but is not strong enough to reverse it apart from certain locally-restricted areas. However, the effects of strongly absorbing aerosols, such as soot, which tend to warm the atmosphere, as well as the indirect effects of aerosols on clouds have not been taken into account. These will have to be considered in future climate simulations.

Chapter 5

A closer look: case study of the cyclone *Grace*

5.1 Introductory remarks

The climatological approach described in the previous chapter was chosen to investigate the influence of scattering aerosols on the development of extratropical cyclones in a warmer climate. In this chapter, the question of whether the track as well as certain characteristics along the cyclone track of an individual cyclone are influenced by anthropogenic aerosols is addressed by an alternative approach. For this purpose, a case study setup was chosen. The idea behind it is as follows: for an individual cyclone that developed over the region of the North Atlantic that is under the influence of the pollution from North America one set of model simulations was performed with all aerosols accounted for and another set of simulations was performed without the contribution of the anthropogenic aerosol emissions. This way, differences in the cyclonic development are easily attributable to the changes in the boundary conditions. Differences between the two ensembles may be expected in the aerosol burden, the aerosol optical depth (AOD), precipitation and the amount of radiation reaching the earth's surface along the cyclone track.

The choice of a suitable cyclone depended on several factors. Due to the available emission inventory (AeroCom; Dentener et al., 2006), a cyclone in the year 2000 was required. The cyclone to be chosen should reach a sufficient intensity, should exist longer than just a couple of days and should not be stationary. Similarly to the argument in Chapter 4, that while cyclones are strongest in the winter months, the aerosol influence is stronger in summer due to the enhanced photochemical reactions, a cyclone occurring in spring or autumn was preferred.

After having systematically studied the tracks of cyclones observed throughout the year 2000 in the operational weather charts archived at the Seewetteramt, Hamburg, and other synoptic weather charts (Berliner Wetterkarte, 2000; DWD, 2000), the cyclone that was named *Grace* by the Institute of Meteo-

rology, Free University of Berlin, was chosen for the case study experiment.

Cyclone *Grace*. *Grace* belonged to a family of cyclones that crossed the North Atlantic in early March, 2000. It first appeared on the Berliner Wetterkarte (2000) at about 46°W and 41°N at 00UTC on March 8, 2000. Fig. 5.1 shows the track of *Grace* as estimated from synoptic weather charts. The initial core pressure of the cyclone was about 1000 hPa. While travelling northeastward toward Iceland, the core pressure decreased to about 995 hPa. On March 10, 2000, the cyclone split south of Iceland and changed its direction, heading now towards southern Scandinavia. While passing over Denmark and Poland, *Grace* filled up. Its core pressure was about 1010 hPa when it reached the Black Sea on March 13, 2000. From there, it travelled towards the Caspean Sea and filled completely.

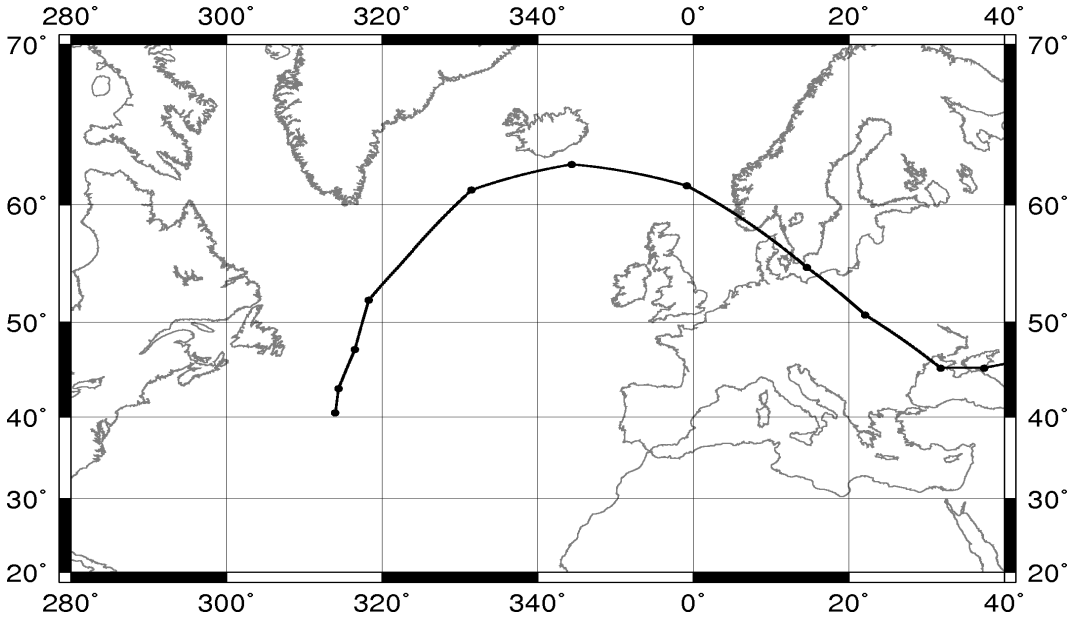

Figure 5.1: Track of cyclone *Grace* starting at 00UTC, March 8, 2000. Track positions, which are indicated every 12 h by filled circles, were estimated from synoptic weather charts.

Experimental setup. For a comprehensive description of the atmospheric state, a single model realisation is not sufficient. Therefore, ensembles of simulations are more and more used in climate modelling. The ensemble members differ slightly in their initial conditions. One approach to determine a set of ensemble members in ECHAM5 is to infinitesimally perturb the prognostic variables divergence, vorticity and temperature in the uppermost model layer. After an integration time period of at least one month, this perturbation is revoked. For each ensemble member, the same model is then used to continue the integration. This approach was technically not feasible for the current case study setup which is constrained by the nudging. As an alternative, the nudging coefficients can be slightly altered to introduce the perturbation in initial conditions in the model (E. Roeckner, pers. comm.).

The ensemble simulations were conducted with ECHAM5-HAM. First, the model was integrated twice in nudged mode from October 1999 to the end of January 2000. The first of these integrations was performed using the full AeroCom emission inventory. This integration forms the basis of the *AllAero* ensemble. The second integration was performed with the identical model setup, but the anthropogenic contributions to the emission inventory, i.e. anthropogenic SO_2 emissions as well as emissions from fossil fuel and biofuel use and wildfires, were neglected. This integration forms the basis of the *NoAnthrAero* ensemble. Between February 1, 2000, and March 6, 2000, the relaxation time for vorticity was then changed from the standard value of 6 hours to obtain the individual ensemble members. The new relaxation time for vorticity was varied in 10-minute intervals from 5 to 7 hours so that 13 simulations were performed within each ensemble. On 00:00 UTC, March 7, 2000, the nudging was switched off. For each ensemble member, the model integration then continued in forecast mode until March 17, 2000.

For simplification, the SST of the starting time of the ensemble integration in forecast mode—00UTC, March 7, 2000—was kept as a constant lower boundary condition in the model. This is reasonable since the SST changed only very little in the ERA40 data set.

5.2 Results

5.2.1 Comparison of the two ensembles

Fig. 5.2 shows the emissions of the five key aerosol components which are considered in the aerosol module HAM—sulphur, dust, black carbon, particulate organic matter and sea salt—during the case study period. The anthropogenic contribution is clearly discernible for sulphur with the major ship routes across the North Atlantic (Fig. 5.2.1) superimposed on the natural DMS emissions (Fig. 5.2.2). For black carbon (Fig. 5.2.3 and 5.2.4) and particulate organic matter (Fig. 5.2.5 and 5.2.6), the emission sources in North America and Europe are dominant. The emissions of dust (Fig. 5.2.7 and 5.2.8) and sea salt (Fig. 5.2.9 and 5.2.10) show only small differences.

The corresponding aerosol burdens averaged over the ensembles and the case study period are presented as averages in Fig. 5.3. Surprisingly, the highest atmospheric sulphur burdens do not coincide with the largest emission sources (Fig. 5.3.1 and 5.3.2 compared to Fig. 5.2.1 and 5.2.2), in particular when considering Europe and northern Africa. A possible explanation for this imbalance will be discussed in Section 5.2.2. The burdens of black carbon, particulate organic matter and dust (Fig. 5.3.3 and Fig. 5.3.5 to 5.3.8) indicate northward transport of these aerosol species from the tropics and subtropics towards Iceland and the Norwegian Sea.

To ensure the reliability of the case study results, the ensemble averages were compared with results of the ECHAM5-HAM reference experiment presented by Stier et al. (2005) who conducted a one-year

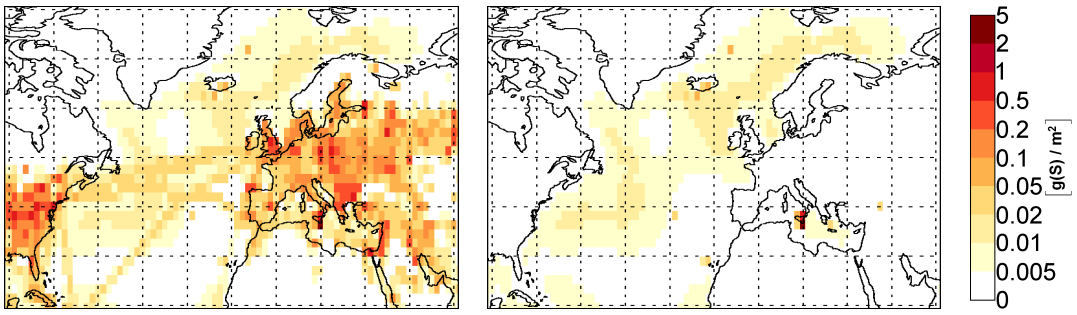

5.2.1: AllAero sulphur

5.2.2: NoAnthrAero sulphur

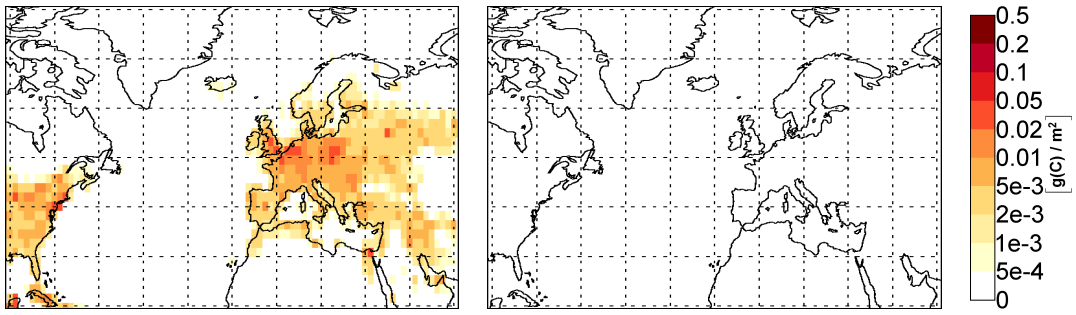

5.2.3: AllAero black carbon

5.2.4: NoAnthrAero black carbon

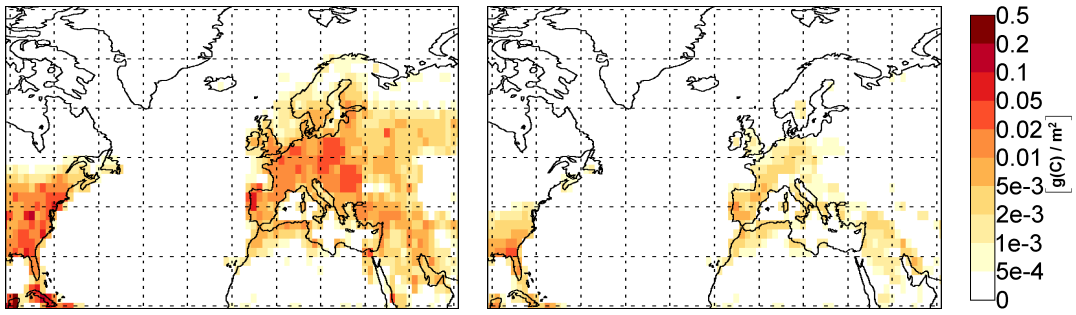

5.2.5: AllAero particulate organic matter

5.2.6: NoAnthrAero particulate organic matter

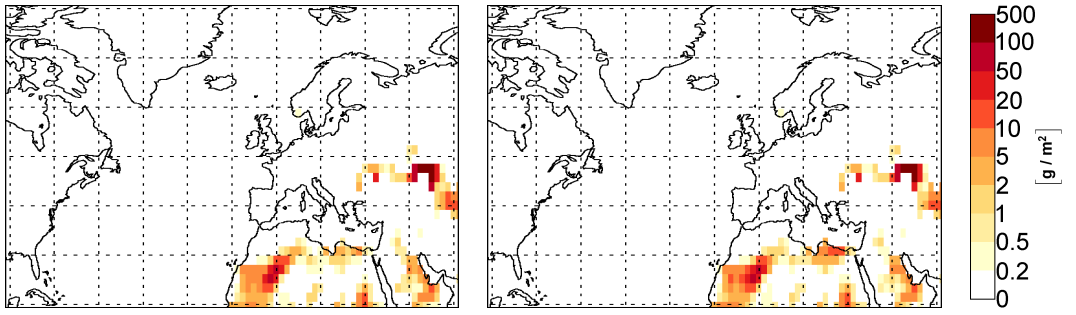

5.2.7: AllAero dust

5.2.8: NoAnthrAero dust

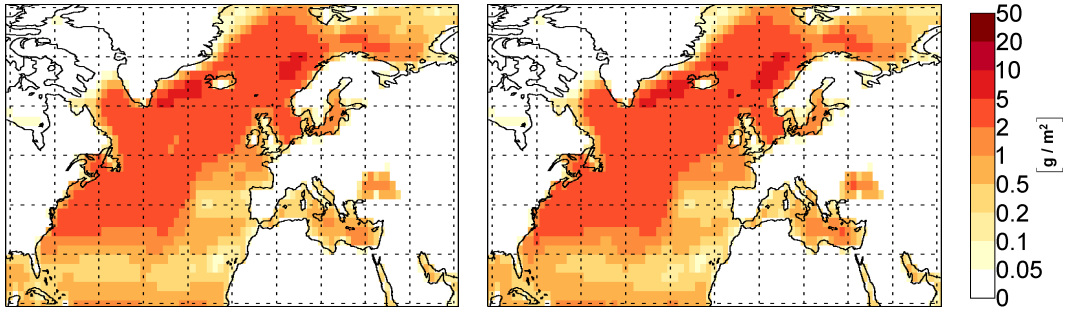

5.2.9: AllAero sea salt

5.2.10: NoAnthrAero sea salt

Figure 5.2: Emissions averaged over the ensembles AllAero (left) and NoAnthrAero (right) for Mar 7–17, 2000.

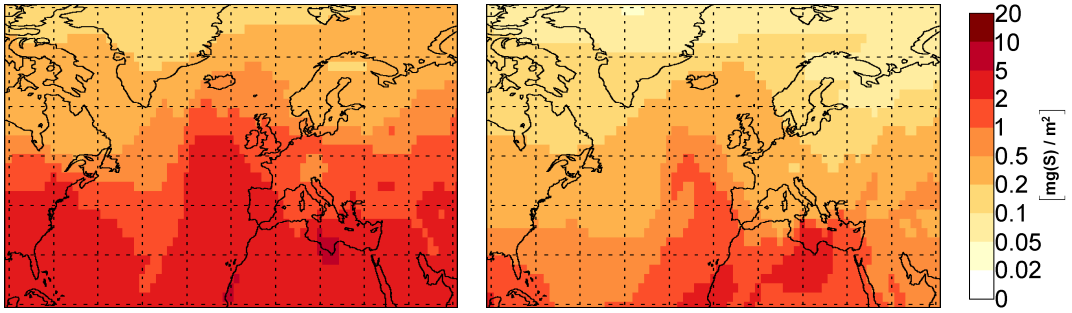

5.3.1: AllAero SO_4^{2-} 5.3.2: NoAnthrAero SO_4^{2-}

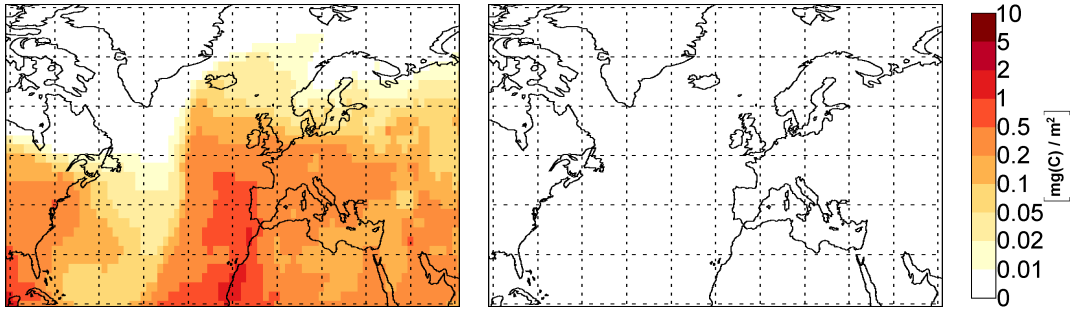

5.3.3: AllAero black carbon 5.3.4: NoAnthrAero black carbon

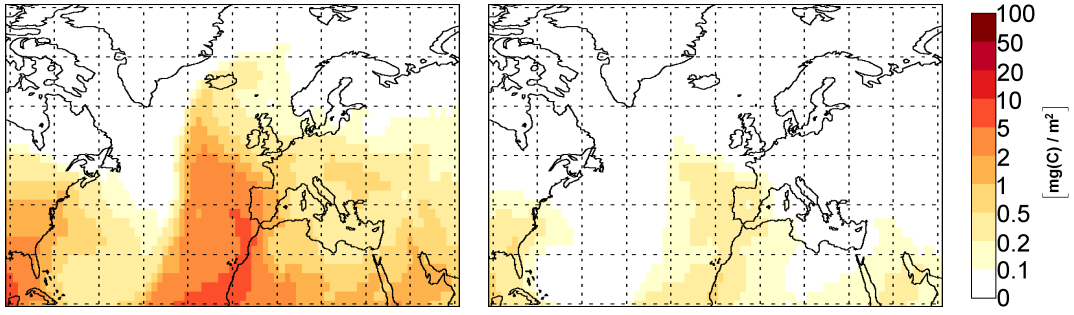

5.3.5: AllAero particulate organic matter 5.3.6: NoAnthrAero particulate organic matter

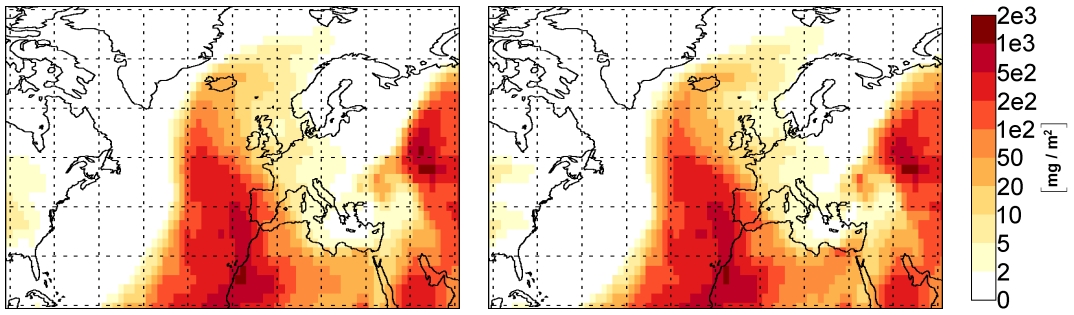

5.3.7: AllAero dust 5.3.8: NoAnthrAero dust

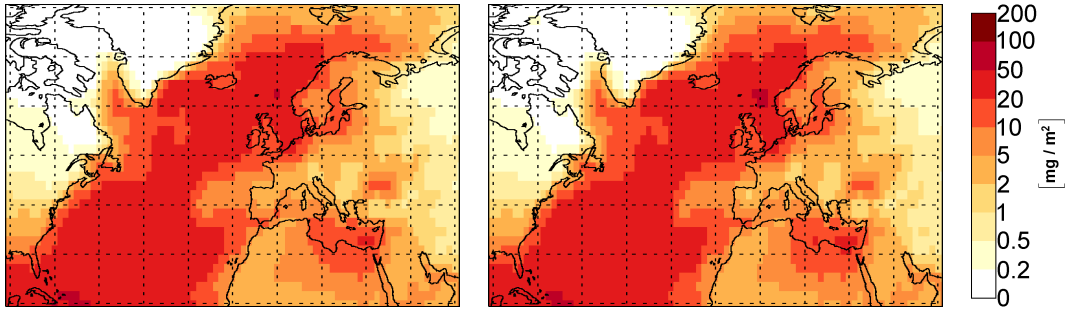

5.3.9: AllAero sea salt 5.3.10: NoAnthrAero sea salt

Figure 5.3: Aerosol burdens averaged over the ensembles AllAero (left) and NoAnthrAero (right) for Mar 7–17, 2000.

nudged simulation for the year 2000 with an earlier version of the model. For March 2000, the results of both model versions are very similar if nudging is used. Once the nudging is switched off, though, the surface wind speed frequency distribution shifts to higher wind speeds which in turn leads to an overestimation of the dust emissions (Timmreck & Schulz, 2004). Therefore, the dust emissions and burdens have to be treated with caution here.

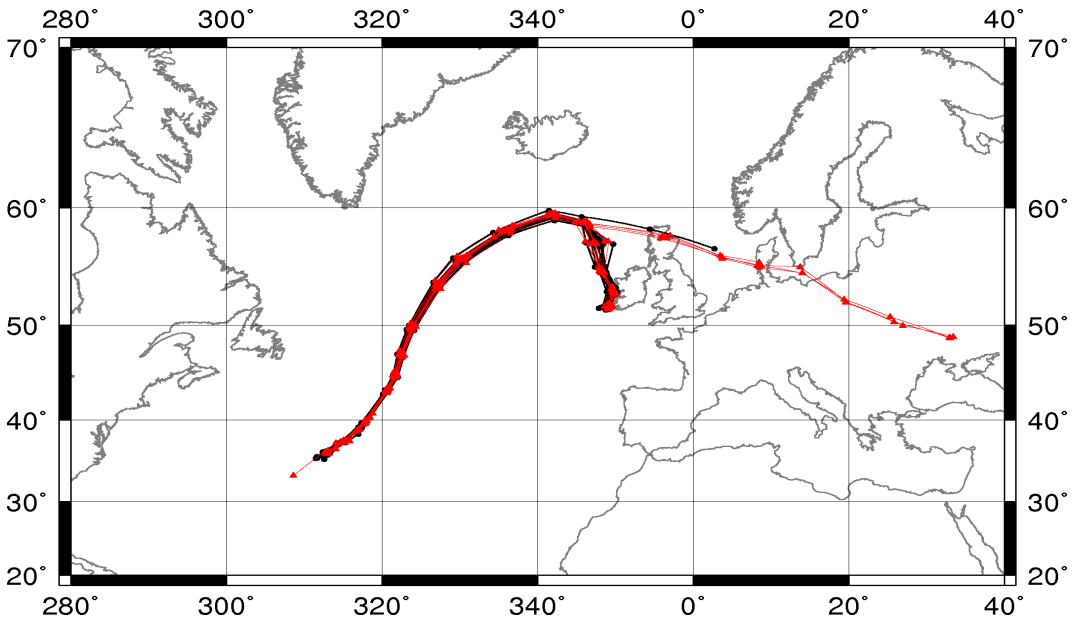

Figure 5.4: Tracks of cyclone *Grace* as detected in the ensembles AllAero (black) and NoAnthrAero (red), starting 00UTC, March 8. The filled circles and triangles indicate the cyclone positions every six hours.

Fig. 5.4 depicts the tracks of cyclone *Grace* for both ensembles as determined from tracking maxima of $\xi_{850\,\mathrm{hPa}}$ with TRACK. Compared to the track estimated from synoptic charts (Fig. 5.1), the modelled tracks are systematically displaced to the south. This southward displacement is well-known when comparing MSLP-based tracks with vorticity-based tracks (Sinclair, 1994; Mailier et al., 2006).

With regard to the effect of anthropogenic aerosols, no effect on the cyclone tracks is discernible. For both AllAero and NoAnthrAero, the tracks follow very similar routes until 18UTC, March 10, 2000. At that time, the cyclone splits and TRACK attributes a higher probability to the southern branch although the eastern branch was actually followed in reality. One ensemble member of AllAero and four ensemble members of NoAnthrAero followed the eastern branch as well. However, the ensembles were too small to test whether this different behaviour of AllAero and NoAnthrAero is robust.

The following figures depict different variables along the cyclone tracks. The values were calculated as the average of the four grid points closest to each cyclone position. Since *Grace* was first detected in all ensemble members at 6UTC, March 8, 2000, the ensemble plots start on this date.

The SO_4^{2-} burden (Fig. 5.5) shows systematically higher burdens for AllAero than for NoAnthrAero, as expected. In AllAero, the burden decreases strongly in the first day due to wet deposition of SO_4^{2-}

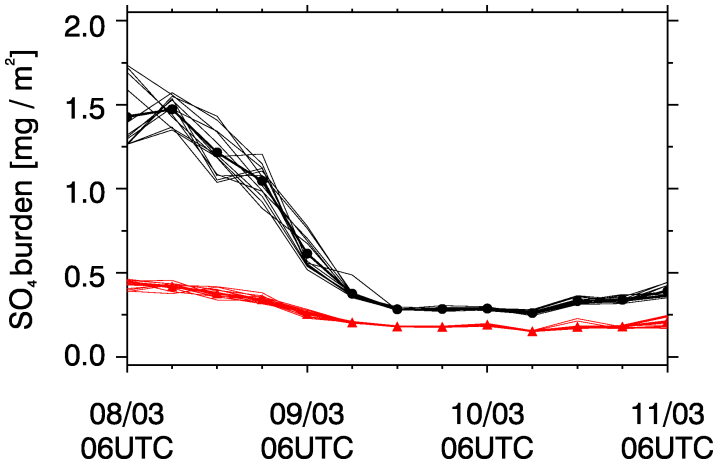

Figure 5.5: SO_4^{2-} burden along the track of cyclone *Grace* for AllAero (black) and NoAnthrAero (red) with filled circles triangles representing the ensemble averages. The abscissa shows the time every 6 hours starting on March 8, 2000.

(cf. Fig. 5.10.6). It levels off at noon, March 9, 2000, and increases again once the cyclone nears Europe. In NoAnthrAero, the burden also decreases in the beginning. The increase in the vicinity of Europe is much less pronounced.

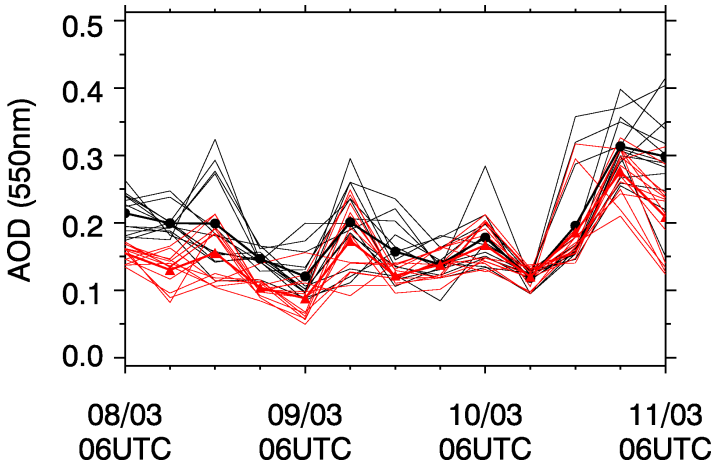

Figure 5.6: AOD (550nm) along-track of cyclone *Grace* for AllAero (black) and NoAnthrAero (red). The filled black circles (AllAero) and red triangles (NoAnthrAero) represent the ensemble averages.

For the AOD at 550 nm (Fig. 5.6), the ensemble average of AllAero is slightly higher than the one of NoAnthrAero until 18UTC, March 9, 2000. This can be explained by the higher SO_4^{2-} burden in AllAero compared to NoAnthrAero (Fig. 5.5). After that date, though, the contribution of dust to the AOD dominates so that the difference between AllAero and NoAnthrAero is negligible.

Fig. 5.7 shows the clear sky net surface solar radiation. Here, the diurnal variation in the radiation is obvious, as is the northward movement of the cyclone since the amplitude of the diurnal variation decreases. However, despite the different aerosol loading in both ensembles, there is no difference in the clear sky net surface solar radiation between the ensembles. This indicates that the direct radiative aerosol effect is negligible along the track.

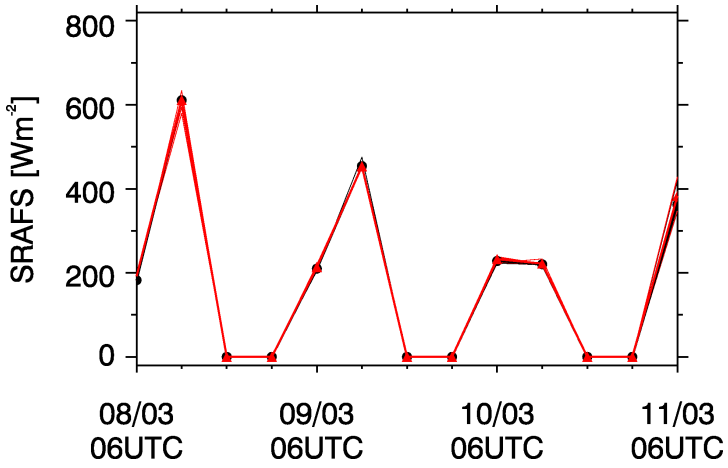

Figure 5.7: As Fig. 5.5, but for net surface solar radiation (clear sky).

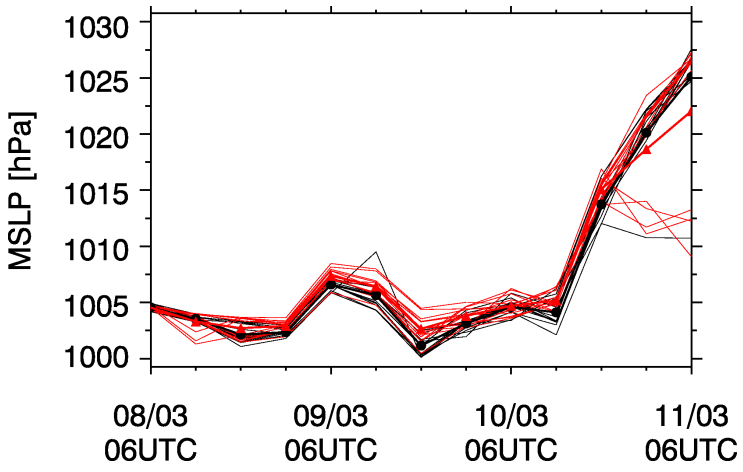

Figure 5.8: As Fig. 5.5, but for MSLP.

The differences in MSLP along the track (Fig. 5.8) are very small. This is consistent with the fact that the cyclone tracks of both ensembles are located closely together geographically. The ensemble members following the eastern branch after the split of the cyclone centre cause a slightly smaller NoAnthrAero ensemble average after 18UTC, March 10, 2000, compared to the AllAero ensemble mean. However, one has to bear in mind that by then the simulation has been proceeding in the forecast mode for more than three days. Thus, differences between the two ensembles at this time may also be due to the uncertainty inherent in the chaotic nature of the atmosphere.

The precipitation along the tracks (Fig. 5.9) shows a larger spread of the ensemble members than, e.g., MSLP, which is probably due to the large spatial variations in precipitation in relation to the cyclone position. Therefore, the calculation of the precipitation from the four grid points surrounding the cyclone centre does not capture this parameter well.

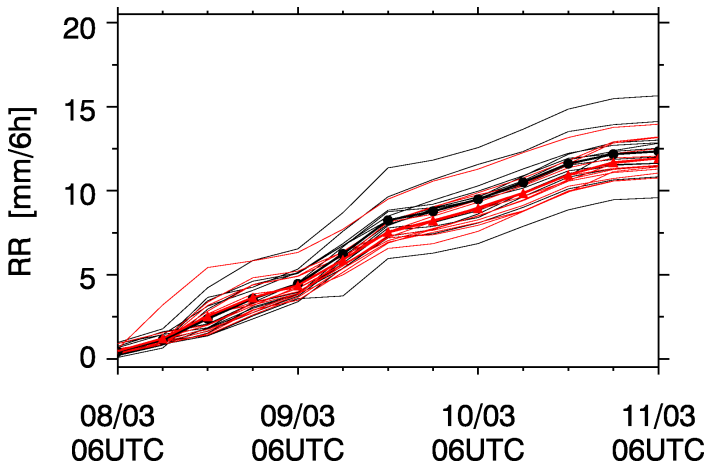

Figure 5.9: As Fig. 5.5, but for precipitation.

5.2.2 SO_x from European sources over the Sahara

As alluded to above, there is an imbalance in the geographic distribution of the main source regions of sulphate precursors and the regions with the highest sulphate burden over Europe and northern Africa. A look at the concentrations of SO_2 and SO_4^{2-} in the surface model layer, the prevailing winds in this layer and the sinks of both species helps to clarify the processes taking place in the model (Fig. 5.10).

The pattern in the near-surface concentration of SO_2 (Fig. 5.10.1) reflects the main emission sources (Fig. 5.2.1). The pattern in the near-surface concentration of SO_4^{2-} (Fig. 5.10.2), on the other hand, more closely resembles the pattern in the SO_4^{2-} column burden (Fig. 5.3.1). The prevailing winds for the 10-day period of March 7–17, 2000, also shown in Fig. 5.10.1 and 5.10.2, indicate a southward transport of both SO_2 and SO_4^{2-} across the Mediterranean into northern Africa where easterly winds dominate. Since the interactive dry deposition scheme used in ECHAM5-HAM (Ganzeveld et al., 1998; Stier et al., 2005) calculates lower dry deposition of SO_2 for bare soils compared to soils covered with vegetation, the dry deposition of SO_2 in northern Africa is smaller than in Europe (Fig. 5.10.3). For SO_4^{2-}, the dry deposition is even lower (Fig. 5.10.4). Due to the lack of precipitation in the Sahara, wet deposition for both species is negligible as well (Fig. 5.10.5 and 5.10.6). At the same time, the gas-phase production of SO_4^{2-} shows a maximum near Malta and Tripoli (Fig. 5.11.2). Over the Mediterranean, SO_4^{2-} is also produced in the liquid phase (Fig. 5.11.1).

Owing to the inefficient sink processes, SO_4^{2-} accumulates over Libya and is transported westward across the Sahara. Over the North Atlantic, a part of this SO_4^{2-} is then transported to the north. Off the west coast of the Iberian Peninsula, it mixes with the SO_4^{2-} originating from ship emissions. The anticyclonic circulation centred over southern England, finally, explains the high sulphate burden west of Ireland (Fig. 5.3.1).

The open questions now are: how representative is the circulation described above of the average circulation in this region? And: can the westward transport of SO_4^{2-} across the Sahara be verified?

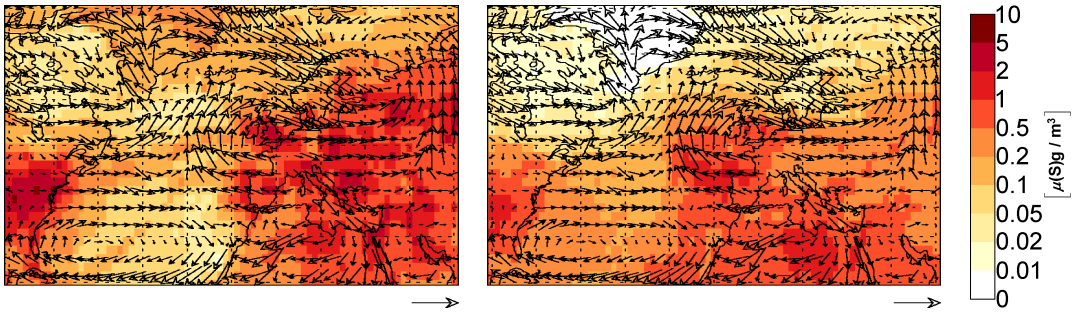

5.10.1: SO_2 concentration

5.10.2: SO_4^{2-} concentration

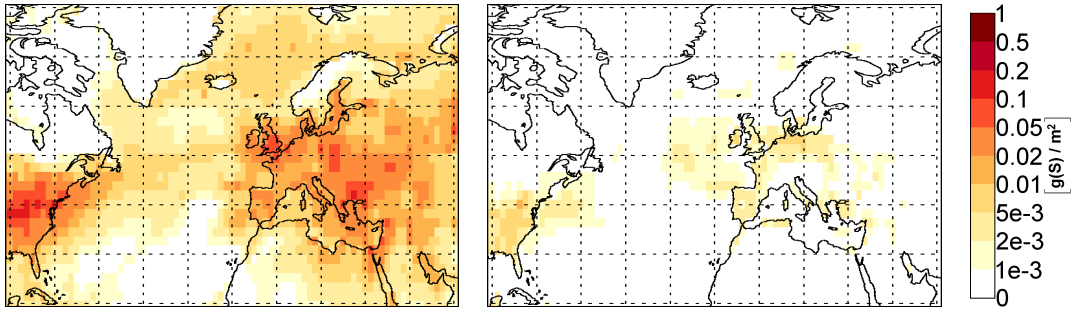

5.10.3: SO_2 dry deposition

5.10.4: SO_4^{2-} dry deposition

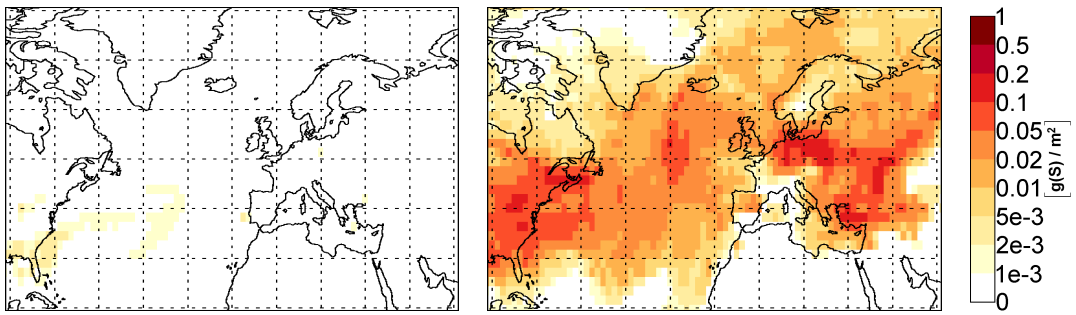

5.10.5: SO_2 wet deposition

5.10.6: SO_4^{2-} wet deposition

Figure 5.10: AllAero ensemble averages: concentration of SO_2 (left) and SO_4^{2-} (right) at about 1000 hPa with vectors depicting wind speed and direction in the same layer, dry deposition and wet deposition for SO_2 (left) and SO_4^{2-} (right) averaged over Mar 7–17, 2000. The arrow below the maps in Fig. 5.10.1 and 5.10.2 represents a wind speed of 10 m/s.

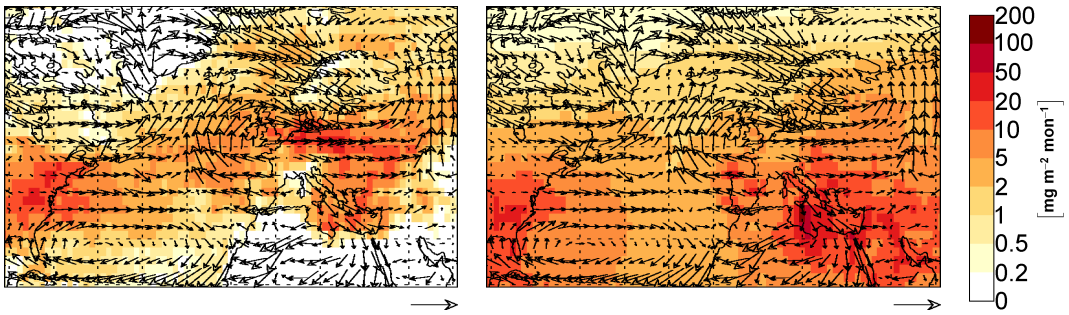

5.11.1: Liquid phase 5.11.2: Gas phase

Figure 5.11: AllAero ensemble average: SO_4^{2-} production in the liquid (left) and gaseous (right) phase averaged March 7–17, 2000 (AllAero ensemble average). The vectors depict the average wind speed and direction at about 1000 hPa. The arrow below the maps represents a wind speed of 10 m/s.

To address the first question, the ERA40 geopotential height and wind fields at 1000 hPa were studied. In the case study period, a blocking high was centred over France in the simulation. In ERA40, the centre of the blocking high is located further west (Fig. 5.12.1) which can be explained by the different averaging period used for case study experiment (March 7–17, 2000) and ERA40 (March 1–31, 2000). Similar blocking highs occurred in 8 of the 45 years covered by ERA40 (1961, 1966, 1973, 1978, 1983, 1988, 1990, 1997). On average, though, the high pressure region is located further southwest in the North Atlantic (Fig. 5.12.2) which inhibits northward transport from Africa or west of Portugal. The circulation of the case study period cannot be considered as a representative of the circulation over Europe and North Africa in March.

The second question is more difficult to address due to the lack of observational data in North Africa in 2000. Satellite observations are only partially suitable, as well. Fig. 5.13 shows the AOD of the small mode fraction, i.e. particles smaller than 1 μm, for March as obtained from MODIS. The main contributors to the small mode fraction AOD are SO_4^{2-}, black carbon and particular organic matter. While the MODIS data confirm the high AOD values seen in the eastern North Atlantic in the simulation, they do not prove or disprove the transport across the Sahara. The question, therefore, cannot be answered within the scope of this study.

5.3 Conclusions

In order to investigate the influence of aerosols on the cyclone track and selected meteorological parameters along-track, two ensembles were produced in a case study setup. For one ensemble, ECHAM5-HAM was integrated with the full aerosol emissions from the AeroCom emission inventory. For the other, the anthropogenic contributions to these emissions were omitted.

Concerning the characteristics of the chosen cyclone, *Grace*, no discernible influence of the aerosols

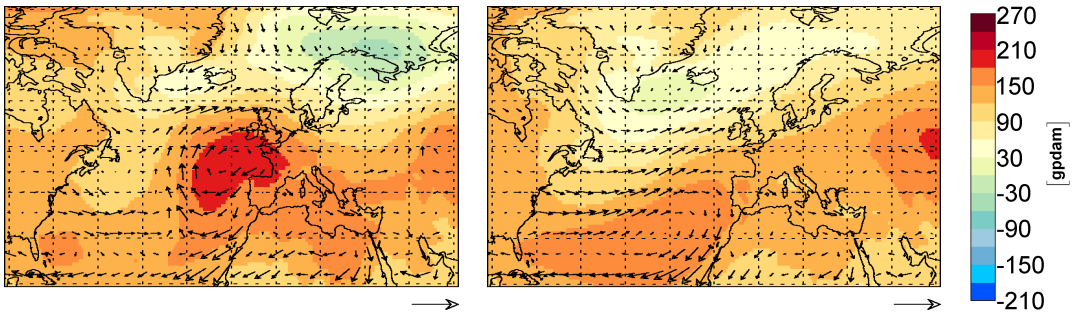

5.12.1: March, 2000 5.12.2: Average March, 1958–2002

Figure 5.12: ERA40 geopotential height and wind vectors at 1000 hPa in March for the year 2000 (left) and averaged over 1958–2002 (right). The arrow below the maps represents a wind speed of 10 m/s.

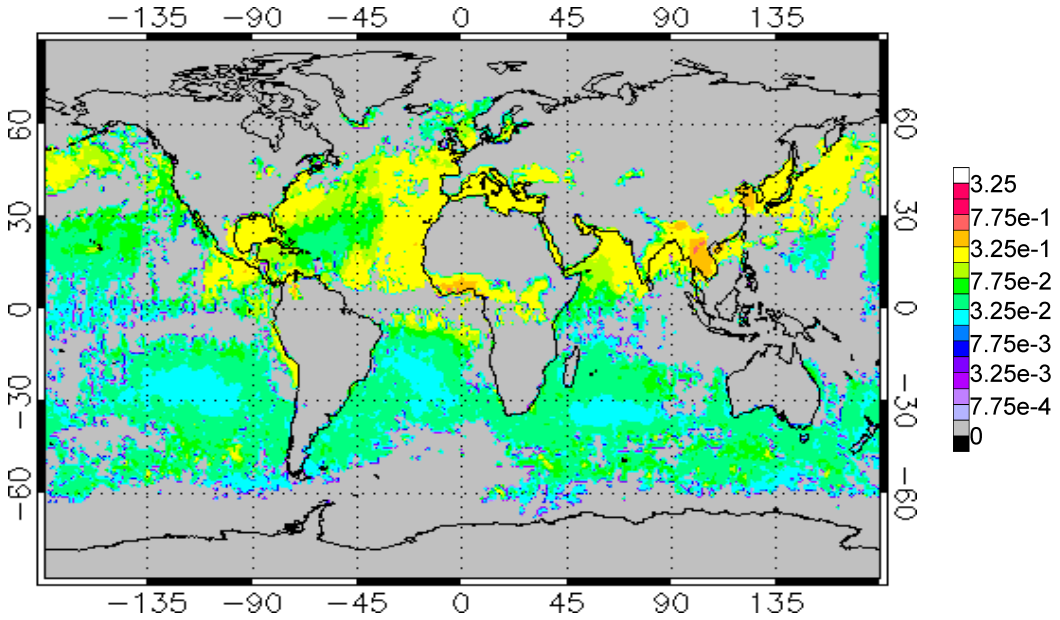

Figure 5.13: MODIS AOD (550nm) of the small mode fraction (particles with diameters less than 1μm) for March, 2000. Areas for which less than 15 retrievals were recorded are masked grey.

could be detected. This may be due to a number of reasons: (1) the aerosol effects are possibly too small due to the relatively small differences in aerosol concentration between both ensembles or (2) the internal dynamics of the cyclone may be too large compared to the effects that aerosols may have so that the latter play no role in the development of the cyclone. Furthermore, the case study setup may be insufficient, in particular with regard to the SST, which was kept constant during the case study period. To estimate the effect of the constant SST, the simulation with the standard nudging coefficients (Table 2.1) was repeated with the SST both uniformly reduced and increased by 1 K. These simulations differed only very little from the simulation performed with the original SST distribution. The results of the case study therefore suggest that anthropogenic aerosols affect cyclone characteristics only on a long-term basis. There is no indication for an influence on an established cyclone. This conclusion does not contradict the results of Chapter 4 which showed that sulphate aerosol attenuates the greenhouse gas effect on cyclonic activity.

Regarding the long-distance transport of European SO_2 to Africa, future research should focus on evaluating the dry deposition in the model. Since 2000, the number of AERONET stations (Aerosol Robotic Network; http://aeronet.gsfc.nasa.gov) in North Africa has increased from less than 10 to more than more than 20 in 2007, although the majority of the stations are still located outside of the Sahara. The aerosol reanalysis to be produced within the GEMS project (Global earth-system monitoring using space and in-situ data) may be useful for this evaluation, as well. Defining a tracer in the model may also help to establish the history of the SO_4^{2-} that accumulates in North Africa—it was not possible to determine whether the largest contribution to the accumulating SO_2 was from Mount Vesuvius or from anthropogenic sources. Performing simulations without natural SO_4^{2-} sources may also help to answer this question.

Chapter 6

Conclusions and outlook

Extratropical cyclones originating over the North Atlantic are fundamental to the everyday weather in Europe. In the past, studies of the response of cyclonic activity to global climate change have mainly focussed on the effect caused by increasing greenhouse gas concentrations. It is still under debate how the number, intensity and location of extratropical cyclones respond to these changes since two competing energetic effects—a decreasing meridional temperature gradient and an increasing latent heat content of the atmosphere—take place simultaneously. Radiatively active aerosol particles play a role in the changing energy availability, as well, and should therefore be taken into account in this context.

This study addressed three specific questions concerning the influence of aerosols on North Atlantic cyclones with the help of the objective feature tracking algorithm TRACK.

Is there an aerosol signal in the past? From the 1960s to the 1990s, the anthropogenic emissions both decreased over North America and Europe. Therefore, the cyclonic activity in the North Atlantic/ European region was investigated in these two decades. The study evaluated the ERA40 reanalysis and a transient model simulation of the coupled atmosphere-ocean general circulation model (AOGCM) ECHAM5-HAM/MPIOM-HAMOCC5. Reanalysis and model showed good agreement from a climatological point of view, i.e., the AOGCM reproduced the general pattern of cyclone track density, genesis and lysis regions as well as intensity and lifetime. Time series related to cyclonic activity, in particular a count of deep cyclones (core pressure below 950 hPa) and the North Atlantic Oscillation Index, exhibited discrepancies, though. These discrepancies, however, could not be taken as an indication for the performance of the model since only one realisaton of the model was used for the comparison.

In ERA40, the northwestward shift of track density and mean cyclone intensities from the 1960s to the 1990s corresponded to the change from a predominantly negative to a predominantly positive NAO phase as shown by the ERA40 NAO index. In the AOGCM, on the other hand, the NAO exhibited stronger interannual variability compared to the reanalysis. Consequently, the inconsistent change in the patterns of track density and mean cyclone intensities between the two decades is reasonable.

The decades 1961–1970 and 1991–2000 were compared since the accompanying decrease in the aerosol load was expected to lead to a change in the patterns of track density and other cyclone-related parameters opposite to what can be seen in Chapter 4. However, there was no indication for such an aerosol signal in the data.

Are there aerosol effects in the future? In the second part of this study, the influence of aerosols on the distribution and intensity of cyclones in the future was analysed. For this purpose, a set of transient simulations of ECHAM4/OPYC3 (Roeckner et al., 1999) was used. Here, the results presented by Roeckner et al. (1999) were expanded on by focussing on the behaviour of North Atlantic cyclones in the simulations. ECHAM4/OPYC3 represents a proven and tested AOGCM. Its interactive sulphur cycle scheme was state-of-the-art when the simulations were performed and is comparable to approaches taken in other, more current GCMs. At the time when the study was performed for this doctoral thesis, no comparable simulations of ECHAM5-HAM were available.

The transient ECHAM4/OPYC3 simulations were particularly suitable to address the question above since they allowed the separation of the greenhouse gas and the direct sulphate aerosol effects. Such a separation between the effects of the two forcings on cyclonic behaviour had not been attempted previously.

The effects of greenhouse gases and scattering sulphate aerosol of anthropogenic origin when comparing a present to a future time period can be summarised as follows:

Temperature: The greenhouse gas effect caused a warming in summer and winter whereas the direct radiative effect of SO_4^{2-} led to a cooling. The sulphate-induced cooling only attenuated the greenhouse gas-induced warming, though.

Baroclinicity: Anthropogenic greenhouse gases tended to reduce the baroclinicity of the atmosphere over the North Atlantic/European region while SO_4^{2-} tended to increase it.

Track density: Over Europe, the track density exhibited a northward shift in winter in the greenhouse gas scenario. The sulphate aerosol had the opposite effect, albeit of a smaller magnitude.

Cyclone intensity: While the number of cyclones with core pressures below 970 hPa increased significantly in the future when considering only greenhouse gases, it changed only insignificantly when also taking the direct sulphate effect into account.

The increasing sulphate concentration thus dampened the simulated response of the climate system to the greenhouse gas forcing, but could, in general, not reverse it. Interestingly, the strongest response to the aerosol forcing often coincided spatially with the region of the strongest response to the greenhouse gas forcing and not the region of the strongest emission sources.

Do aerosols influence an individual cyclone? The third part of this study analysed the influence of aerosols on specific meteorological parameters along the track of an individual cyclone. For this purpose, a case study experiment was performed by simulating the cyclone *Grace* which developed over the North Atlantic in March 2000. Two ensembles were produced with ECHAM5-HAM: one included the full AeroCom emission inventory, the other only the subset of the emission inventory comprised by natural emissions. Concerning the temporal evolution of selected meteorological parameters along the track of the cyclone *Grace*, the inclusion of anthropogenic aerosols caused no discernible effect compared to the ensemble which included only the emissions from natural aerosol sources. The results suggest that aerosol effects on cyclones occur only on a long-term basis, as shown in the previous part of this study, and that the difference in the aerosol burden of the ensembles wis not sufficient to cause a detectable difference in the development of the cyclone *Grace*. The setup of the case study experiment or, respectively, its subsequent analysis proved to be inappropriate to answer the above question. Furthermore, while the nudging was imperative to perform the case study simulations, its effects of forcing the model to the observed climatology may outweigh the aerosol effects.

Outlook

Within the framework of this study, only a part of the complex interactions between aerosols and cyclones could be examined. In particular, the influence of the direct sulphate effect was analysed. To study indirect aerosol effects or the effects of other types of aerosols, especially the effects of strongly absorbing aerosols such as soot, ECHAM5-HAM (Stier et al., 2005), which is now available, constitutes an important tool.

An interesting next step to the work presented here would be to use equilibrium simulations that allow to study the effect of anthropogenic aerosol species or the effect of main emission source regions separately. A set of such simulations is planned for ECHAM5-HAM. Due to the internal variability of the atmosphere, such a set of equilibrium simulations should preferably contain several realisations of each emission scenario. However, ECHAM5-HAM requires a large amount of computing power. Therefore, producing ensembles of the different emission scenarios may not be feasible.

With the regard to cyclones, the equilibrium simulations may improve the understanding of the mechanisms involved in the interaction of aerosols and cyclones. While the comparison of individual cyclones of separate equilibrium simulations would not be possible, new insight may be gained by examining the average properties of specific cyclone classes. E.g., cyclones could be classified according to their genesis region which would preferably be chosen in relation to the main emission source regions. When studying parameters along the cyclone tracks, care should be taken to include not only the four gridpoints closest to the cyclone centre, but rather to determine the whole area influenced by the passing cyclone.

One method to do so is the watershed segmentation method (Muskulus & Jacob, 2005).

Koren et al. (2005) found a strong correlation between the presence of aerosols and the structural properties of convective clouds in daily satellite data over the North Atlantic. They conclude that pollution, desert dust and biomass burning aerosols systematically invigorate convective clouds. Given this aerosol influence on convective clouds, the convection associated with the cold fronts of cyclones should be examined with regard to the influence of aerosol indirect effects on the cyclone's warm conveyor belt, which plays a major role in the cyclone's transport of water vapour, and hence latent energy. For this purpose, an algorithm to objectively detect fronts in gridded data is needed (e.g., Hewson, 1998). The interactions of aerosols and frontal convection should be studied with a model capable of resolving mesoscale processes while at the same time accounting for both direct and indirect aerosol effects.

Appendix A

Cyclone climatologies

The following table provides a comprehensive overview of cyclone climatologies. Care was taken not to restrict the presented studies to the region considered in this disseration only.

Table A.1: Cyclone climatologies. For abbreviations see Appendix B.

Author(s)	Data source	Horizontal resolution	Sampling time interval [h]	Analysis period	Tracking done?	Area	Season
Alpert et al. (1990a)	ECMWF analyses	2.5° ×2.5°	12	1982–1987	Yes	Med: 0–60°N, 0–60°E	Monthly
Bartholy et al. (2006)	ERA40	2.5° ×2.5°	6	1957–2002	Yes	NAE: 30°–75°N, 45°W–40°E	DJF, JJA
Bell & Bosart (1989)	NMC analyses	2° ×5°	12	1962–1977	Yes	NH: 20°–90°N	Monthly
Benestad & Chen (2006)	NMC ds195.5	2.5° ×2.5°	12	1955–1994	No	NAE: 20°–75°N, 80°W–40°E	Annual, monthly
	ERA40		24	1958–2002			
Blender et al. (1997)	ECMWF analyses	T106	6h	1990–1994	Yes	NAE: 30°–80°N, 80°W–30°E	NDJFM
Campins et al. (2006)	HIRLAM(INM)-0.5deg	0.5° ×0.5°	6h	1995–2003	Yes	Med: 15.5°–65°N, 66.5°W–30°E	Seasonal
Eichler & Higgins (2006)	ERA40	2.5° ×2.5°	6	1971–2000	Yes	PNA: 0–70°N, 110°E–0	JFM, AMJ, JAS, OND
	NCEP/NCAR			1950–2002			
Favre & Gershunov (2006)	NCEP/NCAR	2.5° ×2.5°	24	1950–2001	Yes	NP: 0–90°N, 80°E–110°W	JFM
Geng & Sugi (2001)	NCEP/NCAR	2.5° ×2.5°	6	1958–1998	Yes	NA: 45°–80°N, 60°W–0	DJF
Graham & Diaz (2001)	NCEP/NCAR	2.5° ×2.5°	6	1949–1998	Yes	NP: 30°–50°N, 150°W–30°E	DJFM
Gulev et al. (2001)	NCEP/NCAR	2.5° ×2.5°	6	1958–1999	Yes	NH	JFM
Haak & Ulbrich (1996)	ECMWF analyses	T63	24	1980–1993	No	NA: 30°–90°N, 60°W–60°E	Monthly
Hanson et al. (2004)	ERA15 + ECMWF analyses	2.5° ×2.5°	6	1979–2001	Yes	NAE: 20°–80°N, 80°W–30°E	ONDFJM
	NCEP/NCAR						
Hirsch et al. (2001)	NCEP/NCAR	2.5° ×2.5°	6	1951–1997	Yes	US east coast	ONDJFMA
Hodges et al. (2003)	ERA15 + ECMWF analyses	T42	6	1979–2001	Yes	Global	DJF, JJA
	NCEP/NCAR			1979–1996			

Table A.1: Continued from previous page.

Author(s)	Data source	Horizontal resolution	Sampling time interval [h]	Analysis period	Tracking cyclones	Area	Season
	NCEP/DOE			1979–1995			
	NASA GEOS-1			1980–1993			
Hoskins & Hodges (2002)	ERA15 + ECMWF analyses	T42	6	1979–2000	Yes	NH extratropics	DJF
Hoskins & Hodges (2005)	ERA40	T42	6	1958–2002	Yes	SH extratropics	Seasonal
Jones & Simmonds (1993)	Numerical analyses BoM	≈500 km at 45°S	24	1975–1990	Yes	SH	Seasonal
Keable et al. (2002)	NCEP/NCAR	n. s.	6	1958–1997	Yes	SH	Seasonal
Keller et al. (2006)	NCEP/NCAR	2.5°×2.5°	6	1977–2003	No	NP	NDJFM
Key & Chan (1999)	NCEP/NCAR	2.5°×2.5°	12	1958–1997	Yes	Latitude zones: 0–30°, 30°–60°, 60°–90°; certain regions	Seasonal
Lambert (1988)	ECMWF/WMO data set	n. s.	24	1980–1984	No	Global	Winter
	CCC GCM I	T20	24	5a			
Lambert (1996)	NCAR MSLP data + NMC Canada operational analyses	5°×5°	24	1899–1991	No	NH	DJF
Lambert et al. (2002)	NCEP/NCAR	n. s.	12	1979–1988	No	NH, SH: extratropics	Winter
	BMRC, CCC, COLA, CSIRO, CSU, DERF, ECMWF, GLA, GSFC, MRI, RPN, UGAMP, UKMO AMIP simulations	Various	12/24				
	ERA15	n. s.	12				
Lim (2005)	NCEP/DOE	T62	6	1979–2000	Yes	SH, NH	Seasonal
Lim & Simmonds (2007)	ERA40	125 km	6	1979–2000	Yes	SH: 25°–90°S	JJA
Maheras et al. (2001)	NCEP/NCAR	2.5°×2.5°	6	1958–1997	No	Med: 0–65°N, 20°W–50°E	Seasonal, daily
Nieto et al. (2005)	NCEP/NCAR	2.5°×2.5°	24	1958–1998	Yes	NH: 20°–70°N	Monthly
Paciorek et al. (2002)	NCEP/NCAR	2.5°×2.5°	12	1948–1999	No	NH: 20°–70°N	DJF
Pezza & Ambrizzi (2003)	NCEP/NCAR	2.5°×2.5°	24	1973–1996	Yes	SH	JJA
Picornell et al. (2001)	HIRLAM(INM)-0.5deg	0.5°×0.5°	6	1995–1999	Yes	Med: 29°–49°N, 12°W–18°E	Seasonal
Pinto et al. (2005)	NCEP/NCAR	T62, T42	6, 12	1958–1998	Yes	NH: 20°–90°N	ONDJFM
Rudeva & Gulev (2007)	NCEP/NCAR	2.5°×2.5°	1	1948–2004	Yes	NH	JFM, JAS
Schneidereit et al. (2007)	ERA40	T106	6	1958–2002	Yes	NA: 20°–90°N, 90°W–40E	DJF
Serreze et al. (1993)	NMC SLP set	≈400 km	24	1952–1989	Yes	Arctic: 55°–90°N	DJF, JJA
Serreze (1995)	NMC SLP set	≈400 km	12	1973–1992	Yes	Arctic: 35°–90°N	winter, summer

Table A.1: Continued from previous page.

Author(s)	Data source	Horizontal resolution	Sampling time interval [h]	Analysis period	Tracking cyclones	Area	Season
Sickmöller et al. (2000)	ERA15 + ECMWF analyses	1.25°×1.25°	6	1980–1997	Yes	NA, NP: 30°–80°N	DJF
Simmonds & Keay (2000a)	NCEP/NCAR	2.5°×2.5°	6	1958–1997	Yes	SH: extratropics	Seasonal
Sinclair (1994)	ECMWF analyses	2.5°×2.5°	12	1980–1986	Yes	SH: 30°–90°S	DJF, JJA, DJFM, JJAS, annual
Sinclair (1995)	ECMWF analyses	2.5°×2.5°	12	1980–1986	Yes	SH: 30°–90°S	NDJFMA, MJJASO, annual
Smith et al. (2002)	NCEP/NCAR	2.5°×2.5°	12	1953–1999	No	Global, but only NH & eastern North America shown	DJF, Oct, Dec, Feb, Apr
Spanos et al. (2003)	NCEP/NCAR	2.5°×2.5°	6	1958–1997	No	Med: 30°–50°N, 5°–35°E	AMJJASO
Trigo et al. (1999)	ERA15 + initialised reanalysis	T106	6	1979–1996	Yes	Med: 24.75°–50.625°N, 15.75°W–45°E	Monthly
Trigo et al. (2002)	ECMWF initialised reanalysis	T106	6	1979–1996	Yes	Med: 24.75°–50.625°N, 15.75°W–45°E	Monthly
Trigo (2006)	ERA40	T106	6	1958–2000	Yes	NAE: 20°–75°N, 85°W–70°E	DJFM
	NCEP/NCAR	2.5°×2.5°					
Wang et al. (2006)	ERA40	250 km × 250 km	6	1958–2001	Yes	NH, SH: 30°–70°	JFM, AMJ, JAS, OND
	NCEP/NCAR						
Wernli & Schwierz (2006)	ERA40	1°×1°	6	1958–2001	Yes	Global	Seasonal
Zhang et al. (2004)	NCEP/NCAR	2.5°×2.5°	6	1948–2002	Yes	Arctic: 30°–90°N	ONDJFM, AMJJAS

Appendix B

Abbreviations and acronyms

AERONET	Aerosol Robotic Network
AMJ	April, May, June
AOD	Aerosol Optical Depth
AOGCM	Atmosphere-Ocean General Circulation Model
BC	Black Carbon
BoM	Bureau of Meteorology, Australia
CCC GCM	Canadian Climate Centre General Circulation Model
CCCma GCM	Canadian Centre for Climate Modelling and Analysis General Circulation Model
CCN	Cloud Condensation Nucleus/Nuclei
CDNC	Cloud Droplet Number Concentration(s)
CFC	Chlorofluorocarbon
DJF	December, January, February
DOE	Department of Energy
ECHAM	European Centre HAmburg Model
ECMWF	European Centre for Medium-Range Weather Forecasts
ENSO	El Niño Southern Oscillation
EOF	Empirical Orthogonal Function
ERA	ECMWF ReAnalysis
EZMW	Europäisches Zentrum für mittelfristige Wettervorhersage (ECMWF)
GCM	General Circulation Model
GEMS	Global Earth-system Monitoring using Space and in-situ data
GEOS	Goddard Earth Observing System
GM	Greenwich Meridian
HCFC	Hydrochlorofluorocarbon

HFC	Hydrofluorocarbon
HIRLAM	High Resolution Limited Area Model
HOPE	Hamburg Ocean Primitive Equation model
IFS	Integrated Forecasting System
IGY	International Geophysical Year (July 1957 to December 1958)
INM	Instituto Nacional de Meteorologia—National Institute of Meteorology, Spain
JAS	July, August, September
JFM	January, February, March
JJA	June, July, August
JMA	Japan Meteorological Agency
Med	Mediterranean
MJJASO	May, June, July, August, September, October
MPIOM	Max Planck Institute Ocean Model
MSLP	Mean Sea Level Pressure
NA	North Atlantic
NAE	North Atlantic/Europe
NASA	National Aeronautics and Space Administration
NAOI	North Atlantic Oscillation Index
NAO	North Atlantic Oscillation
NCAR	National Center for Atmospheric Research
NCEP	National Center for Environmental Prediction
NDJFM	November, December, January, February, March
NDJFMA	November, December, January, February, March, April
NH	Northern Hemisphere
NMC	National Meteorological Center
NP	North Pacific
n. s.	not specified
NWP	Numerical Weather Prediction
OND	October, November, December
ONDJFM	October, November, December, January, February, March
ONDJFMA	October, November, December, January, February, March, April
OPYC	Ocean in isoPYcnal Coordinates
POM	Particulate Organic Matter
RRTM	Rapid Radiation Transfer Model
SH	Southern Hemisphere

SRES	Special Report on Emission Scenarios
SST	Sea Surface Temperature
SYNOP	Surface Synoptic Observation
UKMO	United Kingdom Meteorological Office
US	United States

Bibliography

ACKERMAN, A., TOON, O., STEVENS, D., HEYMSFIELD, A., RAMANATHAN, V., AND WELTON, E. (2000). Reduction of tropical cloudiness by soot. *Science* **288**, 1042–1047.

AFFELD, B. (1996). *Zugbahnen der Tiefdruckgebiete in täglichen ECMWF-Analysen über dem Nordatlantik*. Master's thesis, Universität Hamburg. 101pp.

AKYILDIZ, V. (1985). Systematic errors in the behavior of cyclones in ECMWF operational models. *Tellus* **37A**, 297–308.

ALBRECHT, B. (1989). Aerosols, cloud microphysics, and fractional cloudiness. *Science* **245**, 1227–1230.

ALEXANDERSSON, H., SCHMITH, T., IDEN, K., AND TUOMENVIRTA, H. (1998). Long-term trend variations of the storm climate over NW Europe. *Global Atmos. Ocean System* **6**, 97–120.

ALPERT, P., NEEMAN, B. U., AND SHAY-EL, Y. (1990a). Climatological analysis of Mediterranean cyclones using ECMWF data. *Tellus* **42A**, 65–77.

ALPERT, P., NEEMAN, B. U., AND SHAY-EL, Y. (1990b). Interannual variability of cyclone tracks in the in the mediterranean. *J. Climate* **3**, 1474–1478.

ANDERSON, D. (2000). *Feature tracking validation of storm tracks in model data*. Ph.D. thesis, University of Reading.

ANDERSON, D., HODGES, K. I., AND HOSKINS, B. J. (2003). Sensitivity of feature based analysis methods of storm tracks to the form of background field removal. *Mon. Wea. Rev.* **131**, 565–573.

ÅNGSTRÖM, A. (1962). Atmospheric turbidity, global illumination and planetary albedo of the earth. *Tellus* **14**, 435–450.

ANTHES, R. A. (1974). Data assimilation and initialization of hurricane prediction models. *J. Atmos. Sci.* **31**, 702–719.

ARAKAWA, A. AND LAMB, V. R. (1977). Computational design of the basic dynamical processes of the UCLA general circulation model. *Methods Comput. Phys.* **17**, 173–265.

AYRAULT, F. AND JOLY, A. (2000a). Une nouvelle typologie des dépressions météorologique: Classification des phases de maturation. *C. R. Acad. Sci. Paris, série IIa* **330**, 167–172.

AYRAULT, F. AND JOLY, A. (2000b). Une nouvelle typologie des dépressions météorologique: Nouvelle perspective climatologique. *C. R. Acad. Sci. Paris, série IIa* **330**, 173–178.

BACON, S. AND CARTER, D. (1991). Wave climate changes in the North-Atlantic and North-Sea. *Int. J. Climatol.* **11**, 545–558.

BAEHR, C., POUPONNEAU, B., AYRAULT, F., AND JOLY, A. (1999). Dynamical characterization of the FASTEX cyclogenesis cases. *Q. J. R. Meteorol. Soc.* **125**, 3469–3494.

BARDIN, M. Y. AND POLONSKY, A. B. (2005). North Atlantic Oscillation and synoptic variability in the European-Atlantic region in winter. *Izvestia Atmos. Ocean Phys.* **41**, 127–136.

BARTHOLY, J., PONGRÁCZ, R., AND PATTANTYÚS-ÁBRAHÁM, M. (2006). European cyclone track analysis based on ECMWF ERA-40 data sets. *Int. J. Climatol.* **26**, 1517–1527.

BAUER, M. AND DEL GENIO, A. D. (2006). Composite analysis of winter cyclones in a GCM: Influence on climatological humidity. *J. Climate* **19**, 1652–1672.

BEERSMA, J. J., RIDER, K. M., KOMEN, G. J., KAAS, E., AND KHARIN, V. V. (1997). An analysis of extra-tropical storms in the North Atlantic region as simulated in a control and 2xCO_2 time-slice experiment with a high-resolution atmospheric model. *Tellus* **49A**, 347–361.

BELL, G. D. AND BOSART, L. F. (1989). A 15-year climatology of northern hemisphere 500 mb closed cyclone and anticyclone centers. *Mon. Wea. Rev.* **117**, 2142–2162.

BENESTAD, R. AND CHEN, D. (2006). The use of a calculus-based cyclone identification method for generating storm statistics. *Tellus* **58A**, 473–486.

BENGTSSON, L., HODGES, K., AND ESCH, M. (2007a). Tropical cyclones in a T159 resolution global climate model: Comparison with observations and re-analyses. *Tellus* **59A**, 396–416.

BENGTSSON, L., HODGES, K., ESCH, M., KEENLYSIDE, N., KORNBLUEH, L., LUO, J.-J., AND YAMAGATA, T. (2007b). How may tropical cyclones change in a warmer climate? *Tellus* **59A**, 539–561.

BENGTSSON, L., HODGES, K., AND FROUDE, L. (2005). Global observations and forecast skill. *Tellus* **57A**, 515–527.

BENGTSSON, L., HODGES, K., AND HAGEMANN, S. (2004a). Sensitivity of large-scale atmospheric analyses to humidity observations and its impact on the global water cycle and tropical and extratropical weather systems in ERA40. *Tellus* **56A**, 202–217.

BENGTSSON, L., HODGES, K., AND HAGEMANN, S. (2004b). Sensitivity of the ERA40 reanalysis to the observing system: Determination of the global atmospheric circulation from reduced observations. *Tellus* **56A**, 456–471.

BENGTSSON, L., HODGES, K. I., AND ROECKNER, E. (2006a). Storm tracks and climate change. *J. Climate* **19**, 3518–3543.

BENGTSSON, L., HODGES, K. I., ROECKNER, E., AND BROKOPF, R. (2006b). On the natural variability of the pre-industrial European climate. *Clim. Dyn.* **27**, 743–760.

BERLINER WETTERKARTE (2000). Tägliche Wetterkarten März 2000. Published by Berliner Wetterkarte e. V. and the Institute for Meteorology, Free University of Berlin.

BLACKMON, M. L. (1976). A climatological spectral study of the 500 mb geopotential height of the northern hemisphere. *J. Atmos. Sci.* **33**, 1607–1623.

BLENDER, R., FRAEDRICH, K., AND LUNKEIT, F. (1997). Identification of cyclone track regimes in the North Atlantic. *Q. J. R. Meteorol. Soc.* **123**, 727–741.

BRENGUIER, J., PAWLOWSKA, H., SCHÜLLER, L., PREUSKER, R., FISCHER, J., AND FOUQUART, Y. (2000). Radiative properties of boundary layer clouds: Droplet effective radius versus number concentration. *J. Atmos. Sci.* **57**, 803–821.

BRINKOP, S. AND ROECKNER, E. (1995). Sensitivity of a general-circulation model to parameterizations of cloud-turbulence interactions in the atmospheric boundary-layer. *Tellus* **47A**, 197–220.

BROMWICH, D. H., FOGT, R. L., HODGES, K. I., AND WALSH, J. E. (2007). A tropospheric assessment of the ERA-40, NCEP, and JRA-25 global reanalyses in the polar regions. *J. Geophys. Res.* **112**. Art. No. D10111.

BYRKJEDAL, Ø., KVAMSTØ, N. G., MELAND, M., AND JANSEN, E. (2006). Sensitivity of last glacial maximum climate to sea ice conditions in the Nordic Seas. *Clim. Dyn.* **26**, 473–487.

CAMPINS, J., JANSÀ, A., AND GENOVÉS, A. (2006). Three-dimensional structure of western Mediterranean cyclones. *Int. J. Climatol.* **26**, 323–343.

CAO, Z. AND ZHANG, D.-L. (2004). Tracking surface cyclones with moist potential vorticity. *Adv. Atmos. Sci* **21**, 830–835.

CARNELL, R. E. AND SENIOR, C. A. (1998). Changes in mid-latitude variability due to increasing greenhouse gases and sulfate aerosols. *Clim. Dyn.* **14**, 369–383.

CARNELL, R. E., SENIOR, C. A., AND MITCHELL, J. F. B. (1996). An assessment of measures of storminess: Simulated changes in northern hemisphere winter due to increasing CO_2. *Clim. Dyn.* **12**, 467–476.

CARTER, D. AND DRAPER, L. (1988). Has the northeast Atlantic become rougher? *Nature* **322**, 494.

CHANDLER, M. AND JONAS, J. (1999). Atlas of extratropical cyclones (1961- 1998). NASA Goddard Institute for Space Studies and the Center for Climate System Research at Columbia University. New York, NY, USA.

CHANG, E. AND SONG, S. (2006). The seasonal cycles in the distribution of precipitation around cyclones in the western North Pacific and Atlantic. *J. Atmos. Sci.* **63**, 815–839.

CHARNEY, J. G. (1947). The dynamics of long waves in a baroclinic westerly current. *J. Meteorol.* **4**, 135–162.

CLAUSSEN, M., LOHMANN, U., ROECKNER, E., AND SCHULZWEIDA, U. (1994). A global data set of land-surface parameters. Max Planck Institut für Meteorologie, Report No. 135, Hamburg, Germany, 23 pp.

CONDRON, A., BIGG, G., AND RENFREW, I. (2006). Polar mesoscale cyclones in the northeast Atlantic: Comparing climatologies from ERA-40 and satellite imagery. *Mon. Wea. Rev.* **134**, 1518–1533.

DACRE, H. F. (2004). *Climatology and development mechanisms of frontal waves*. Ph.D. thesis, Department of Meteorology, University of Reading.

DEAN, D. (1993). *A Northern Hemisphere climatology of 500hPa trough merger and fracture*. Master's thesis, State University of New York at Albany. 234pp.

DEAN, D. B. AND BOSART, L. F. (1996). Northern hemisphere 500-hPa trough merger and fracture: A climatology and case study. *Mon. Wea. Rev.* **124**, 2644–2671.

DENTENER, F., KINNE, S., BOND, T., BOUCHER, O., COFALA, J., GENEROSO, S., P.GINOUX, S.GONG, HOELZEMANN, J. J., ITO, A., L.MARELLI, PENNER, J. E., PUTAUD, J.-P., TEXTOR, C., M.SCHULZ, VAN DER WERF, G. R., AND WILSON, J. (2006). Emissions of primary aerosol and precursor gases in the years 2000 and 1750, prescribed datasets for AeroCom. *Adv. Chem. Phys.* **6**, 4321–4344.

DIERCKX, P. (1981). An algorithm for surface fitting with spline functions. *SIAM J. Numer. Anal.* **19**, 1286–1304.

DIERCKX, P. (1984). Algorithms for smoothing data on the sphere with tensor product splines. *Computing* **32**, 319–342.

DOS SANTOS MESQUITA, M. (2006). *Tracking Summer Extra-Tropical Storms: A Climatological Overview and Variability in the Northern Hemisphere*. Master's thesis, Geophysical Institute, University of Bergen.

DWD (2000). Wetterkarte. Amtsblatt des Deutschen Wetterdienstes D7311 A.

EADY, E. T. (1949). Long waves and cyclone waves. *Tellus* **1**, 33–52.

EICHLER, T. AND HIGGINS, W. (2006). Climatology and ENSO-related variability of North American extratropical cyclone activity. *J. Climate* **19**, 2076–2093.

FAVRE, A. AND GERSHUNOV, A. (2006). Extra-tropical cyclonic/anticyclonic activity in North-Eastern Pacific and air temperature extremes in western North America. *Clim. Dyn.* **26**, 617–629.

FEICHTER, J., KJELLSTRÖM, E., RODHE, H., DENTENER, F., LELIEVELD, J., AND ROELOFS, G.-J. (1996). Simulation of the tropospheric sulfur cycle in a global climate model. *Atmos. Env.* **30**, 1693–1707.

FEICHTER, J., LOHMANN, U., AND SCHULT, I. (1997). The atmospheric sulfur cycle and its impact on the shortwave radiation. *Clim. Dyn.* **13**, 235–246.

FEICHTER, J., ROECKNER, E., LOHMANN, U., AND LIEPERT, B. (2004). Nonlinear aspects of the climate response to greenhouse gas and aerosol forcing. *J. Climate* **17**, 2384–2398.

FEINGOLD, G., EBERHARD, W., VERON, D., AND PREVIDI, M. (2003). First measurements of the Twomey indirect effect using ground-based remote sensors. *Geophys. Res. Lett.* **30**. Art. No. 1287.

FEREK, R., HEGG, D., HOBBS, P., DURKEE, P., AND NIELSEN, K. (1998). Measurements of ship-induced tracks in clouds off the Washington coast. *J. Geophys. Res.* **103**, 23199–23206.

FISCHER-BRUNS, I., FEICHTER, J., AND BANSE, D. F. (2007). Subm. to Clim. Dyn.

FISCHER-BRUNS, I., VON STORCH, H., GONZÁLES-ROUCO, J. F., AND ZORITA, E. (2005). Modelling the variability of midlatitude storm activity on decadal to century time scales. *Clim. Dyn.* **25**, 461–476.

FOUQUART, Y. AND BONNEL, B. (1980). Computations of solar heating of the Earth's atmosphere: A new parameterization. *Beitr. Phys. Atmosph.* **53**, 35–62.

FRANKE, R. (1994). Die nordatlantischen Orkantiefs mit einem Kerndruck von 950 hPa und weniger während der letzten 38 Jahre. *Der Wetterlotse* **570**, 199–207.

FROUDE, L. S. R. (2005). *The Predictability of Storm Tracks*. Ph.D. thesis, Environmental Systems Sciene Centre, University of Reading.

FROUDE, L. S. R., BENGTSSON, L., AND HODGES, K. I. (2007a). The predictability of extratropical storm tracks and the sensitivity of their prediction to the observing system. *Mon. Wea. Rev.* **135**, 315–333.

FROUDE, L. S. R., BENGTSSON, L., AND HODGES, K. I. (2007b). The prediction of extratropical storm tracks by the ECMWF and NCEP ensemple prediction systems. *Mon. Wea. Rev.* **135**, 2545–2567.

FYFE, J. C. (2003). Extratropical southern hemisphere cyclones: Harbingers of climate change? *J. Climate* **16**, 2802–2805.

GAFFNEY, S. J. (2004). *Probabilistic Curve-Aligned Clustering and Prediction with Regression Mixture Models*. Ph.D. thesis, University of California, Irvine. Available online at http://www.datalab.uci.edu/papers/sgaffney_thesis.pdf (accessed 29/09/2007).

GAFFNEY, S. J., ROBERTSON, A. W., SMYTH, P., CAMARGO, S. J., AND GHIL, M. (2007). Probabilistic clustering of extratropical cyclones using regression mixture models. *Clim. Dyn.* **29**.

GANZEVELD, L., LELIEVELD, J., AND ROELOFS, G. (1998). A dry deposition parameterization for sulfur oxides in a chemistry and general circulation model. *J. Geophys. Res.* **103**, 5679–5694.

GENG, Q. AND SUGI, M. (2001). Variability of the North Atlantic cyclone activity in winter analyzed from NCEP-NCAR reanalysis data. *J. Climate* **14**, 3863–3873.

GENG, Q. AND SUGI, M. (2003). Possible change of extratropical cuyclone activituy due to enhanced greenhouse gases and sulfate aerosol–study with a high-resolution AGCM. *J. Climate* **16**, 2262–2274.

GIBSON, J., KÅLLBERG, P., UPPALA, S., NOMURA, A., HERNANDEZ, A., AND SERRANO, E. (1997). ERA description. ECMWF Re-Analysis Final Rep. Series 1, 71 pp.

GIORGI, F. AND CHAMEIDES, W. (1986). Rainout lifetimes of highly soluble aerosols and gases as inferred from simulations with a general-circulation model. *J. Geophys. Res.* **91**, 14367–14376.

GODFRED-SPENNING, C. R. AND SIMMONDS, I. (1996). An analysis of Antarctic sea-ice and extratropical cyclone associations. *Int. J. Climatol.* **16**, 1315–1332.

GOLDFARB, D. (1969). Extension of Davidons variable metric method to maximization under linear inequality and equality constraints. *SIAM J. Appl. Math.* **17**, 739–764.

GRAHAM, N. AND DIAZ, H. (2001). Evidence for intensification of North Pacific winter cyclones since 1948. *Bull. Am. Meteor. Soc.* **82**, 1869–1893.

GRASSL, H. (1975). Albedo reduction and radiative heating of clouds by absorbing aerosol particles. *Beitr. Phys. Atmosph.* **48**, 199–210.

GRAY, S. AND DACRE, H. (2006). Classifying dynamical forcing mechanisms using a climatology of extratropical cyclones. *Q. J. R. Meteorol. Soc.* **132**, 1119–1137.

GREEVES, C. Z., POPE, V. D., STRATTON, R. A., AND MARTIN, G. M. (2006). Representation of northern hemisphere winter storm tracks in climate models. *Clim. Dyn.* .

GRIGORIEV, S., GULEV, S. K., AND ZOLINA, O. (2000). Innovative software facilitates cyclone tracking and analysis. *EOS Trans. Amer. Geophys. Union* **81**, 170.

GULDBERG, A., KAAS, E., DEQUE, M., YANG, S., AND THORSEN, S. (2005). Reduction of systematic errors by empirical model correction: Impact on seasonal prediction skill. *Tellus* **57A**, 575–588.

GULEV, S., JUNG, T., AND RUPRECHT, E. (2002). Climatology and interannual variability in the intensity of synoptic-scale processes in the North Atlantic from the NCEP-NCAR reanalysis data. *J. Climate* **15**, 809–828.

GULEV, S. K., ZOLINA, O., AND GRIGORIEV, S. (2001). Extratropical cyclone variability in the northern hemisphere winter from the NCEP/NCAR reanalysis data. *Clim. Dyn.* **17**, 795–809.

HAAK, U. AND ULBRICH, U. (1996). Verification of an objective cyclonle climatology for the North Atlantic. *Meteorol. Z.* **5**, 24–30.

HAGEMANN, S. (2002). *An improved land surface parameter dataset for global and regional climate models*. Tech. rep., Max-Planck-Institut für Meteorologie, Hamburg. Report 336, Max-Planck-Institut für Meteorologie, Hamburg.

HANSEN, J., SATO, M., AND RUEDY, R. (1997). Radiative forcing and climate response. *J. Geophys. Res.* **102**, 6831–6864.

HANSON, C. E., PALUTIKOF, J. P., AND DAVIES, T. D. (2004). Objective cyclone climatologies of the North Atlantic— a comparison between the ECMWF and NCEP reanalyses. *Clim. Dyn.* **22**, 757–769.

HAYDEN, B. P. (1981). Cyclone occurrence mapping–equal-area or raw frequencies. *Mon. Wea. Rev.* **109**, 168–172.

HAYWOOD, J. M. AND SHINE, K. P. (1995). The effect of anthropogenic sulfate and soot aerosol on the clear sky planetary radiaton budget. *Geophys. Res. Lett.* **22**, 603–606.

HEWSON, T. D. (1998). Objective fronts. *Meteorol. Appl.* **5**, 37–65.

HIBLER, W. (1979). Dynamic thermodynamic sea ice model. *J. Phys. Oceanogr.* **9**, 815–846.

HIRSCH, M. E., DEGAETANO, A. T., AND COLUCCI, S. J. (2001). An East Coast winter storm climatology. *J. Climate* **14**, 882–899.

HODGES, K. I. (1994). A general method for tracking analysis and its application to meterological data. *Mon. Wea. Rev.* **122**, 2573–2586.

HODGES, K. I. (1995). Feature tracking on the unit sphere. *Mon. Wea. Rev.* **123**, 3458–3465.

HODGES, K. I. (1996). Spherical nonparameteric estimators applied to the UGAMP model integration for AMIP. *Mon. Wea. Rev.* **124**, 2914–2932.

HODGES, K. I. (1998). Feature-point detection using distance transforms: Application to tracking tropical convective complexes. *Mon. Wea. Rev.* **126**, 785–795.

HODGES, K. I. (1999a). Adaptive constraints for feature tracking. *Mon. Wea. Rev.* **127**, 1362–1373.

HODGES, K. I. (1999b). Extension of spherical nonparametric estimators to nonisotropic kernels: An oceanographic application. *Mon. Wea. Rev.* **127**, 214–227.

HODGES, K. I., HOSKINS, B. J., BOYLE, J., AND THORNCROFT, C. (2003). A comparison of recent reanalysis datasets using objective feature tracking: Storm tracks and tropical easterly waves. *Mon. Wea. Rev.* **131**, 2012–2037.

HODGES, K. I. AND THORNCROFT, C. D. (1997). Distribution and statistics of African mesoscale convective weather systems based on the ISCCP Meteosat imagery. *Mon. Wea. Rev.* **125**, 2821–2837.

HOPSCH, S., THORNCROFT, C., HODGES, K., AND AIYYER, A. (2007). West African storm tracks and their relationship to Atlantic tropical cyclones. *J. Climate* **20**, 2468–2483.

HOSKINS, B. J. AND HODGES, K. I. (2002). New perspectives on the northern hemisphere winter storm tracks. *J. Atmos. Sci.* **59**, 1041–1061.

HOSKINS, B. J. AND HODGES, K. I. (2005). A new perspective on southern hemisphere storm tracks. *J. Climate* **18**, 4108–4129.

HURRELL, J. W., KUSHNIR, Y., VISBECK, M., AND OTTERSEN, G. (2003). An overview of the North Atlantic oscillation. In *The North Atlantic Oscillation: Climate Significance and Environmental Impact* (Edited by J. W. Hurrell, Y. Kushnir, G. Ottersen, & M. Visbeck), Geophysical Monograph Series 134, pp. 1–35. AGU.

IPCC (1994). *IPCC Technical Guidelines for Assessing Climate Change Impacts and Adaptations. Part of the IPCC Special Report to the First Session of the Cnverfence of the Parties to the UN Framework Convention onClimate Change, Working Group II, Intergovernmental Panel on Climate Change*. CARTER, T. R., PARRY, M. L., HARASAWA, H., AND NISHIOKA, S. Eds. University College London, United Kingdom, and Center for Environmental Research, National Institute for Environmental Studies, Tsukuba, Japan, 59 pp.

IPCC (1996). *Climate Change 1995: The Science of Climate Change. Contribution of Working Group I to the Second Assessment Report of the Intergovernmental Panel on Climate Change*. HOUGHTON, J. T., FILHO, L. G. M., CALLENDAR, B. A., HARRIS, N., KATTENBERG, A., AND MASKELL, K. Eds. Cambridge University Press, 572 pp.

IPCC (2000). *IPCC Special Report on Emission Scenarios*. NAKICENOVIC, N., ALCAMO, J., DAVIS, G., DE VRIES, B., FENHANN, J., GAFFIN, S., GRÜBLER, K. G. A., JUNG, T. Y., KRAM, T., LA ROVERE, E. L., MICHAELIS, L., MORI, S., MORITA, T., PEPPER, W., PITCHER, H., PRICE, L., RAIHI, K., ROEHRL, A., ROGNER, H.-H., SANKOVSKI, A., SCHLESINGER, M., SHUKLA, P., SMITH, S., SWART, R., VAN ROOIJEN, S., VICTOR, N., AND DADI, Z. Eds. Cambridge University Press, 599 pp.

IPCC (2001). *Climate Change 2001: The Scientific Basis. Contribution of Working Group I to the Third Assessment Report of the Intergovernmental Panel on Climate Change*. HOUGHTON, J. T., DING, Y., GRIGGS, D., NOGUER, M., VAN DER LINDEN, P. J., AND XIAOSU, D. Eds. Cambridge University Press, 944 pp.

IPCC (2007). *Climate Change 2007: The Physical Science Basis. Contribution of Working Group I to the Fourth Assessment Report of the Intergovernmental Panel on Climate Change*. SOLOMON, S., QIN, D., MANNING, M., CHEN, Z., MARQUIS, M., AVERYT, K. B., TIGNOR, M., AND MILLER, H. L. Eds. Cambridge University Press, 996 pp.

JEUKEN, A., SIEGMUND, P., HEIJBOER, L., FEICHTER, J., AND BENGTSSON, L. (1996). On the potential of assimilating meteorological analyses in a global climate model for the purpose of model validation. *J. Geophys. Res.* **101**, 16939–16950.

JONES, A., ROBERTS, D., AND SLINGO, A. (1994). A climate model study of indirect radiative forcing by anthropogenic sulphate aerosols. *Nature* **370**, 450–453.

JONES, D. A. AND SIMMONDS, I. (1993). A climatology of southern hemisphere extratropical cyclones. *Clim. Dyn.* **9**, 131–145.

JUNG, T., GULEV, S., RUDEVA, I., AND SOLOVIOV, V. (2006). Sensitivity of extratropical cyclone characteristics to horizontal resolution in the ECMWF model. *Q. J. R. Meteorol. Soc.* **132**, 1839–1857.

KANAMITSU, M., EBISUZAKI, W., WOOLEN, J., POTTER, J., AND FIORINO, M. (2000). An overview of ncep/doe reanalysis2. Proc. Second Int. WCRP Conf. on Reanalysis, Wokefield Park, Reading, United Kingdom, WCRP-109, WMO/TD-No. 985, 14.

KARELSKY, S. (1961). Monthly and seasonal anticyclonicity and cyclocinicity in the Australian region–15 years (1946–1960) averages. Met. Study No. 13, AGPS, Canberra.

KEABLE, M., SIMMONDS, I., AND KEAY, K. (2002). Distribution and temporal variability of 500 hPa cyclone characteristics in the southern hemisphere. *Int. J. Climatol.* **22**, 131–150.

KELLER, L. M., MORGAN, M. C., HOUGHTON, D. D., AND LAZEAR, R. A. (2006). Synoptic-dynamic climatology of large scale cyclones in the North Pacific. *Mon. Wea. Rev.* **134**.

KEY, J. R. AND CHAN, A. C. K. (1999). Multidecadal global and regional trends in 1000 mb and 500 mb cyclone frequencies. *Geophys. Res. Lett.* **26**, 2053–2056.

KHAIROUTDINOV, M. AND KOGAN, Y. (2000). A new cloud physics parameterization in a large-eddy simulation model of marine stratocumulus. *Mon. Wea. Rev.* **128**, 229–243.

KIEHL, J., SCHNEIDER, T., PORTMANN, R., AND SOLOMON, S. (1999). Climate forcing due to tropospheric and stratospheric ozone. *J. Geophys. Res.* **104**, 31239–31254.

KISTLER, R., KALNAY, E., COLLINS, W., SAHA, S., WHITE, G., WOOLLEN, J., CHELLIAH, M., EBISUZAKI, W., KANAMITSU, M., KOUSKY, V., VAN DEN DOOL, H., JENNE, R., AND FIORINO, M. (2001). The NCEP-NCAR 50-year reanalysis: Monthly means CD-ROM and documentation. *Bull. Am. Meteor. Soc.* **82**, 247–267.

KLEIN, W. H. (1957). *Principal tracks and mean frequencies of cyclones and anticyclones in the Northern Hemisphere*. Tech. rep., U.S. Weather Bureau. U.S. Weather Bureau Research Paper 40, 60 pp.

KLOSTER, S., FEICHTER, J., REIMER, E., SIX, K., STIER, P., AND WETZEL, P. (2006). DMS cycle in the marine ocean-atmosphere system - a global model study. *Biogeosci.* **3**, 29–51.

KNIPPERTZ, P., ULBRICH, U., AND SPETH, P. (2000). Changing cyclones and surface wind speeds over the North Atlantic and Europe in a transient GHG experiment. *Clim. Res.* **15**, 109–122.

KÖNIG, W., SAUSEN, R., AND SIELMANN, F. (1993). Objective identification of cyclones in GCM simulations. *J. Climate* **6**, 2217–2231.

KÖPPEN, W. (1881). Die Zugbahnen der barometrischen Minima in Europa und auf dem nordatlantischen Ocean und ihr Einfluß auf Wind und Wetter bei uns. *Mittlgn. d. geogr. Gesellschaft in Hamburg* **1**, 76–97.

KOREN, I., KAUFMAN, Y., ROSENFELD, D., REMER, L., AND RUDICH, Y. (2005). Aerosol invigoration and restructuring of Atlantic convective clouds. *Geophys. Res. Lett.* **32**. Art.No. L14828.

KRÜGER, O. AND GRASSL, H. (2002). The indirect aerosol effect over Europe. *Geophysical Research Letters* **29**. Art. No. 1925.

KRÜGER, O. AND GRASSL, H. (2004). Albedo reduction by absorbing aerosols over China. *Geophys. Res. Lett.* **31**. Art. No. L02108.

LAMBERT, S. J. (1988). A cyclone climatology of the Canadian Climate Centre general circulation model. *J. Climate* **1**, 109–115.

LAMBERT, S. J. (1995). The effects of enhanced greenhouse warming on winter cyclone frequencies and strengths. *J. Climate* **8**, 1447–1452.

LAMBERT, S. J. (1996). Intense extratropical northern hemisphere winter cyclone events: 1899–1991. *J. Geophys. Res.* **101**, 21319–21325.

LAMBERT, S. J. (2004). Changes in winter cyclone frequencies and strengths in transient enhanced greenhouse warming simulations using two coupled climate models. *Appl. Opt.* **42**, 173–181.

LAMBERT, S. J. AND FYFE, J. C. (2006). Changes in winter cyclone frequencies and strengths simulated in enhanced greenhouse warming experiments: Results from the models participating in the IPCC diagnostic exercise. *Clim. Dyn.* **26**, 713–728.

LAMBERT, S. J., SHENG, J., AND BOYLE, J. (2002). Winter cyclone frequencies in thirteen models participating in the Atmospheric Model Intercomparison Project (AMIP1). *Clim. Dyn.* **19**, 1–16.

LE MARSHALL, J. F. AND KELLY, G. A. M. (1981). A January and July climatology of the southern hemisphere based on daily numerical analyses. *Aust. Meteorol. Mag.* **29**, 65–85.

LE TREUT, H. AND KALNAY, E. (1990). Comparison of observed and simulated cyclone frequency distribution as determined by an objective method. *Atmósfera* **3**, 57–71.

LECKEBUSCH, G. C., KOFFI, B., ULBRICH, U., PINTO, J. G., SPANGEHL, T., AND ZACHARIAS, S. (2006). Analysis of frequency and intensity of European winter storm events from a multi-model perspective, at synoptic and regional scales. *Clim. Res.* **31**, 59–74.

LECKEBUSCH, G. C. AND ULBRICH, U. (2004). On the relationship between cyclones and extreme wind events over Europe under climate change. *Global Planet. Change* **44**, 181–193.

LEFEVRE, R. J. AND NIELSEN-GAMMON, J. W. (1995). An objective climatology of mobile troughs in the northern hemisphere. *Tellus* **47A**, 638–655.

LEFOHN, A. S., HUSAR, J. D., AND HUSAR, R. B. (1999). Estimating historical anthropogenic global sulfur emission patterns for the period 1850–1990. *Atmos. Env.* **33**, 3435–3444.

LEONARD, S. R., TURNER, J., AND VAN DER WAL, A. (1999). An assessment of three automatic depression tracking schemes. *Meteorol. Appl.* **6**, 173–183.

LIEPERT, B. G., FEICHTER, J., LOHMANN, U., AND ROECKNER, E. (2004). Can aerosols spin down the water cycle in a warmer and moister world? *Geophys. Res. Lett.* **31**. L06207.

LIM, E.-P. (2005). *Global changes in synoptic activity with increasing atmospheric* CO_2. Ph.D. thesis, School of Earth Sciences, University of Melbourne. Available online from the University of Melbourne ePrints Repository.

LIM, E.-P. AND SIMMONDS, I. (2006). Effect of changes in latitudinal temperature gradient and vertical stability on SH winter extratropical cyclones simulated in a warmer climate. Subm. to J. Clim.

LIM, E.-P. AND SIMMONDS, I. (2007). Southern hemisphere winter extratropical cyclone characteristics and vertical organization observed with the ERA-40 reanalysis data in 1979—2001. *J. Climate* **20**, 2675–2690.

LIN, H. AND LEAITCH, R. (1997). Development of an in-cloud aerosol activation parameterization for climate modelling. WMO Workshop on measurement of cloud properties for forcasts of weather, 328-335, World Meteorological Organization, Geneva, 1997.

LIN, S. AND ROOD, R. (1996). Multidimensional flux-form semi-lagrangian transport schemes. *Mon. Wea. Rev.* **124**, 2046–2070.

LINDZEN, R. S. AND FARRELL, B. (1980). A simple approximate result for the maximum growth rate of baroclinic instabilities. *J. Atmos. Sci.* **37**, 1648–1654.

LIONELLO, P., DALAN, F., AND ELVINI, E. (2002). Cyclones in the Mediterranean region: The present and the doubled CO_2 climate scenarios. *Clim. Res.* **22**, 147–159.

LOHMANN, U. (2002). A glaciation indirect aerosol effect caused by soot aerosols. *Geophys. Res. Lett.* **29**. Art. No. 1052.

LOHMANN, U. AND FEICHTER, J. (2005). Global indirect aerosol effects: A review. *Adv. Chem. Phys.* **5**, 715–737.

LOHMANN, U., FEICHTER, J., CHUANG, C., AND PENNER, J. (1999). Prediction of the number of cloud droplets in the ECHAM GCM. *J. Geophys. Res.* **104**, 9169–9198.

LOHMANN, U. AND KÄRCHER, B. (2002). First interactive simulations of cirrus clouds formed by homogeneous freezing in the echam general circulation model. *J. Geophys. Res.* **107**.

LOHMANN, U. AND ROECKNER, E. (1996). Design and performance of a new cloud microphysics scheme developed for the ECHAM general circulation model. *Clim. Dyn.* **12**, 557–572.

LÖPTIEN, U. AND RUPRECHT, E. (2005). Effect of synoptic systems on the variability of the North Atlantic Oscillation. *Mon. Wea. Rev.* **133**, 2894–2904.

LÖPTIEN, U., ZOLINA, O., GULEV, S., LATIF, M., AND SOLOVIOV, V. (2007). Cyclone life cycle characteristics over the northern hemisphere in coupled GCMs. Subm. to Clim. Dyn.

LOTT, F. (1999). Alleviation of stationary biases in a gcm through a mountain drag parameterization scheme and a simple representation of mountain lift forces. *Mon. Wea. Rev.* **127**, 788–801.

LOTT, F. AND MILLER, M. J. (1997). A new subgrid-scale orographic drag parameterization: Its formulation and testing. *Q. J. R. Meteorol. Soc.* **123**, 101–127.

LOUIS, J. (1979). Parametric model of vertical eddy fluxes in the atmosphere. *Boundary-Layer Meteorol.* **17**.

LOZANO, I., DEVOY, R. J. N., MAZ, W., AND ANDERSEN, U. (2004). Storminess and vulnerability along the Atlantic coastlines of Europe: Analysis of storm records and of a greenhouse gases induced climate scenario. *Mar. Geol.* **210**, 205–225. Sp. Iss. SI.

LUKSCH, U., RAIBLE, C., BLENDER, R., AND FRAEDRICH, K. (2005). Decadal cyclone variability in the North Atlantic. *Meteorol. Z.* **14**, 747–753.

MAHERAS, P., FLOCAS, H. A., PATRIKAS, I., AND ANAGNOSTOPOULOU, C. (2001). A 40 year objective climatology of surface cyclones in the Mediterranean region: Spatial and temporal distributions. *Int. J. Climatol.* **21**, 109–130.

MAIER-REIMER, E., KRIEST, I., SEGSCHNEIDER, J., AND WETZEL, P. (2005). The HAMburg ocean carbon cycle model HAMOCC5.1 - technical description release 1.1,. Reports on Earth System Science, 14, Max Planck Institute for Meteorology, Hamburg, Germany, available from: http://www.mpimet.mpg.de, 50 pp.

MAILIER, P. J., STEPHENSON, D. B., FERRO, C. A. T., AND HODGES, K. I. (2006). Serial clustering of extratropical cyclones. *Mon. Wea. Rev.* **134**, 2224–2240.

MARSLAND, S., HAAK, H., JUNGCLAUS, J., LATIF, M., AND ROSKE, F. (2003). The Max-Planck-Institute global ocean/sea ice model with orthogonal curvilinear coordinates. *Ocean Modelling* **5**, 91–127.

MARTIN, G., DEARDEN, C., GREEVES, C., HINTON, T., INNESS, P., JAMES, P., POPE, V., RINGER, M., SLINGO, J., STRATTON, R., AND YANGANG, G.-Y. (2004). *Evaluation of the atmospheric performance of HadGAM/GEM1*. Tech. rep., UK Met Office. Hadley Centre technical note 54.

MCCABE, G. J., CLARK, M. P., AND SERREZE, M. C. (2001). Trends in northern hemisphere surface cyclone frequency and intensity. *J. Climate* **14**, 2763–2768.

MCCORMIC, R. A. AND LUDWIG, J. H. (1967). Climate modifications by atmospheric aerosols. *Science* **156**, 1358–1359,.

MCDONALD, R. E. (2007). Future changes in northern hemisphere extra-tropical cyclones. To be submitted to Clim. Dyn.

MERKEL, U. AND LATIF, M. (2002). A high resolution AGCM study of the El Niño impact in the North Atlantic/European sector. *Geophys. Res. Lett.* **29**. Art. No. 1291.

MILLER, M., PALMER, T., AND SWINBANK, R. (1989). Parametrization and influence of subgridscale orography in general-circulation and numerical weather prediction models. *Meteorol. Atmos. Phys.* **40**, 84–109.

MLAWER, E. J., TAUBMAN, S. J., BROWN, P. D., IACONO, M. J., AND CLOUGH, S. J. (1997). Radiative transfer for inhomogeneous atmospheres: RRTM, a validated correlated-k model for the longwave. *J. Geophys. Res.* **102**, 16663–16682.

MORCRETTE, J.-J., SMITH, L., AND FOUQUART, Y. (1986). Pressure and temperature dependence of the absorption in longwave radiation parameterizations. *Beitr. Phys. Atmosph.* **59**, 455–469.

MURPHY, B. F., PETTRE, P., AND SIMMONDS, I. (2002). Effects of changing baroclinicity on the southern hemisphere extratropical circulation. *Q. J. R. Meteorol. Soc.* **128**, 1807–1826.

MURRAY, R. J. AND SIMMONDS, I. (1991a). A numerical scheme for tracking cyclone centers from digital data. Part I: Development and operation of the scheme. *Aust. Meteorol. Mag.* **39**, 155–166.

MURRAY, R. J. AND SIMMONDS, I. (1991b). A numerical scheme for tracking cyclone centers from digital data. Part II: Application to January and July general circulation model simulations. *Aust. Meteorol. Mag.* **39**, 167–180.

MUSKULUS, M. AND JACOB, D. (2005). Tracking cyclones in regional model data: The future of Mediterranean storms. *Adv. Geosc.* **2**, 13–19.

NIETO, R., GIMENO, L., DE LA TORRE, L., RIBERA, P., GALLEGO, D., GARCÍA-HERERA, R., GARCÍA, J. A., NUÑEZ, M., REDAÑO, A., AND LORENTE, J. (2005). Climatological features of cutoff low systems in the northern hemisphere. *J. Climate* **18**, 3085–3103.

NORDENG, T. E. (1994). Extended versions of the convection parametrization scheme at ECMWF and their impacts upon the mean climate and transient activity of the model in the tropics. ECMWF Tech. Memo. 206, 25 pp.

OBERHUBER, J. M. (1993). Simulation of the Atlantic circulation with a coupled sea ice-mixed layer-isopycnal general circulation model. Part I: Model description. *J. Phys. Oceanogr.* **23**, 808–829.

OLSON, J., WATTS, J., AND ALLISON, L. (1983). Carbon in live vegetation of major world ecosystems. ORNL-5862, Oak Ridge National Laboratory, Oak Ridge, TN.

OVERLAND, J. E. AND PEASE, C. H. (1982). Cyclone climatology of the Bering Sea and its relation to sea ice extent. *Mon. Wea. Rev.* **110**, 5–13.

PACIOREK, C. J., RISBY, J. S., VENTURA, V., AND ROSEN, R. D. (2002). Multiple indices of northern hemisphere cyclone activity, winters 1949-99. *J. Climate* **15**, 1573–1590.

PETTERSEN, S. (1956). *Weather Analysis and Forecasting*. vol. 1. 2nd Edition. McGraw-Hill. 422 pp.

PEZZA, A. AND AMBRIZZI, T. (2005). Dynamical conditions and synoptic tracks associated with different types of cold surge over tropical South America. *Int. J. Climatol.* **25**, 215–241.

PEZZA, A. B. AND AMBRIZZI, T. (2003). Variability of southern hemisphere cyclone and anticyclone behavior: Further analysis. *J. Climate* **16**, 1075–1083.

PICORNELL, M. A., JANSÀ, A., GENOVÉS, A., AND CAMPINS, J. (2001). Automated database of mesocyclones from the HIRLAM(INM)-0.5° analyses in the western Mediterranean. *Int. J. Climatol.* **21**, 335–354.

PINCUS, R. AND BAKER, M. (1994). Precipitation, solar absorption, and albedo susceptibility in marine boundary layer clouds. *Nature* **372**, 250–252.

PINTO, J. (2002). *Influence of Large-Scale Atmospheric Circulation and Baroclinic Waves on the Variability of Mediterranean Rainfall.*. Ph.D. thesis, Mitteilungen aus dem Institut für Geophysik und Meteorologie der Universität zu Köln, Heft 151.

PINTO, J. G., SPANGEHL, T., ULBRICH, U., AND SPETH, P. (2005). Sensitivities of a cyclone detection and tracking algorithm: Individual tracks and climatology. *Meteorol. Z.* **14**, 823–838.

PINTO, J. G., SPANGEHL, T., ULBRICH, U., AND SPETH, P. (2006). Assessment of winter cyclone activity in a transient ECHAM4-OPYC3 GHG experiment. *Meteorol. Z.* **15**, 279–291.

PINTO, J. G., ULBRICH, U., LECKEBUSCH, G. C., SPANGEHL, T., REYERS, M., AND ZACHARIAS, S. (2007). Changes in storm track and cyclone activity in three SRES ensemble experiments with the ECHAM5/MPI-OM1 GCM. *Clim. Dyn.* **29**, 195–210.

PORCÙ, F., CARRASSI, A., MEDAGLIA, C. M., PRODI, F., AND MUGNAI, A. (2007). A study on cut-off low vertical structure and precipitation in the Mediterranean region. *Meteorol. Atmos. Phys.* **96**, 121–140.

RADINOVIC, D. (1987). Mediterranean cyclones and their influence on the weather and climate. WMO, PSMP Report Ser. No. 24, 131pp, Geneva, Switzerland.

RAIBLE, C. C. (2007). On the relation between extremes of midlatitude cyclones and the atmospheric circulation using ERA40. *Geophys. Res. Lett.* **234**. Art. No. L07703.

RAIBLE, C. C. AND BLENDER, R. (2004). Northern hemisphere midlatitude cyclone variability in GCM simulations with different ocean representations. *Clim. Dyn.* **22**, 239–248.

RAIBLE, C. C., DELLA-MARTA, P. M., SCHWIERZ, C., WERNLI, H., AND BLENDER, R. (2007a). Northern hemisphere extratropical cyclones: A comparison of detection and tracking methods and different reanalyses. Accepted for publication by Mon. Wea. Rev.

RAIBLE, C. C., YOSHOMORI, M., STOCKER, T. F., AND CASTY, C. (2007b). Extreme midlatitude cyclones and their implications for precipitation and wind speed extremes in simulations of the Maunder minimum versus present day conditions. *Clim. Dyn.* **28**, 409–423.

REED, R. J., HOLLINGSWORTH, A., HECKLEY, W. A., AND DELSOL, F. (1986). *An evaluation of the performance of the ECMWF operational forecasting system in analyzing and forecasting tropical easterly wave disturbances Part I : Synoptic investigation*. Tech. Rep. 58, ECMWF.

REITAN, C. H. (1974). Frequencies of cyclones and cyclogenesis for North America. *Mon. Wea. Rev.* **102**, 861–868.

REITAN, C. H. (1979). Trends in the frequencies of cyclone activity over North America. *Mon. Wea. Rev.* **107**, 1684–1688.

RINGER, M. A., MARTIN, G. M., GREEVES, C. Z., HINTON, T. J., JAMES, P. M., POPE, V. D., SCAIFE, A. A., STRATTON, R. A., INNESS, P. M., SLINGO, J. M., AND YANG, G. (2006). The physical properties of the atmosphere in the new Hadley Centre Global Environmental Model (HadGEM1). Part II: Aspects of variability and regional climate. *J. Climate* **19**, 1302–1326.

ROCKEL, B., RASCHKE, E., AND WEYRES, B. (1991). A parameterization of broad band radiative transfer properties of water, ice, and mixed clouds. *Beitr. Phys. Atmosph.* **64**, 1–12.

ROECKNER, E. (1995). Parameterization of cloud radiative properties in the ECHAM4 model. Proc. WCRP Workshop on Cloud Microphysics Parameterizations in Global Atmospheric Circulation Models, Kananaskis, AB, Canada, WCRP, 105-116.

ROECKNER, E., ARPE, K., BENGTSSON, L., CLAUSSEN, C. M., DÜMENIL, L., ESCH, M., GIORGETTA, M., SCHLESE, U., AND SCHULZWEIDA, U. (1996a). *The atmospheric general circulation model ECHAM-4: Model description and simulation of present-day climate*. Tech. rep., Max-Planck-Institute for Meteorology, Hamburg, Germany. Report No. 218, 90pp.

ROECKNER, E., BAEUML, G., BONVENTURA, L., BROKOPF, R., ESCH, M., GIORGETTA, M., HAGEMANN, S., KIRCHNER, I., KORNBLUEH, L., MANZINI, E., RHODIN, A., SCHLESE, U., SCHULZWEIDA, U., AND TOMPKINS, A. (2003). The atmospheric general circulation model ECHAM5. Part i: Model description. Report 349, Max Planck Institute for Meteorology, Hamburg, Germany, available from http://www.mpimet.mpg.de.

ROECKNER, E., BENGTSSON, L., FEICHTER, J., LELIEVELD, J., AND RODHE, H. (1999). Transient climate change simulations with a coupled atmosphere-ocean GCM including the tropospheric sulfur cycle. *J. Climate* **12**, 3004–3032.

ROECKNER, E., OBERHUBER, J., BACHER, A., CHRISTOPH, M., AND KIRCHNER, I. (1996b). ENSO variability and atmospheric response in a global coupled atmosphere-ocean GCM. *Clim. Dyn.* **12**, 737–754.

ROELOFS, G. AND LELIEVELD, J. (1995). Distribution and budget of O_3 in the troposphere calculated with a chemistry general-circulation model. *J. Geophys. Res.* **100**, 20983–20998.

RUDEVA, I. AND GULEV, S. (2007). Climatology of cyclone size characteristics and their changes during the cyclone life cycle. *Mon. Wea. Rev.* **135**, 2568–2587.

RUPRECHT, E., SCHRÖDER, S. S., AND UBL, S. (2002). On the relation between NAO and water vapour transport towards europe. *Meteorol. Z.* **11**, 395–401.

SALARI, V. AND SETHI, I. K. (1990). Feature point correspondence in the presence of occlusion. *IEEE Trans. PAMI* **12**, 87–91.

SARDESHMUKH, P. D. AND HOSKINS, B. J. (1984). Spatial smoothing on the sphere. *Mon. Wea. Rev.* **112**, 2524–2529.

SATO, M., HANSEN, J., MCCORMICK, M., AND POLLACK, J. (1993). Stratospheric aerosol optical depths, 1850–1990. *J. Geophys. Res.* **98**, 22987–22994.

SCHINKE, H. (1993). On the occurrence of deep cyclones over Europe and the North Atlantic in the period 1930–1991. *Beitr. Phys. Atmosph.* **66**, 223–237.

SCHNEIDEREIT, A. (2007). *Zyklonenstatistik in Reanalysen des ECMWF (ERA-40) und in Szenarienrechnung des ECHAM/MPI-OM*. Master's thesis, Institut fü Meteorologie, Universität Hamburg. 131pp.

SCHNEIDEREIT, A., BLENDER, R., FRAEDRICH, K., AND LUNKEIT, F. (2007). Icelandic climate and North Atlantic cyclones in ERA-40 reanalyses. *Meteorol. Z.* **16**, 17–23.

SCHUBERT, M. (1996). *Analyse der Zyklonenzugbahen über dem Nordatlantik in Kontroll- und Szenarienrechnungen*. Master's thesis, Institut für Meteorologie, Universität Hamburg. 121pp.

SCHUBERT, M., PERLWITZ, J., BLENDER, R., FRAEDRICH, K., AND LUNKEIT, F. (1998). North Atlantic cyclones in CO_2-induced warm climate simulations: Frequency, intensity and tracks. *Clim. Dyn.* **14**, 827–837.

SCHUBERT, S. D., ROOD, R. B., AND PFAENDTNER, J. (1993). An assimilated dataset for earth science applications. *Bull. Am. Meteor. Soc.* **74**, 2331–2342.

SCHULZ, M., DE LEEUW, G., AND BALKANSKI, Y. (2004). Emission of atmospheric trace compounds. Chap, Sea-salt aerosol source functions and emissions, pp. 333-359, Ed. Kluwer, 2004.

SEPP, M., POST, P., AND JAAGUS, J. (2005). Long-term changes in the frequency of cyclones and their trajectories in central and northern Europe. *Nordic Hydrology* **36**, 297–309.

SERREZE, M. C. (1995). Climatological aspects of cyclone development and decay in the Arctic. *Atmos. - Ocean* **33**, 1–23.

SERREZE, M. C., BOX, J. E., BARRY, R. G., AND WALSH, J. E. (1993). Characteristics of Arctic synoptic activity, 1952–1989. *Meteorol. Atmos. Phys.* **51**, 147–164.

SERREZE, M. C., CARSE, F., BARRY, R. G., AND ROGERS, J. C. (1997). Icelandic low cyclone activity: Climatological features, linkages with the NAO, and relationships with the recent changes in the northern hemisphere circulation. *J. Climate* **10**, 453–464.

SETHI, I. K. AND JAIN, R. (1987). Finding trajectories of feature points in a monocular image sequence. *IEEE Trans. PAMI* **9**, 56–73.

SICKMÖLLER, M., BLENDER, R., AND FRAEDRICH, K. (2000). Observed winter cyclone tracks in the northern hemisphere in re-analysed ECMWF data. *Q. J. R. Meteorol. Soc.* **126**, 591–620.

SIMMONDS, I. AND KEAY, K. (2000a). Mean southern hemisphere extratropical cyclone behavior in the 40-year NCEP-NCAR reanalysis. *J. Climate* **13**, 873–885.

SIMMONDS, I. AND KEAY, K. (2000b). Variability of southern hemisphere extratropical cyclone behavior, 1958–97. *J. Climate* **13**, 550–561.

SIMMONDS, I. AND LAW, R. (1995). Associations between Antarctic katabatic flow and the upper level winter vortex. *Int. J. Climatol.* **15**, 403–421.

SIMMONDS, I. AND MURRAY, R. J. (1999). Southern extratropical cyclone behavior in ECMWF analyses during the FROST Special Observing Periods. *Wea. Forecasting* **14**, 878–891.

SIMMONDS, I. AND WU, X. R. (1993). Cyclone behaviour response to changes in winter southern hemisphere sea-ice concentration. *Q. J. R. Meteorol. Soc.* **119**, 1121–1148.

SIMMONS, A., BURRIDGE, D., JARRAUD, M., GIRARD, C., AND WERGEN, W. (1989). The ECMWF medium-range prediction models development of the numerical formulations and the impact of increased resolution. *Meteorol. Atmos. Phys.* **40**, 28–60.

SINCLAIR, M. R. (1994). An objective cyclone climatology for the southern hemisphere. *Mon. Wea. Rev.* **122**, 2239–2256.

SINCLAIR, M. R. (1995). A climatology of cyclogenesis for the southern hemisphere. *Mon. Wea. Rev.* **123**, 1601–1619.

SINCLAIR, M. R. (1997). Objective identification of cyclones and their circulation, intensity and climatology. *Wea. Forecasting* **12**, 591–608.

SINCLAIR, M. R., RENWICK, J. A., AND KIDSON, J. W. (1997). Low-frequency variability of southern hemisphere sea level pressure and weather system activity. *Mon. Wea. Rev.* **125**, 2531–2543.

SINCLAIR, M. R. AND WATTERSON, I. G. (1999). Objective assessment of extratropical weather systems in simulated climates. *J. Climate* **12**, 3467–3485.

SIX, K. AND MAIER-REIMER, E. (1996). Effects of plankton dynamics on seasonal carbon fluxes in an ocean general circulation model. *Global Biogeochem. Cycles* **10**, 559–583.

SMITH, B. A., BOSART, L. F., AND KEYSER, D. (2002). A global 500 hPa cutoff cyclone climatology: 1953–1999. 19^{th} Conf. on Weather and Forecasting, San Antonio, TX.

SOLANKI, S. AND KRIVOVA, N. (2003). Can solar variability explain global warming since 1970? *J. Geophys. Res.* **108**.

SONG, Y. (2007). *Modeling of atmospheric circulation at mid- and high latitudes of the Northern Hemisphere - evaluation studies using ARPEGE*. Ph.D. thesis, University of Bergen. Available online at http://hdl.handle.net/1956/2368. Accessed 19/09/2007.

SORTEBERG, A., KVAMSTØ, N. G., AND BYRKJEDAL, Ø. (2005). Wintertime Nordic Seas cyclone variability and its impact on oceanic volume transports into the Nordic Seas. In *The Nordic Seas: An Integrated Perspective* (Edited by H. Drange, T. Dokken, T. Furevik, R. Gerdes, & W. Berger), vol. 158 of *Geophysical Monograph Series*, pp. 137–156. American Geophysical Union, Washington, DC.

SPANOS, S., MAHERAS, P., KARACOSTAS, T., AND PENNAS, P. (2003). Objective climatology of 500-hPa cyclones in central and east Mediterranean region during warm-dry period of the year. *Theor. Appl. Climatol.* **75**, 167–178.

STEIN, O. AND HENSE, A. (1994). A reconstructed time series of the number of extreme low pressure events since 1880. *Meteorol. Z.* **1**, 43–46.

STIER, P., FEICHTER, J., KINNE, S., KLOSTER, S., VIGNATI, E., WILSON, J., GANZEVELD, L., TEGEN, I., WERNER, M., BALKANSKI, Y., SCHULZ, M., BOUCHER, O., MINIKIN, A., AND PETZOLD, A. (2005). The aerosol climate model ECHAM5-HAM. *Adv. Chem. Phys.* **5**, 1125–1156.

STIER, P., FEICHTER, J., ROECKNER, E., KLOSTER, S., AND ESCH, M. (2006). The evolution of the global aerosol system in a transient climate simulation from 1860 to 2100. *Adv. Chem. Phys.* **6**, 3059–3076.

STRATTON, R. A. (2004). *Report on aspects of variability in high-resolution versions of HadAM3*. Tech. rep., UK Met Office. Hadley Centre Technical Note 53.

STRETEN, N. A. AND TROUP, A. J. (1973). A synoptic climatology of satellite observed cloud vortices over the Southern Hemisphere. *Q. J. R. Meteorol. Soc.* **99**, 56–72.

SUNDQVIST, H., BERGE, E., AND KRISTJÁNSSON, J. E. (1989). Condensation and cloud parameterization studies with a mesoscale numerical weather prediction model. *Mon. Wea. Rev.* **117**, 1641–1657.

TALJAARD, J. J. (1967). Development, distribution and movement of cyclones and anticyclones in the southern hemisphere during the IGY. *J. Appl. Meteor.* **6**, 973–987.

TANRÉ, D., GELEYN, J. F., AND SLINGO, J. (1984). First results of the introduction of an advanced aerosol-radiation interaction in the ECMWF low resolution global model. Aerosols and Their Climatic Effects: Proceedings of the Meetings of Experts, Williamsburg, Va., 28-30 March 1983, edited by H. E. Gerber and A. Deepak, pp. 133-3177, A. Deepak, Hampton, Va.

TAYLOR, K. E. (1986). An analysis of the biases in traditional cyclone frequency maps. *Mon. Wea. Rev.* **114**, 1481–1490.

TEGEN, I., HARRISON, S. P., KOHFELD, K., PRENTICE, I. C., COE, M., AND HEIMANN, M. (2002). Impact of vegetation and preferential source areas on global dust aerosol: Results from a model study. *J. Geophys. Res.* **107**.

TERRY, J. AND ATLAS, R. (1996). Objective cyclone tracking and its applications to ERS-1 scatterometer forecast impact studies. In *Preprints,* 15^{th} *Conference On Weather Analysis and Forecasting*, pp. 146–149. Amer. Meteor. Soc.

THORNCROFT, C. AND HODGES, K. I. (2001). African easterly wave variability and its relationship to Atlantic tropical cyclone activity. *J. Climate* **14**, 1166–1179.

TIEDTKE, M. (1989). A comprehensive mass flux scheme for cumulus parameterization in large-scale models. *Mon. Wea. Rev.* **117**, 1779–1800.

TIMMRECK, C. AND SCHULZ, M. (2004). Significant dust simulation differences in nudged and climatological operation mode of the AGCM ECHAM. *J. Geophys. Res.* **109**.

TRIGO, I. F. (2006). Climatology and interannual variability of storm-tracks in the Euro-Atlantic sector: A comparison between ERA-40 and NCEP/NCAR reanalyses. *Clim. Dyn.* **26**, 127–143.

TRIGO, I. F., BIGG, G. R., AND DAVIES, T. D. (2002). Climatology of cyclogenesis mechanisms in the Mediterranean. *Mon. Wea. Rev.* **130**, 549–569.

TRIGO, I. F., DAVIES, T. D., AND BIGG, G. R. (1999). Objective climatology of cyclones in the Mediterranean region. *J. Climate* **12**, 1685–1696.

TWOMEY, S. (1974). Pollution and planetary albedo. *Atmos. Env.* **8**, 1251–1256.

UBL, S. (2001). *Variabilität von Zykloneneigenschaften über dem Nordatlantik*. Master's thesis, Institut für Meereskunde an der Universität Kiel.

UENO, K. (1991a). Climatological features of extratropical cyclone activities on the middle latitudes of the northern hemisphere. *Climatological Notes, Institute of Geosc., Univ. Tsukuba* **40**, 77–90.

UENO, K. (1991b). Distribution of extratropical cyclone activity in the middle latitudes of the northern hemisphere. *Geogr. Rev. Japan Ser. A* **64**, 801–817. *In Japanese*.

UENO, K. (1993). Interannual variability of surface cyclone tracks, atmospheric circulation patterns, and precipitation patterns in winter. *J. Meteorol. Soc. Japan* **71**, 655–671.

UPPALA, S., KALLBERG, P., SIMMONS, A., ANDRAE, U., DA COSTA BECHTOLD, V., FIORINO, M., GIBSON, J., HASELER, J., HERNANDEZ, A., KELLY, G., LI, X., ONOGI, K., SAARINEN, S., SOKKA, N., ALLAN, R., ANDERSSON, E., ARPE, K., BALMASEDA, M., BELJAARS, A., VAN DE BERG, L., BIDLOT, J., BORMANN, N., CAIRES, S., CHEVALLIER, F., DETHOF, A., DRAGOSAVAC, M., FISHER, M., FUENTES, M., HAGEMANN, S., HOLM, E., HOSKINS, B., ISAKSEN, L., JANSSEN, P., JENNE, R., MCNALLY, A., MAHFOUF, J.-F., MORCRETTE, J.-J., RAYNER, N., SAUNDERS, R., SIMON, P., STERL, A., TRENBERTH, K., UNTCH, A., VASILJEVIC, D., VITERBO, P., AND WOOLLEN, J. (2005). The ERA-40 re-analysis. *Q. J. R. Meteorol. Soc.* **131**, 2961–3012.

VALCKE, S., ABD D. DECLAT, A. C., AND TERRAY, L. (2003). OASIS ocean atmosphere sea ice soil users' guide. CERFACS Tech. Rep. TR/CMGC/03/69, Toulouse, France, 85 pp.

VAN BEBBER, W. J. (1891). Die Zugstraßen der barometrischen Minima nach den Bahnenkarten der Deutschen Seewarte für den Zeitraum 1875–1890. *Meteorol. Z.* **8**, 361–366.

VIGNATI, E., WILSON, J., AND STIER, P. (2004). M7: An efficient size resolved aerosol microphysics module for large-scale aerosol transport models. *J. Geophys. Res.* **303**, 1309–1311.

VON STORCH, H. AND ZWIERS, F. W. (2002). *Statistical Analysis in Climate Research*. Cambridge University Press, 494 pp.

WALKER, G. T. (1923). Correlation in seasonal variations of weather, VIII: A preliminary study of world weather. Mem. Ind. Meteor. Dept. (Poona), 24, 275-332.

WALLAND, D. J. AND SIMMONDS, I. (1997). Modelled atmospheric response to changes in northern hemisphere snow cover. *Clim. Dyn.* **13**, 25–34.

WANG, C.-C. AND ROGERS, J. C. (2001). A composite study of explosive cyclogenesis in different sectors of the North Atlantic. Part I: Cyclone structure and evolution. *Mon. Wea. Rev.* **129**, 1481–1499.

WANG, X., SWAIL, V., AND ZWIERS, F. (2006). Climatology and changes of extratropical cyclone activity: Comparison of ERA-40 with NCEP-NCAR reanalysis for 1958–2001. *J. Climate* **19**, 3145–3166.

WANG, X. L., SWAIL, V. R., AND ZWIERS, F. W. (2004). Changes in extra-tropical storm tracks and cyclone activities as derived from two global reanalyses and the Canadian CGCM2 projections of future climate. In *Proceedings of the 8th International Workshop on Wave Hindcasting and Forecasting*. North Shore, Oahu, Hawaii.

WASA (1998). Changing waves and storms in the northeast Atlantic? *Bull. Am. Meteor. Soc.* **79**, 741–760.

WASSERMANN, S., SCHMITT, C., KOTTMEIER, C., AND SIMMONDS, I. (2006). Coincident vortices in Antarctic wind fields and sea ice motion. *Geophys. Res. Lett.* **33**.

WATTERSON, I. (2006). The intensity of precipitation during extratropical cyclones in global warming simulations: A link to cyclone intensity? *Tellus* **58**, 82–97.

WERNLI, H. AND SCHWIERZ, C. (2006). Surface cyclones in the ERA-40 dataset (1958–2001). Part I: Novel identification method and global climatology. *J. Atmos. Sci.* **63**, 2486–2507.

WHITE, P. P. Ed. (2003). *IFS Documentation Cycle CY23R4*. ECMWF. Available online at http://ecmwf.com/research/ifsdocs/CY23r4/index.html, accessed on 09/11/2007.

WHITE, W. AND SIMMONDS, I. (2006). Sea surface temperature-induced cyclogenesis in the Antarctic circumpolar wave. *J. Geophys. Res.* **111**.

WHITTAKER, L. M. AND HORN, L. H. (1984). Northern hemisphere extratropical cyclone activity for four midseason months. *J. Climate* **4**, 297–310.

WILE, K. L. (2006). Differences in the frequency and the distribution of intense extratropical cyclone events in a model simulated doubled CO_2 environment. In *Proceedings of the 18th Conference on Climate Variability and Change*.

WILLIAMSON, D. AND RASCH, P. (1994). Water-vapor transport in the NCAR-CCM2. *Tellus* **46A**, 34–51.

WILLIAMSON, D. L. (1981). Storm track representation and verification. *Tellus* **33**, 513–530.

WILSHUSEN, M. (1996). *Bestimmung und Auswertung von Zyklonenzugbahnen aus Beobachtungsdaten über dem Nordpazifik*. Master's thesis, Institut für Meteorologie, Universität Hamburg. 123pp.

WOLFF, J.-O., MAIER-REIMER, E., AND LEGUTKE, S. (1997). The hamburg ocean primitive equation model HOPE. Technical Report 13, German Climate Computer Center (DKRZ), Hamburg, Germany.

YU, H., KAUFMAN, Y., CHIN, M., FEINGOLD, G., REMER, L., ANDERSON, T., BALKANSKI, Y., BELLOUIN, N., BOUCHER, O., CHRISTOPHER, S., DECOLA, P., KAHN, R., KOCH, D., LOEB, N., REDDY, M., SCHULZ, M., TAKEMURA, T., AND ZHOU, M. (2006). A review of measurement-based assessments of the aerosol direct radiative effect and forcing. *Adv. Chem. Phys.* **6**, 613–666.

ZACHARIAS, S. (2006). *Einfluß der Nordatlantikoszillation auf die Entwicklung extremer Zyklonen*. Master's thesis, Institut für Geophysik und Meteorologie, Universität zu Köln.

ZHANG, X., WALSH, J. E., ZHANG, J., BHATT, U. S., AND IKEDA, M. (2004). Climatology and interannual variability of Arctic cyclone activity: 1948–2002. *J. Climate* **17**, 2300–2317.

ZHANG, Y. AND WANG, W.-C. (1997). Model-simulated northern winter cyclone and anticyclone activity under a greenhouse warming scenario. *J. Climate* **10**, 1616–1634.

ZHU, X., SUN, J., LIU, Z., LIU, Q., AND MARTIN, J. E. (2007). A synoptic analysis of the interannual variability of winter cyclone activity in the Aleutian low region. *J. Climate* **20**, 1523–1538.

ZOLINA, O. AND GULEV, S. (2001). Variability of the ocean-atmosphere fluxes associated with atmospheric cyclones. WCRP/SCOR Workshop on Intercomparison and Validation of Ocean-Atmosphere Flux Fields, Potomac, MD.

ZOLINA, O. AND GULEV, S. K. (2002). Improving the accuracy of mapping cyclone numbers and frequencies. *Mon. Wea. Rev.* **130**, 748–759.

ZOLINA, O. AND GULEV, S. K. (2003). Synoptic variability of ocean-atmosphere turbulent fluxes associated with atmospheric cyclones. *J. Climate* **16**, 2717–2734.

My no-frills acknowledgements

Abhay Devasthale, Adetutu Mary Aghedo, Ákos Horváth, Alex Krüger, Alexandra Jahn, Almut Arneth, Almut Gaßmann, Alvaro de Oña, Álvaro Valdebenito, Amélie Kirchgäßner, Andrea Lammert, Andreas Gillmann, Andreas Meyer-Träger, Angela Messing-Banse, Angelika Heil, Anke Seiffert, Anling Richter, Anna Barbara Herold, Anne Kubin, Anne Müller, Anne Smets, Annette Freibauer, Annette Kirk, Annika Jahnke-Bornemann, Antje Weitz, Anusha Warnasooriya, Barbara Zinecker, Bärbel Langmann, Becky Whittenburg, Benjamin Kürten, Bernhard Effertz, Bettina Addicks, Bettina Diallo, Betty Carlin, Birgit Grothmann, Birgit Hünicke, Birgit Meier, Birthe Jacobs, Brian Hoskins, Bruno de Greve, Carola Kauhs, Caroline Narayan, Caryn Radlove, Charmini Kodituwakku, Cheng Tiantao, Christian Banse, Christian Klepp, Christiana Lefebvre, Christiane Fluche, Christiane Orlopp, Christiane Schmidt, Christiane Zitzkat, Christin Sperling, Christina Greeves, Christine Nam, Christine Schleupner, Christof Möller, Christoph Raible, CIS, Claas Teichmann, Claire Granier, Claudia Fennig, Claudia Timmreck, Clotilde Dubois, Constanze Fritz, Corinna Hoose, Cornelia Fessler, Cornelia Kampmann, Cornelia Retz, Daniel Kühnrich, Daniela Jacob, Daniela Matei, David Grawe, Diana Circhetta de Marrón, Diane Galgon, Dietrich Stadtländer, Dirk Notz, DKRZ, Eik Steinbach, Elina Marmer, Elisabeth Kruse, Elke Lord, Elke Meyer, Elke Nechwatal, Els Nagel-Soepenberg, Emilia Sperling, Erich Roeckner, Erik Meyerhof, Ernst Maier-Reimer, Eva Krause, Evelyn Jäkel, Evelyn Wolters, Evert Nagel-Soepenberg, Felix Landerer, Fiona McLay, Florian Niemöller, Florian Plehn, Florian Rauser, Focko Meier, Francesca Guglielmo, Frank Lunkeit, Frank Schühlein, Frauke Pascheke, Friedemann Fischer, Gabriela Sousa-Santos, Gabriele Fuchs, Galina Churkina, Glenn Havelock, Goetz Föser, Gorden Griem, Gregor Leckebusch, Gudrun Rosenhagen, Guido Schröder, Gundi Kleinhoff, Guy Brasseur, Guy Schurgers, Gwen Bryde, Hanna Stadelhofer, Hannes Thiemann, Hans Luthardt, Hans von Storch, Hans-Hermann Winter, Harri Kokkola, Hartmut Graßl, Hauke Schmidt, Heini Wernli, Heinz Jürgen Punge, Helena Burg, Helmuth Haak, Henrike Janßen, Holger Goettel, Hui Wan, Ilona Liesner, Ian Rutt, IMPRS-ESM, Ingrid Engvall, Irene Fischer-Bruns, Irene Stemmler, Irina Domscheit, Ivonne Anders, Jacob Sperling, James Bradley, Jan Kazil, Jana Brunke, Jana Essebier, Jasmin Emrani, Jeannine Kämpfer, Jennifer Sesabo, Jens Herrmann, Jens Kieser, Jessica Rodehorst, Jin-Song von Storch, Joaquim Pinto, Jochem Marotzke, Jörg Winterfeldt, Johann Feichter, Johann Jungclaus, Johanna Baehr, Johannes Quaas, Jonas Alexander, Jorge Martins, Judith J. Hoelzemann, Julia Pongratz, Julia Schreiner, Julia Spreitz, Julius Sperling, Kai Lessmann, Kai Zhang, Karin Thieme, Karsten Fennig, Kathleen Esfeld, Kathrin Kunze, Katja Rindfleisch, Katrin Baumgarten, Katrin Heinrichs, Kerstin Eppert, Kerstin Prömmel, Kevin Hodges, Kevin Sieck, Kirstin Koppelin, Kirstin Lippelt, Klara Bezpalcova, Knut Fiedler, Kornelia Müller, Kristina Trusilova, Kristine Klapheck, Kurt Georg Hooss, Lambert Rasche, Lennart Bengtsson, Li Qian, Lilo Jacob, Lola Kotova, Luca Criscuolo, Luca Pozzoli, Luis Kornblüh, Malte Heinemann, Malte Schwoon, Manu Anna Thomas, Manuela Barth, Marc Oliver Rieger, Marco Giorgetta, Marco Restelli, Marcus Herold, Mareike Swadzba, Mareile Rösner, Maria Froeling, Maria Paz Chidichimo, Marielle Saunois, Marilyn Levinson, Martin Claussen, Martin Döring, Martin Schultz, Martin Wild, Martina Jung, Martina Schulze, Matthias Demuzere, Matthias Hort, Mechthild Klann, Melissa Anne Pfeffer, Merike Schultz, Michael Botzet, Michael Rose, Mikhail Dobrynin, Miren Vizcaino Trueba, MPI-Met, Monia Schärli, Monika Esch, Nadia Kamoun, Nadin Jakob, Nadine Meyer, Nadine Siemens, Nadine Stiebitz, Nanna Egermann, Natalia Calvo, Nico Friedrich, Nicole Wilkens, Nidia Martinez, Niklas Schreiber, Nikolaus Groll, Nikolay Koldunov, Norbert Noreiks, Olaf Krüger, Olaf Seydel, Olaf Schmidt, Olaf Stein, Ole Poulsen, Ole Ross, Patrick Wetzel, Paulina Gaska, Philine Bunte, Philip Stier, Philipp Weis, Rebekka Posselt, Reiner Letscher, Reiner Schnur, Reinhard Budich, Reinhard Schiemann, Reinhard Zöllner, René Hommel, Renate Schönfeld, Renate Spingler, Richard Blender, R. Franke, Richard Tol, Rita Seiffert, Robert Köppe, Rüdiger Banse, Ruth McDonald, Sabine Philipps, Sabrina Melchionna, Sandra Lindner, Sandra Zaremba, Sandrine Aubrun, Sarojini Beena-Balan, Sebastian Rast, Silvia Kloster, Simona Bartelt, Stefan Hagemann, Stefan Kinne, Stefan Manneck, Stefan Sperling, Stefanie vom Hoff, Stephan Bakan, Stephanie Prien, Susanna Kube, Susanne Arndt, Susanne Müller-Kademann, Susanne Winking, Sven Kotlarski, Swati Gehlot, Sylvia Bohnenstengel, Tanja Walter, Tim Erbrecht, Tina Kanzek, Thomas Bruns, Thomas Fuchs, Tim Vahle-Hinz, Tobias Hehnen, Tomas Lovato, Tom Lembcke, Torben Koenigk, Torsten Allwardt, Torsten Weber, Traute Crüger, Triin Lapimaa, Tullio Aurelio, Ulla Heikkilae, Ulrich Hamann, Ulrich Seiffert, Ulrike Heckötter, Ulrike Löptien, Ulrike Lohmann, Ulrike Niemeier, Ursula Bungert, Ute Banse, Ute Neugebauer, Ute Schönborn-Gieße, Uwe Schulzweida, Valentina Sicardi, Victor vom Hoff, Vivian Wendt, Vladimir Vlahovic, Wolfgang Bott, Wolfgang Müller, Xiuhua Zhu, Yiran Peng, Yogesh Tiwari:

Thank you.


Cheppalle... Dio mio, mandami la voglia di studiare...
FUUUUUUUUUUUUUUUUUUU
VOGLIA
Ei, lassù! Stavo scherzando !!!
erodan

Publikationsreihe des MPI-M
„Berichte zur Erdsystemforschung“ , „*Reports on Earth System Science*“, ISSN 1614-1199
Sie enthält wissenschaftliche und technische Beiträge, inklusive Dissertationen.

Berichte zur Erdsystemforschung Nr.1 Juli 2004	**Simulation of Low-Frequency Climate Variability in the North Atlantic Ocean and the Arctic** Helmuth Haak
Berichte zur Erdsystemforschung Nr.2 Juli 2004	**Satellitenfernerkundung des Emissionsvermögens von Landoberflächen im Mikrowellenbereich** Claudia Wunram
Berichte zur Erdsystemforschung Nr.3 Juli 2004	**A Multi-Actor Dynamic Integrated Assessment Model (MADIAM)** Michael Weber
Berichte zur Erdsystemforschung Nr.4 November 2004	**The Impact of International Greenhouse Gas Emissions Reduction on Indonesia** Armi Susandi
Berichte zur Erdsystemforschung Nr.5 Januar 2005	**Proceedings of the first HyCARE meeting, Hamburg, 16-17 December 2004** Edited by Martin G. Schultz
Berichte zur Erdsystemforschung Nr.6 Januar 2005	**Mechanisms and Predictability of North Atlantic - European Climate** Holger Pohlmann
Berichte zur Erdsystemforschung Nr.7 November 2004	**Interannual and Decadal Variability in the Air-Sea Exchange of CO2 - a Model Study** Patrick Wetzel
Berichte zur Erdsystemforschung Nr.8 Dezember 2004	**Interannual Climate Variability in the Tropical Indian Ocean: A Study with a Hierarchy of Coupled General Circulation Models** Astrid Baquero Bernal
Berichte zur Erdsystemforschung Nr9 Februar 2005	**Towards the Assessment of the Aerosol Radiative Effects, A Global Modelling Approach** Philip Stier
Berichte zur Erdsystemforschung Nr.10 März 2005	**Validation of the hydrological cycle of ERA40** Stefan Hagemann, Klaus Arpe and Lennart Bengtsson
Berichte zur Erdsystemforschung Nr.11 Februar 2005	**Tropical Pacific/Atlantic Climate Variability and the Subtropical-Tropical Cells** Katja Lohmann
Berichte zur Erdsystemforschung Nr.12 Juli 2005	**Sea Ice Export through Fram Strait: Variability and Interactions with Climate**- Torben Königk
Berichte zur Erdsystemforschung Nr.13 August 2005	**Global oceanic heat and fresh water forcing datasets based on ERA-40 and ERA-15** Frank Röske
Berichte zur Erdsystemforschung Nr.14 August 2005	**The** HAM**burg** O**cean** C**arbon** C**ycle Model HAMOCC5.1 - Technical Description Release 1.1** Ernst Maier-Reimer, Iris Kriest, Joachim Segschneider, Patrick Wetzel
Berichte zur Erdsystemforschung Nr.15 Juli 2005	**Long-range Atmospheric Transport and Total Environmental Fate of Persistent Organic Pollutants - A Study using a General Circulation Model** Semeena Valiyaveetil Shamsudheen

Publikationsreihe des MPI-M
„Berichte zur Erdsystemforschung“ , „*Reports on Earth System Science*“, ISSN 1614-1199
Sie enthält wissenschaftliche und technische Beiträge, inklusive Dissertationen.

Publikationsreihe des MPI-M
„Berichte zur Erdsystemforschung“ , „*Reports on Earth System Science*“, ISSN 1614-1199
Sie enthält wissenschaftliche und technische Beiträge, inklusive Dissertationen.

Publikationsreihe des MPI-M
„Berichte zur Erdsystemforschung“ , „*Reports on Earth System Science*“, ISSN 1614-1199
Sie enthält wissenschaftliche und technische Beiträge, inklusive Dissertationen.



ISSN 1614-1199